An initial investigation into the application of surfactin, a biosurfactant, as an alternative desulphurisation agent, for the prevention of acid mine drainage, via froth flotation

by

André Rossouw Augustyn

Thesis presented in partial fulfilment
of the requirements for the Degree

of

MASTER OF ENGINEERING
(EXTRACTIVE METALLURGICAL ENGINEERING)

in the Faculty of Engineering
at Stellenbosch University

Supervisor

Dr. M. Tadie

Co-Supervisor

Dr. R. W. M. Pott

December 2020

DECLARATION

By submitting this thesis electronically, I declare that the entirety of the work contained therein is my own, original work, that I am the sole author thereof (save to the extent explicitly otherwise stated), that reproduction and publication thereof by Stellenbosch University will not infringe any third party rights and that I have not previously in its entirety or in part submitted it for obtaining any qualification.

Date: *December 2020*

ABSTRACT

Coal mining plays a significant part in the South African economy. One of the largest problems associated with coal mining is acid mine drainage (AMD), which is produced through the oxidation of sulphide-minerals, in the presence of water and a suitable oxidant. AMD is toxic to the surrounding environment and causes lasting damage.

Froth flotation is a viable option for the desulphurisation of coal tailings which cause AMD. Global trends towards more sustainable and environmentally friendly surfactants have led to the investigation of biosurfactants as replacements for synthetic surfactants used in flotation. Surfactin, a microbial biosurfactant, may be promising as a desulphurisation agent, due to its molecular structure and the anionic nature of its functional groups, indicating the potential for preferential chelation of pyrite. The aim of this research was to determine the effectiveness of surfactin as a collector in desulphurisation of coal through froth flotation, as a mitigation strategy for the formation of acid mine drainage.

The first objective was achieved using surface tension to determine the critical micelle concentration of the surfactin sample, found to be 4.5 mg/L, to determine a practical surfactin concentration range, which was used for further experimentation.

Surfactin adsorption on both the surface of coal and pyrite was confirmed through zeta potential and FTIR analysis and indicated a greater interaction with both the surface of coal and pyrite in the neutral and alkaline pH ranges, signifying that ionisation of the surfactin carboxylic groups plays a significant role in adsorption. The attachment mechanism of surfactin to the surface of coal was confirmed to be hydrophobic physisorption between the aliphatic functional groups of surfactin molecules and the carbonaceous surface functional groups of coal, but results indicated that there was a limited number of surfactin adsorption sites. In contrast, the attachment mechanism of surfactin onto the surface of pyrite was chemisorption to either Fe-hydroxide sites or through interaction of the amide groups on surfactin with sulphur on the pyrite surface. Surfactin demonstrated a cleaning effect on both the surface of coal and pyrite, which may contribute to the increase in hydrophobicity.

Surfactin acted as a collector of both coal and pyrite at most operating conditions, however, there were instances at which surfactin had little to no effect on the hydrophobicity of coal or pyrite, and in the case of coal, surfactin acted as a depressant at pH 8. Generally, surfactin was a more effective collector of coal in the acidic pH range, and of pyrite in the alkaline pH range. This differential activity allows for the preferential flotation of either coal or pyrite.

The final objective was to determine the coal desulphurisation system operating conditions, and based on this preliminary study, those were determined to be at pH 10 and 5 mg/L surfactin concentration. This provided a 56.2% pyrite recovery and 47.8 % coal recovery. As a preliminary study, this research achieved its aim and indicated that surfactin shows great potential as an effective agent for the desulphurisation of coal through froth flotation.

OPSOMMING

Steenkoolwinning speel ’n beduidende rol in die Suid-Afrikaanse ekonomie. Een van die grootste probleme wat met steenkoolmyne geassosieer word is suurmyndreinering (AMD), wat geproduseer word tydens die oksidasie van sulfiedminerale in die teenwoordigheid van water en ’n gepaste oksidant. AMD is toksies vir die omliggende omgewing en veroorsaak blywende skade.

Skuimflottering is ’n lewensvatbare opsie vir die ontswaeling van steenkooluitskotte wat AMD veroorsaak. Globale tendense na meer volhoubare en omgewingsvriendelike surfaktante het na die ondersoek van biosurfaktante as plaasvervangers vir sintetiese surfaktante wat gebruik word in flottering, gelei. Surfaktien, ’n mikrobiese biosurfaktant, kan belowend wees as ’n ontswaelingsmiddel as gevolg van sy molekulêre struktuur en die anioniese natuur van sy funksionele groepe, wat die potensiaal vir voorkeurchelasie van piriet aandui. Die doel van hierdie navorsing was om die effektiwiteit van surfaktien as ’n versamelaar in ontswaeling van steenkool deur skuimflottering te bepaal, as ’n mitigasiestrategie vir die formasie van suurmyndreinering.

Die eerste doel is bereik deur oppervlakspanning te gebruik om die kritiese miselkonsentrasie van die surfaktiensteekproef te bepaal, gevind om 4.5 mg/L te wees, om ’n praktiese surfaktienkonsentrasiebestek te bepaal, wat gebruik is vir verdere eksperimentering.

Surfaktienadsorpsie op beide die oppervlaktes van steenkool en piriet is bevestig deur zetapotensiaal en FTIR-analise en het ’n groter interaksie met beide die oppervlak van steenkool en piriet in die neutrale en alkaliese pH-bestekke aangedui, wat aandui dat ionisering van die surfaktien se karboksiliese groepe ’n beduidende rol speel in adsorpsie. Die aanhegtingsmeganisme van die surfaktien op die oppervlakte van steenkool is bevestig om hidrofobiese fisisorpsie tussen die alifatiese funksionele groepe van surfaktienmolekules en die koolstofhoudende oppervlak funksionele groepe van steenkool te wees, maar resultate het aangedui dat daar ’n beperkte aantal surfaktienadsorpsie verbindingsplekke was. In kontras was die aanhegtingsmeganisme van surfaktien op die oppervlak van piriet chemisorpsie na Fe-hidroksied verbindingsplekke of deur interaksie van die amiedgroepe op surfaktien met sulfur op die pirietoppervlak. Surfaktien het ’n skoonmaakeffek op beide die oppervlaktes van steenkool en piriet gedemonstreer, wat tot die toename in hidrofobisiteit kon bydra.

Surfaktien het as ’n versamelaar van beide steenkool en piriet opgetree by meeste bedryfskondisies, maar daar was egter gevalle waar surfaktien min tot geen effek op die hidrofobisiteit van steenkool of piriet gehad het nie, en in die geval van steenkool, het surfaktien as ’n depressant opgetree by pH 8. Oor die algemeen was surfaktien ’n meer effektiewe versamelaar van steenkool in die suur pH-bestek, en van piriet in die alkaliese pH-bestek. Hierdie differensiële aktiwiteit laat die voorkeur flottering toe van of steenkool of piriet.

Die finale doel was om die steenkool ontswaelingstelsel se bedryfskondisies te bepaal, en gebaseer op hierdie voorafgaande studie is hierdie bepaal om by pH 10 en 5 mg/L surfaktienkonsentrasie te wees. Dit het ’n 56.2% pirietherwinning en 47.8% steenkoolherwinning voorsien. As ’n voorafgaande studie,

het hierdie navorsing sy doel bereik en aangedui dat surfaktien groot potensiaal toon as ’n effektiewe middel vir die ontswaeling van steenkool deur skuimflottering.

ACKNOWLEDGEMENTS

I would like to express my sincere gratitude to the following people for their direct and indirect contributions that made this research possible:

- Dr. M. Tadie and Dr. R.W. Pott for supervising my project and for their support.
- The staff at the analytical facility at the Department of Process Engineering of Stellenbosch University.
- The facilities staff of the Department of Process Engineering of Stellenbosch University.
- The Department of Process Engineering of Stellenbosch University for a postgraduate bursary.
- My family and friends, even though they had no idea what I was speaking about.

ARTICLES ARISING FROM THIS WORK

Articles in preparation

Article 1: The use of surfactin, a biosurfactant, as a flotation agent for coal, in the desulphurisation of coal via flotation.

Article 2: The use of surfactin, a biosurfactant, as a flotation agent for pyrite, in the desulphurisation of coal via flotation.

TABLE OF CONTENTS

LIST OF FIGURES

LIST OF TABLES

NOMENCLATURE

AMD	Acid mine drainage	-
ARD	Acid rock drainage	-
Asp	Aspartic amino acid (aspartate residue)	-
C	Carbon	-
CMC	Critical micelle concentration	mg/L
FTIR	Fourier transform infrared spectroscopy	-
Glu	Glutamic amino acid (glutamate residue)	-
H	Hydrogen	-
k	Flotation rate constant	min^{-1}
Fe	Iron	-
HPLC	High-performance liquid chromatograph	-
ICCP	The International Committee for Coal and Organic Petrology	-
IEP	isoelectric point	-
LC-MS	Liquid chromatography-mass spectroscopy	-
Leu	Leucine amino acid	-
M	Molarity	mol/L
NaCl	Sodium chloride	-
$NaHCO_3$	Sodium bicarbonate	-
O	Oxygen	-
pKa	Acid dissociation constant	-
PSD	Particle size distribution	-
PZC	Point of zero charge	-
P_{80}	Particle size at 80% particle pass	µm
R	Recovery	%
ROM	Run-of-mine	-
S	Sulphur	-
T	Time	min
Tris	tris(hydroxymethyl)aminomethane	-
Val	Valine amino acid	-
v/v	Volume per volume	%
wt%	Weight percent	%
XRD	X-ray powder diffraction	-

1 INTRODUCTION

1.1 Background

Mining makes up a large part of the South African and African economy as a whole. South Africa produced more than 250 Mt of coal at a value of more than R 110 billion in 2016 (Chamber of Mines of South Africa, 2018). The global demand for coal is expected to trend downwards, nevertheless, the demand for a cheap power source from developing nations is expected to support the demand for coal resources for the foreseeable future (Chamber of Mines of South Africa, 2018). However, coal mining, and mining in general, has traditionally been associated with environmental damage.

The most recent survey estimates that the South African coal mining industry discards more than 11 million tons of ultrafine coal slurry and 42 million tons of discard coal per annum (Department of Minerals and Energy, 2001). Ultrafine and discard coal waste has been linked to spontaneous combustion, dust problems and acid mine drainage (Reddick et al., 2007). One of the biggest causes of environmental damage associated with coal mining is acid mine drainage caused by discard coal and ultrafine coal tailings. AMD is produced by the oxidative dissolution of sulphide-minerals (such as pyrite) in mine structures, mill and process plant tailings and mine waste rock piles resulting in a strongly acidic, aqueous solution, high in ferrous and non-ferrous metal sulphates and salts (Akcil and Koldas, 2006; Georgopoulou et al., 1996; Macingova and Luptakova, 2012; Simate and Ndlovu, 2014). AMD contaminates ground and surface water, affecting the health of the surrounding environment, flora and fauna (Simate and Ndlovu, 2014).

Several methods for mitigating AMD have been investigated and implemented. Froth flotation has been shown to be a viable method for ultrafines desulphurisation and beneficiation (Reddick et al., 2007). The use of surfactants increases the selectivity and efficiency of froth flotation. During desulphurisation, coal flotation makes use of kerosene and dodecane, whereas pyrite flotation makes use of xanthates and dithiocarbonates (Kazadi Mbamba et al., 2013; Lotter et al., 2016). These surfactants are synthetic, generally made from fossil fuels, and can be environmentally toxic (Bach et al., 2016). Xanthates have been shown to bioaccumulate (Xu et al., 1988) and enhance the bioaccumulation of heavy metals in organisms (Block and Pärt, 1986). The degradation product of xanthate, carbon disulphide (CS_2), is the main source of toxicity and has been associated with a number of long-term neurological and reproductive effects (Agency for Toxic Substances and Disease Registry, 2012). Thus, the catch-22 of needing to desulphurise coal tailings to prevent environmental problems, but the current desulphurisation system uses xanthate which causes environmental problems.

There has been a worldwide shift towards safer, more environmentally responsible, and sustainable alternative mining processes. This has driven the investigation into replacing synthetic surfactants with microbially produced biosurfactants (Mulligan, 2009). These biosurfactants can be produced using waste streams and have been shown to be less toxic and more readily biodegradable than their synthetic counterparts (Bodour and Miller-Maier, 1998).

1.2 Research motivation

There have been limited investigations into the use of biosurfactants in flotation. Rhamnolipid biosurfactants were investigated in coal, iron concentrate, phosphate ore and hematite flotation (Khoshdast et al., 2011; Szymanska and Sadowski, 2010) and, surfactin or lychenysin biosurfactants as collectors for goethite flotation (Zouboulis et al., 2003).

Abdel-Khalek and El-Midany (2013) showed that *Bacillus subtilis* bacteria, the microorganism that produces surfactin, can be used to desulphurise coal in a bioflotation system. But bioflotation systems with live microbes present their own set of challenges and thus it is hypothesised that using the pure biosurfactants produced by *Bacillus subtilis* bacteria would be more effective. The attachment of *Bacillus subtilis* bacteria is attributed to lipopolysaccharides, lipoprotein and bacterial surface proteins. Of these molecules, surfactin has been well characterised and has shown promise in previous mineral flotation.

The proposed research hypothesizes that using the biosurfactant, surfactin, produced by *Bacillus subtills*, as a desulphurisation agent in a pure form will be more practical and effective. Another contributing factor is that surfactin shows promise as a desulphurisation agent, due to its amphiphilic molecular structure and the anionic nature of its carboxylic functional groups, indicating the potential for preferential chelation of pyrite.

1.3 Aim and Objectives

This research aims to determine the effectiveness of surfactin as a collector in desulphurisation of coal through froth flotation of coal and pyrite, as a mitigation strategy for the formation of acid mine drainage. Specifically, this proof of concept study will be a preliminary investigation into the practical feasibility of surfactin as a collector for coal and pyrite. The success of this study could lead to a more environmentally friendly alternative for the synthetic surfactants currently used.

Five objectives have been identified in order to achieve the aim and answer the key questions. Firstly, to determine a surfactin concentration range for further experimentation. This objective will guide the surfactin concentration range investigated in the subsequent experimentation. The second objective is to evaluate the effect of the coal and pyrite surface charge on the adsorption of surfactin, to determine how pH and surfactin concentration affect surfactin adsorption. This leads to objective three, which is to evaluate the attachment mechanism of surfactin to the surface of coal and pyrite, to gain more insight into the interaction between coal or pyrite and surfactin The next objective is to evaluate the effect of surfactin on the hydrophobicity of coal and pyrite, which will indicate the applicability of surfactin in a flotation system. Lastly, all previous results will be combined to answer the last objective, which is to determine the potential desulphurisation operating conditions, with respect to using surfactin as a desulphurisation agent.

1.4 Thesis overview

Chapter 2, Literature review, is an overview of the literature associated with the understanding of acid mine drainage, froth flotation, biosurfactants and surfactin, and identify the opportunity and evidence for using surfactin as a potential desulphurisation agent.

Chapter 3, Hypothesis, Aim and Objectives, identifies the hypothesis and the motivation behind it, as well as stating the aim and outlining the associated objectives of this research. The key questions are also identified.

Chapter 4, Methodology, describes the origin, preparation and characterization of the materials used in this study, as well as the methods used to investigate and complete the research objectives.

Chapter 5, Results and Discussion, presents and discusses the results of the investigation into surfactin adsorption onto the surface of coal and pyrite, the associated effect of pH and surfactin concentration on adsorption and hydrophobicity, as well as the recovery and flotation kinetics associated with the flotation of coal and pyrite using surfactin.

Chapter6, Conclusion, provides a general conclusion on the aim achieved and specific conclusions with respect to each specified objective.

Chapter 7, Recommendations, outlines recommended objectives to be completed to further study the novel use of surfactin as a coal desulphurisasion agent.

2 LITERATURE REVIEW

This literature review aims to review and discuss the relevant literature associated with certain aspects of the proposed research. The objectives for the literature review are:

1. Explore acid mine drainage and gain a greater understanding of the cause and the effect.
2. Explore froth flotation for desulphurisation of coal and the associated variables involved.
3. Gain a greater understanding of coal and pyrite surface chemistry and how it affects flotation.
4. Understand biosurfactants and the structure of surfactin.
5. Review the studies done on surfactin adsorption in a mineral processing context.

2.1 Acid mine drainage

Acid mine drainage (AMD) is considered the worst of all the environmental problems associated with mining (Peppas et al., 2000). AMD has severe, far stretching, and long-lasting effects on the environment. To understand the scope and scale of the problem that is AMD, in this section the literature surrounding AMD was reviewed to understand the definition, formation, environmental impact, and prevention and mitigation methods of AMD.

2.1.1 Acid mine drainage: definition and formation

To understand why it is important to prevent acid mine drainage (AMD), we firstly have to understand what exactly AMD is, how it forms and the link to pyrite and coal mining.

Acid mine drainage (AMD), also known as acid rock drainage (ARD), is characterised by a low pH aqueous effluent with a high specific conductivity. High concentrations of base metals, such as manganese, iron and aluminium, and lower concentrations of heavy metals and other elements are usually present in AMD (Peppas et al., 2000). The exact composition of AMD is dependent on the surrounding climate, geology, hydrology and mineralogy, and thus differs markedly from site to site. This makes predicting and planning for AMD exceptionally difficult (Akcil and Koldas, 2006; Kefeni et al., 2017).

In order for AMD to form, three conditions need to be met: the presence of sulphide material, the presence of water, and the presence of an oxidant (primarily atmospheric oxygen, but potentially other chemical sources) (Akcil and Koldas, 2006). AMD forms through a complex series of reactions that depend on the chemical species involved. Simply put, the sulphide minerals are oxidised by the action of water and oxygen to form sulphuric acid. These oxidation reactions are autocatalytic and have been found to be accelerated by microbial activity. Depending on the surrounding environment, some of the generated sulphuric acid is neutralised by acid consuming minerals in the surrounding rock, resulting in the formation of precipitation compounds such as oxyhydroxides, metal hydroxides, gypsum and more complex compounds (Gray, 1997; Peppas et al., 2000). It is this mixture of acidic effluent and the metals and metal precipitates released from the rock minerals that make up AMD.

The AMD process does also occur naturally, but intensive mining operations tend to increase the quantity of sulphide mineral ores exposed to the environment by several orders of magnitude (Akcil and Koldas, 2006). AMD is commonly found at gold and coal mining activities, due to the associated sulphide minerals commonly found in conjunction with these minerals, but has also been associated with lead, zinc, copper,

and silver mining operations (Gray, 1997; Kefeni et al., 2017). Of all the major sulphide minerals associated with AMD, the mineral pyrite is the most significant (Gray, 1997; Kefeni et al., 2017).

2.1.2 Acid mine drainage: environmental impact

Now that acid mine drainage has been defined and the formation and link to coal mining is clear, the reason to prevent AMD, namely the severe environmental impact of AMD, will be explored in this section.

AMD has a significant impact on the environment. AMD contaminates soil and ground- and surface-water, due to the acidity, metal toxicity, salination and sedimentation associated with AMD (Gray, 1997; Peppas et al., 2000). The most common and abundant metal in AMD is Fe(II). Fe(II) is oxidised to form iron oxide precipitate, known for its yellow/orange/brick-red colour. In streams contaminated with AMD, this Fe(II) oxide embeds itself on stream or ocean beds and the formation of ferric hydroxide precipitates lowers the pH of the water. Consequently, microorganisms and aquatic life that live and feed along the stream and ocean beds are severely affected and can die (Agrawal and Sahu, 2009; Han et al., 2017). This death of microorganisms causes a snowballing chain-reaction up the food chain, negatively effecting the stream and surrounding biota (Kefeni et al., 2017; Simate and Ndlovu, 2014).

It has been found that streams contaminated with AMD do not support vegetation in the zones around them. This effect has been found to persist for several kilometres downstream from the AMD source (Naicker et al., 2003). The heavy metals associated with AMD have the ability to accumulate and persist in the ecosystem for extended periods of time. They disrupt the normal metabolic functions of living organisms, causing acute and chronic poisoning, toxicity and disease (Simate and Ndlovu, 2014).

A significant portion of AMD is left untreated as treatment options are either too expensive or plainly inadequate (Akcil and Koldas, 2006). The pollution of water sources by AMD has a serious impact on human health, especially due to acute and long term heavy metal toxicity caused by AMD heavy metal pollutants in the water (Simate and Ndlovu, 2014). AMD is a serious pollution problem for current and future generations and which has been shown to produce prolonged pollution and degradation of the surrounding environment (Broadhurst et al., 2015; Kefeni et al., 2017). Thus, there is a strong case for the prevention of AMD.

2.1.3 Acid mine drainage: prevention and mitigation

The severe environmental impacts associated with acid mine drainage (AMD) have been reviewed and the need to prevent AMD is clear. The next section will review the prevention and mitigation of AMD to avert the associated environmental impacts.

The potential for and severity of AMD is highly site dependent and this makes it difficult and costly to predict (Akcil and Koldas, 2006). AMD remediation methods are largely costly and unaffordable, with very few being cheap and sustainable (Anawar, 2015; Kefeni et al., 2017) .

Control of AMD is generally performed using three main techniques, namely: release control, migration control and source control (Geldenhuis and Bell, 1998). Release control focuses on the collection and treatment of AMD after formation. This makes use of water treatment processes to remove harmful

metals and sulphate, and neutralize the pH to allow the water to be reused or discarded without any harmful environmental effects. Migration control focuses on the AMD transport medium, namely water. The main goal of migration control is the prevention of water entering the AMD site, by employing diversion channels or placing cover materials, to prevent water infiltration. Migration control is more practical with closed or abandoned mines, whereas release control is more practical for working mines. Source control focuses on the prevention and inhibition of AMD generation in the first place. Techniques focus on the exclusion of air or water, or the isolation or removal of sulphide material. The isolation and removal of sulphide material is generally done by desulphurisation of waste streams with techniques such as froth flotation (Geldenhuis and Bell, 1998).

Recent changes in global legislation and more environmental and sustainable thinking, has led to more pro-active approaches to preventing or minimizing AMD. These approaches focus on long-term prevention or reduction of AMD through generating benign mine waste in the first place (Broadhurst et al., 2015; Harrison et al., 2010). One of these approaches is the desulphurisation of the sulphide-bearing waste material before disposal, using physical separation techniques such as froth flotation. The use of flotation for desulphurisation, to minimize AMD, has been shown to be technically feasible (Benzaazoua et al., 2000; Bois et al., 2005; Broadhurst et al., 2015; Hesketh et al., 2010; Kazadi Mbamba et al., 2012).

2.1.4 Acid mine drainage: summary

The oxidation of pyrite in coal mining waste tailings causes the formation of acid mine drainage (AMD). AMD causes harmful, long term environmental pollution. A viable method for the desulphurisation of coal tailings, to prevent AMD formation, is to use froth flotation. In the next section, froth flotation and the use of froth flotation for coal desulphurisation will be reviewed.

2.2 Froth flotation

As discussed in the previous section, froth flotation is a viable method for the desulphurisation of coal tailings to prevent acid mine drainage (AMD). In this section the froth flotation itself and its application to coal desulphurisation will be discussed.

2.2.1 Froth flotation: Overview

Froth flotation makes use of the natural surface characteristics of minerals to separate them. The mineral surface characteristics make the mineral hydrophobic or hydrophilic. Hydrophilic surfaces are readily wetted and thus tend to stay in the bulk liquid. Hydrophobic surfaces repel water and thus are able to attach to air bubbles, allowing them to be floated and thereby separated from the hydrophilic minerals (Wills and Napier-Munn, 2005).

To illustrate the concept of froth flotation, a flotation column will be used as an example. Figure 1 shows a schematic drawing of a froth flotation column. Although the design of the column and air disperser may differ, the operating principle stays the same. The feed to the flotation column is usually a slurry made up of the minerals to be separated. Air is introduced through an air dispersion device that creates air bubbles. The hydrophobic particles in the flotation pulp attach to the raising air bubbles. The bubbles and

attached hydrophobic particles report to and reside in the froth layer formed at the top of the column. The froth eventually overflows and is collected as concentrate, separating the hydrophobic particles from the hydrophilic particles that remain in the column pulp. The hydrophilic particles that remain in the flotation pulp are removed as tailings at the bottom of the column. These tailings are known as “gangue” when they are the undesirable material.

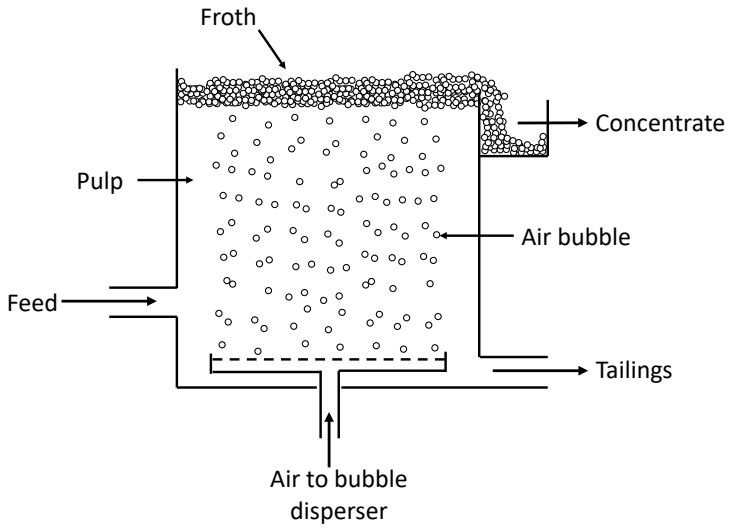

Figure 1: Schematic drawing of a simple froth flotation column. Adapted from Suli et al. (2017).

Froth flotation recovers material through three mechanisms, namely:

1. Selective attachment of minerals to air bubbles.
2. Entrainment of material in the water in the froth.
3. Physical entrapment of the material between particles attached to air bubbles.

Selective attachment is the main mechanism by which the majority of the valuable material is recovered. Entrainment and entrapment are mechanisms which are not particularly selective, and thus these mechanisms cause unwanted gangue material to be recovered with the valuable material. Thus, entrainment and entrapment negatively affect the separation efficiency (SE). These three mechanisms coupled with the interaction of chemical and physical variables, make the system fairly complex (Polat et al., 2003; Wills and Napier-Munn, 2005). The chemical and physical (equipment and operational components) variables within a flotation system are interlinked and interdependent and their relationships are summarised in the form of Klimpel’s triangle (Klimpel and Hansen, 1988), shown in Figure 2.

In this study the focus will be on the chemical components of the flotation system. Specifically, the collectors used in the desulphurisation of coal through froth flotation. The next section will discuss the chemical components of a froth flotation system, what collectors are and how they fit in to the desulphurisation system

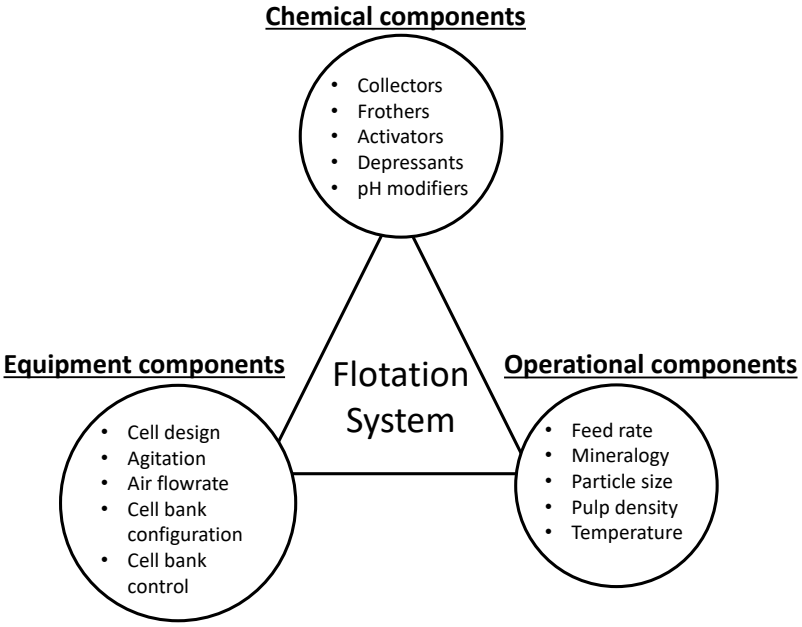

Figure 2: Klimpel's triangle showing the relationships between various components in a flotation system. Adapted from Klimpel and Hansen (1988).

2.2.2 Froth flotation: Chemical enhancement

The majority of minerals are hydrophilic in their natural state and need the addition of chemical agents to assist flotation. These chemical agents can be classified as frothers, activators, dispersants, depressants, pH modifiers or collectors. Greater focus will be on collectors, as they are linked to the aim of the study.

2.2.2.1 Frothers, activators, dispersants, depressants, and pH modifiers

Frothers are reagents that facilitate the production and preservation of fine bubbles, which increases the bubble-particle collision rate and favours increased flotation kinetics. Activators are generally inorganic salts that, as ions in solution, react with and change the surface of a mineral to facilitate increased collector adsorption and thus floatability. Dispersants are used to prevent aggregation of particles and prevent fine particles from coating larger particles. Depressants are used to increase selectivity in flotation by selectively causing certain minerals to become hydrophilic, through the adsorption of hydrophilic species, the blocking of hydrophobic sites on the surface of certain minerals and the desorption of adsorbed collector or activating species (Farrokhpay, 2011; Klimpel and Isherwood, 1991; Wills and Napier-Munn, 2005).

The regulation of pH plays one of the, if not the most important role in flotation. The electrochemical potential, surface charge, ion exchange, adsorption, depression, collector stability, dissolution and oxidation of species are all linked to the pH. Regulators are generally lime, sodium carbonate or sodium hydroxide for alkalinity adjustments, and sulfuric or sulfurous acids for decreasing pH (Wills and Napier-Munn, 2005).

2.2.2.2 Collectors

Few minerals are naturally hydrophobic. In this case reagents, named collectors, are added to the flotation process, where they adsorb onto specific mineral surfaces, rendering the mineral hydrophobic. These collectors are surfactants. They reduce the stability of the hydrated layer between the mineral and the air-bubble. This allows the particle to attach to the air bubble more easily (Nagaraj and Farinato, 2016; Wills and Napier-Munn, 2005).

Non-ionising collectors are generally insoluble and strongly hydrophobic. They adsorb through the natural tendency for hydrophobic species to attract each other and repel water, called hydrophobic interaction. These collectors are used with naturally hydrophobic minerals to improve their floatability (Wills and Napier-Munn, 2005). One example of the use of non-ionising collectors is to enhance the hydrophobicity of coal through “oily collectors” such as diesel oil and kerosene (Dey, 2012; Dey et al., 2014).

Ionising collectors are soluble and made up of a nonpolar hydrocarbon group connected to a polar group. The nonpolar group is hydrophobic. The polar group allows the molecule to be soluble, as well as being the reactive part of the molecule. Ionising collectors are divided into two groups according to the charge on the dissociated polar group: anionic and cationic. Cationic collectors are generally based on amines and ether amines, and are used for non-sulphide flotation. Anionic collectors are further divided into sulfhydryl type, made up of an SH group in undissociated form and commonly used for sulphide flotation, and oxyhydryl type, made up of a OH group and commonly used in non-sulphide.

The focus of this project is to determine if the proposed biosurfactant, surfactin, can perform the same function as xanthate, a sulfhydryl type collector used in pyrite flotation. The structure of surfactin (discussed in greater detail in section 172.7), shows a parallel structure to xanthate in terms of the fact that they both have a polar group and a hydrophobic group. That is the extent of the similarities. Xanthate has a sulfhydryl polar group, whereas the polar group of surfactin consists of carboxylic and amide functional groups. The hydrophobic group of xanthates is also generally shorter than the hydrophobic group of surfactin. The difference in structure does not necessarily mean that surfactin can not perform the same function as xanthates. It is entirely possible that surfactin can be used to float pyrite, same as xanthates, but surfactin instead uses different functional groups to float pyrite, which links to the aim of surfactin being a potential replacement for xanthates as surfactin does not have the sulfhydryl group that causes the negative environmental impact upon the degradation of xanthates.

However, surfactin shows similarities to chelating collectors. Chelating collectors are surfactants that have at least two donor atoms that form a complex with a metal ion (Singh, 1998). The structure of hydroxamate type collectors shows parallels to the carboxylic and amide functional groups found on surfactin. Hydroxamate type collectors have seen use in the flotation of copper oxide and iron ores and show clear strong chelation of copper (Fuerstenau et al., 2000; Singh, 1998). Surfactin has also shown to chelate with copper ions (Mulligan et al., 1999a), and thus a parallel can be drawn between surfactin and hydroxamate collectors. It is unknown at this stage whether surfactin chelation with copper will translate to chelation of iron on the surface of pyrite, and therein lies the opportunity for further research. The

purpose of this research will be to determine if the chelation ability of surfactin translates to pyrite, and whether surfactin can be used as an effective collector of pyrite in the desulphurisation of coal.

2.2.3 Froth flotation: configurations for the desulphurisation of coal tailings

Having discussed the basic operation of a froth flotation system and the use of collectors to increase selectivity, the next section focuses on the flotation configurations commonly used in the desulphurisation of coal using froth flotation. As it is yet unknown whether surfactin will act as a collector or depressant for either coal or pyrite, the effect of surfactin on the floatability of either coal or pyrite will govern the flotation configuration in which surfactin can be used.

The desulphurisation of coal tailings using froth flotation generally makes use of two flotation configurations. The traditional route is the direct flotation configuration, when the valuable material, namely coal, is separated into the froth fraction, leaving the gangue in the tailings. As coal is naturally hydrophobic and the gangue is not, direct flotation makes use of this natural hydrophobicity. The reverse flotation configuration is the opposite of the direct flotation configuration. It is characterised by floating the gangue material, in this case pyrite, with the valuable material remaining in the tailings (Stonestreet and Franzidis, 1988; Wills and Napier-Munn, 2005). The reversal of the traditional flotation route is used to prevent entrainment by removing the gangue phase by flotation, which tends to make up a smaller percentage of the total feed in coal flotation, instead of the bulk coal phase which tends to make up the largest part of the feed to the flotation system. Some entrainment of the desired mineral is inevitable and thus the total coal recovery is lower, but the final grade of the bulk coal phase is higher and was shown to have less gangue materials compared to using a direct flotation system (Stonestreet and Franzidis, 1988).

Kazadi Mbamba et al.(2012) proposed a two-stage process for the desulphurisation of South African coal tailings. The first stage is the direct flotation of coal for the recovery of valuable low-sulphur coal ultrafines that can be transformed into a commercial product. The second stage involves the flotation of pyrite from the first stage tailings, to provide a benign desulphurised gangue material that can be disposed easily without environmental harm. The lower volume of pyrite concentrate is then more viable to be bio-desulphurised. The two-stage process is attractive as it provides a saleable coal product in the first stage and a low volume pyrite concentrate in the second stage, providing additional income as well as reducing the final pyrite disposal costs due to the lower volume.

This study aims to determine the effectiveness of surfactin in either of the two stages of the Kazadi Mbamba et al.(2012) desulphurisation process. If surfactin performs well as a collector of pyrite and a depressant of coal, it will be useful in stage two. If surfactin is an effective collector of coal and depressant of pyrite, it will find application in stage one of the two-stage process. There may also be an opportunity to use surfactin in both stages and use pH to manipulate the selectivity of surfactin for either coal or pyrite. This possibility would need to be investigated.

2.3 Coal and the factors influencing coal flotation

The froth flotation process, its application to the desulphurisation of coal, and the use of collectors to increase selectivity has been discussed. This section aims to review coal composition and coal surface chemistry as it has a large impact the hydrophobicity of coal and on collector adsorption in coal flotation. Understanding the coal surface chemistry will clarify the interaction between the coal surface and the biosurfactant, surfactin, allowing the potential adsorption mechanisms to be determined.

Coal is described as a heterogenous material, consisting of organic and mineral fractions. The organic fractions have different chemical and physical properties according to the plant material it originates from and is classified according to rank (Holuszko and Mastalerz, 2015; ICCP, 2001, 1998; Pickel et al., 2017; Sýkorová et al., 2005).

2.3.1 Coal Rank

Coal rank is used to describe the degree of coalification of the original plant material. The degree of coalification follows the path from low to high rank: lignite, sub-bituminous coal, bituminous coal, semi-anthracite, and anthracite. Sub-bituminous coal is formed when lignite loses its hydroxyl side chains. Further coalification leads to the formation of aromatic rings. The higher the aromaticity of the coal the higher the coal rank, with anthracite having tightly packed aromatic ring clusters. Increase in coal rank is associated with an increase in carbon content and a decrease in oxygen content (Holuszko and Mastalerz, 2015). Thus, a higher coal rank is associated with a greater hydrophobicity as there are more aliphatic and aromatic surface functional groups, and consequently easier to float in froth flotation processes.

2.3.2 Mineral matter associated with coal

Clays, carbonate material, sulphides (mainly pyrite), quartz and glauconite are the dominant minerals associated with South African coals (Kershaw and Taylor, 1992). These minerals are generally hydrophilic and do not float naturally in a froth flotation system (Wen et al., 2017).

2.3.3 Coal surface chemistry

Coal is made up of a hydrocarbon structure. This makes coal naturally hydrophobic. But the various surface functional groups attached to the hydrocarbon structure determine the hydrophobic-hydrophilic character (Holuszko and Mastalerz, 2015).

Oxygen exists on the surface of coal in various forms, namely: carboxyl (-COOH), hydroxyl (-OH, phenol and alcohol), ether (C-O-C), ketone (C=O) and methoxy ($-OCH_3$). These functional groups have been found to be readily oxidized by a small amount of residual oxygen (Dey, 2012; Korobetskii et al., 1990). Oxygen functional groups on the coal surface provide sites for the adsorption of water. Thus, the coal surface functional groups can be directly related to the hydrophobicity-hydrophilicity of coal (Fuerstenau et al., 1983; Holuszko and Mastalerz, 2015).

The determination of coal surface charge is difficult due to the heterogeneous nature of coal (Dey, 2012). Campbell and Sun (1969) proposed that the freshly exposed coal surface, when exposed to atmospheric oxygen, causes the exposed carbon to oxidize. The oxidized surface has characteristics similar to oxide

minerals, with hydroxyl and hydronium ions determining the surface charge. Kelebek et al.(1982) proposed that the surface charge of low rank lignitic coals, due to the abundance of oxygen functional groups, is determined by the degree of dissociation of weakly acidic oxygen functional groups, such as phenolic OH and COO, on the coal surface.

2.3.3.1 Effect of oxidation on coal surface chemistry

Three major aspects are involved in the oxidation of coal: the adsorption of oxygen onto the coal surface, the release of reaction products, and the release of heat. The release of heat may cause further oxidation to occur. Coal oxidization is characterized by a decrease in the hydrophobic carbon sites on the coal surface. This occurs in conjunction with an increase in the hydrophilic sites, through the formation of oxygenated functional groups. Oxidized coal has similar surface properties to low rank coal (Fuerstenau and Diao, 1992; Wen et al., 2017).

2.3.3.2 Effect of pH on coal surface chemistry

Hydroxyl and hydronium ions are the electrokinetic potential determining ions. Thus, an increase in pH, and associated increase in hydroxyl ions (OH^-), causes an increase in the negative surface charges on coal. Inversely, when pH is decreased, the associated increase in hydronium ions (H_3O^+) causes an increase in the acid groups, the negative charges are neutralized and the positive charges are increased. This makes the surface more positive. (Dey, 2012).

2.3.4 Coal zeta potential

To understand the zeta potential, a discussion of the surface charge and the double layer theory is done in this section. Additionally, using zeta potential as a method of distinguishing between chemical and physical surfactant adsorption is discussed.

Mineral particles in water exhibit a surface charge. The charge associated with the particle affects the distribution of counterions near the particle. The first layer of counterions, bound to the particle, is called the Stern layer. The second layer of counterions, more loosely attracted ions, is called the diffuse layer. The Stern and diffuse layer together make up the electrical double layer (EDL). The potential across the double layer, from the Stern layer to the bulk solution, falls exponentially the larger the distance from the particle and is described by the Gouy-Chapman theory (Fuerstenau and Pradip, 2019; Poortinga et al., 2002). The movement of liquid across a solid surface strips off ions in the diffuse layer, giving rise to an electrical potential called the zeta potential. The zeta potential is generally equated to the Stern potential (Fuerstenau and Pradip, 2005). The double layer and the associated electrokinetic potentials are shown schematically in Figure 3.

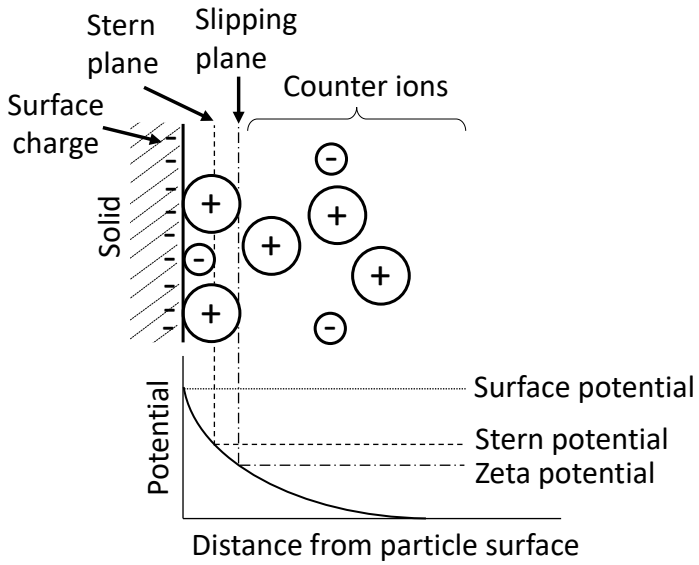

Figure 3: A schematic showing the electrokinetic double layer and the associated electrokinetic potential. Adapted from (Fuerstenau and Pradip, 2019)

Ions that establish the electrical double layer are called potential-determining ions and are commonly hydrogen or hydroxyl ions. For flotation, the most important parameter associated with the electrical double layer is the point of zero surface charge (PZC), also called the isoelectric point (IEP) when working with zeta potential.

The addition of surfactants changes the IEP and the zeta potential response curve of a mineral. The changes to the zeta potential response and IEP can be used to distinguish whether adsorption is through physical or chemical interactions (Fuerstenau and Pradip, 2005). Figure 4 will be used to illustrate the effect of a surfactant on the zeta potential response of a mineral. The indifferent electrolyte curve indicates the zeta potential of a mineral without the addition of a surfactant, with the PZC or IEP indicated by point A. Assuming the mineral is naturally hydrophilic and an anionic surfactant is added to the system, a zeta potential response similar to the dashed line in Figure 4 is obtained. At high pH, the anionic surfactant is not adsorbed (due to electrostatic repulsion between the negatively charged mineral surface and the anionic surfactant) and the zeta potential response is the same as the case without surfactant addition. As the pH is decreased, the mineral surface becomes more positively charged and the anionic surfactant is able to adsorb. At point D, the surfactant starts to form hemimicelles and chain-chain interactions cause reversal of the zeta potential as pH is lowered to the IEP at point C. In the case of a hydrophobic mineral, the addition of an anionic surfactant will cause the IEP to shift lower from point A to point B'. This reflects adsorption of the hydrophobic chain of the surfactant onto the hydrophobic mineral. The curves come together at point E' where the mineral surface charge is sufficiently negatively charged and the repulsive force is large enough to prevent hydrophobic interaction, and thus prevent further adsorption of the anionic surfactant. Anionic surfactant that chemisorb onto the mineral surface, cause a significant shift in the IEP, as seen by the shift from point A to point B". At high pH the curves come together at point E", indicating the point where the electrostatic repulsion between the negatively

charged surface and the anionic surfactant is large enough to prevent chemical adsorption of the surfactant.

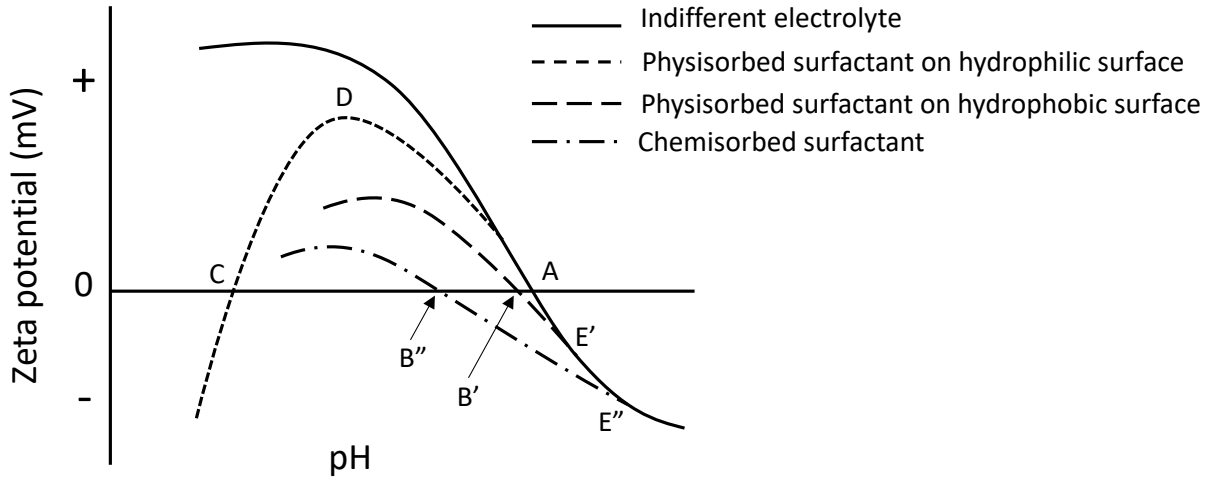

Figure 4: Schematic illustration of the effect of surfactant adsorption on zeta potential. Redrawn from Fuerstenau and Pradip,(2005)

The iso-electric point (IEP) of coal varies due to the heterogenous nature of coal. The IEP of unoxidized coal was found to be 4.2. (Sarikaya and Özbayoğlu, 1995). The IEP of bituminous coal has been reported to be between 3.5 – 4.6 (Kelebek et al., 1982). Weathering of coal, increases oxidation, thereby increasing the number of oxygenated functional groups and making the coal surface more hydrophilic (Dey, 2012). This oxidation causes the shift of the isoelectric point (IEP) to a lower pH value (Kelebek et al., 1982). Thus, the experimental IEP can be compared to literature IEP to determine degree of oxidation and as a way of validating the experimental method used.

2.4 Pyrite and the factors influencing pyrite flotation

The other mineral of importance in the desulphurisation of coal is pyrite. This section aims to review the composition of pyrite and the pyrite surface chemistry as it will affect collector adsorption and thus the floatability of pyrite.

Pyrite, also known as iron disulphide (FeS_2), is the most common sulphide mineral on earth. Subsequently pyrite often exists within coal mines and sulfidic ores as gangue. It is commonly removed by froth flotation (Ahmadi et al., 2018; Moslemi and Gharabaghi, 2017).

2.4.1 Types of pyrite

There are two main types of pyrite: coal-pyrites and mineral-pyrites. The morphology of coal-pyrite and mineral-pyrite is dissimilar and there is significant variance within the specific types. Coal-pyrite is considered poorly crystalline and consequently has a higher surface area. This causes natural coal-pyrite surface to oxidize much faster and have a higher concentration of oxidation products (Khan et al., 1991; Raichur et al., 2001; Yoon et al., 1997). This is important to keep in mind when using mineral-pyrite as a substitute for coal pyrite in this preliminary study.

2.4.2 Pyrite surface chemistry

The surface chemistry of pyrite is largely dependent on the electrochemical potential of the solution/mineral interface. This potential is made up of the cathodic and anodic reactions at the mineral surface. It controls the formation of species that cause pyrite to float, such as elemental sulfur and polysulfides, and species that depress pyrite flotation, such as sulfate and hydroxide/ferric oxide. This electrochemical potential is affected by electrochemical processes such as pyrite oxidation, activation, depression and adsorption of collectors. These processes affect the floatability of pyrite and thus play an important role within control and optimization of the process (Moslemi and Gharabaghi, 2017).

2.4.2.1 Effect of oxidation on pyrite surface chemistry

The rate of oxidation is affected by numerous factors, such as solution electrochemical potential, pH, oxidizing agent type and concentration, temperature, agitation and particle size (Moslemi and Gharabaghi, 2017). Freshly milled pyrite is hydrophilic, due to the high concentration of exposed iron species. As the pyrite starts to oxidize under oxidizing conditions, the iron experiences preferential dissolution, creating iron-deficient areas in the crystal lattice structure. Polysulfide then forms on the surface. This coating behaves hydrophobically, due to lack of metal. Further oxidation leads to the formation of Ferric hydroxide ($Fe(OH)_3$) and $S_xO_y^{2-}$, which form hydrophilic functional groups on the surface of the oxidized pyrite (Buckley and Riley, 1991; Peng et al., 2003; Tao et al., 1994; Zachwieja et al., 1989; Zhu et al., 2002).

2.4.2.2 Effect of pH on pyrite surface chemistry

The relationship between pH and floatability of pyrite is dependent on the ratio of hydrophobic sulfur species to hydrophilic hydroxide species. In alkaline environments, ferrous ions react to form ferrous hydroxides, which continue to react to form ferric hydroxides. These ferric hydroxides precipitate on the pyrite surface (Chander and Briceno, 1987; Ekmekçi and Demirel, 1997; Wang and Forssberg, 1990). As pH increases in the alkaline environment, the rate of formation and stability of these hydrophilic products increases (Cai et al., 2009a, 2009b; Ekmekçi and Demirel, 1997). Hydrophobic sulfur species also form, but they are covered by the more stable hydrophilic species (Wang and Forssberg, 1990). In acidic environments, pyrite has a higher hydrophobicity due to the formation of elemental sulphur or sulphur-based species (Cai et al., 2009a; Ekmekçi and Demirel, 1997; Moslemi et al., 2011; Trahar et al., 1994).

2.4.3 Pyrite zeta potential

Zeta potential, its relation to surface charge and the method of using zeta potential to distinguish between chemical and physical surfactant adsorption has been discussed in the coal zeta potential section (section 122.3.4). This section will briefly discuss the literature surrounding the zeta potential of pyrite.

Fornasiero et al. (1992) performed various studies on the effect of oxidation on the zeta potential of pyrite. The isoelectric point (IEP) of freshly ground pyrite, conditioned for 30 min in an aqueous solution in the presence of argon, occurs at a pH of 1.2. When the pyrite is instead conditioned for 30 min in an aqueous solution in the presence of air, IEP of pyrite changes to approximately pH 2. Conditioning pyrite

for 2 hours in an aqueous solution in the presence of air, causes a significant shift in the IEP to an approximate pH of 5.2. Consequently, the degree of pyrite surface oxidation can be determined from the shift in the IEP of pyrite towards the higher IEP of the metal oxides as oxidation takes place (Fornasiero et al., 1994, 1992; Peng and Grano, 2010). Using the literature IEP of pyrite, the degree of oxidation of the experimental pyrite can be determined by comparison.

2.5 Biosurfactants

The previous sections dealt with coal and pyrite surface chemistry and how it relates to hydrophobicity and froth flotation. The collectors for pyrite commonly used in the desulphurisation of coal, namely xanthates, were shown to have negative environmental and health related effects. An interesting route of investigation would be to determine if a more environmentally friendly biosurfactant, namely surfactin, can be effectively used in place of xanthate collectors. Thus, biosurfactants are discussed in the next section.

To understand biosurfactants, we first have to understand surfactants. Surfactants are molecules that adsorb onto interfaces and alter the interface characteristics. They are attracted to interfaces due to their amphipathic nature (Rosenberg and Ron, 1999).

Biosurfactants are surfactants from a biological source. The production of biosurfactants from bacteria and fungi is easier and faster due to the shorter generation time in comparison to plant and animal growth (Lang, 2002). Microbial biosurfactants can be classified according to their chemical structure and microbial origin (Desai and Banat, 1997). The five major microbial biosurfactant classes are: lipopeptides, phospholipids, glycolipids, neutral lipids and polymeric compounds (Liu et al., 2015). Their molecular structure consists of a hydrophobic moiety and hydrophilic moiety to provide the amphipathic nature. Amino acids, peptides, mono-, oligo- or polysaccharides make up the hydrophilic moiety, whereas unsaturated, saturated, and/or hydroxylated fatty acids or fatty alcohols make up the hydrophobic moiety (Lang, 2002). The aliphatic structure of biosurfactants, made up of a hydrophilic and a hydrophobic moiety, shares the characteristics needed for collectors used in flotation systems. The wide variety of different biosurfactants provides a wide range of polar functional groups that show many similarities to commonly used synthetic collectors in flotation systems, and thus provides a potential avenue for research into their application in flotation systems.

2.5.1 Application of biosurfactants

Biosurfactants have several advantages over synthetic surfactants and show promise as replacements for these synthetic surfactants. Biosurfactants have been shown to have a higher degree of biodegradability, lower toxicity, and higher efficiency towards extreme temperature, salinity and pH compared to synthetic surfactants (Georgiou et al., 1992; Kretschmer et al., 1982; Mnif and Ghribi, 2015; Zajic et al., 1977). Therefore, the potential exists to replace synthetic surfactants with biosurfactant equivalents across a wide range of applications.

2.6 Surfactin

The biosurfactant that has piqued interest as a potential collector in coal desulphurisation is surfactin. This section will explore surfactin and why it shows promise as a potential collector of pyrite.

Surfactin, iturin and fengycin are the most well-known lipopeptides biosurfactants. They are produced by *Bacillus spp.* and are made up of a peptide cycle linked to a fatty acid. The structure divides lipopeptides into surfactin, iturin or fengycin families according to the number of amino acids and the length of the fatty acid chain (Lang, 2002; Rosenberg and Ron, 1999). Arima et al.(1968) are credited as the first to report and name surfactin, and Kakinuma et al.(1969) as the first to determine the chemical structure and amino acid sequence of surfactin. Thus, all the potential applications of surfactin have not yet been explored.

2.6.1 Production of surfactin:

Surfactin is produced by approximately 20 strains of *Bacillus subtilis* (Peypoux et al., 1999) and can be produced on an industrial scale using either a synthetic medium or agro-industrial residue medium. Using agro-industrial residues has the potential to reduce the cost of production. However, approximately 50% - 70% of the production costs are for the recovery and purification of surfactin from the culture medium. The use of ultra-filtration has shown potential as a purification method, due to not requiring any organic solvents, and subsequently reducing costs significantly (Zanotto et al., 2019). This indicates that it is possible to produce surfactin on an industrial scale on industrial waste streams, increasing the sustainability of surfactin, making it more attractive as a potential replacement for synthetic surfactants.

2.7 Structure and properties of surfactin

The structure of surfactin is important as it will determine if surfactin can be used as an effective collector in a froth flotation coal desulphurisation process. This section reviews the literature surrounding the structure of surfactin and the properties associated with that structure.

2.7.1 Structure of surfactin

Surfactin is a cyclic lipopeptide made up of a peptide chain consisting of seven α-amino acids bonded, with a lactone bond, to a hydroxyl fatty acid. The general amino acid sequence is: Glu^1 - Leu^2 - Leu^3 - Val^4 - Asp^5 - Leu^6 - Leu^7 (Liu et al., 2015). The typical structure of surfactin is shown in Figure 5. Natural surfactin is a mixture of isoforms. Differences occur in the hydroxy fatty acid chain length and branching, and by substitution of the amino acids of the peptide ring. These variations are largely determined by the specific *B. subtilis* strain and the environmental and nutritional conditions. Up to 44 analogues have been reported (Kowall et al., 1998). The amino acids that make up the peptide ring are of interest as they have carboxylic and amide functional groups that could interact with pyrite surfaces as well as aliphatic functional groups that may interact with hydrophobic coal surfaces.

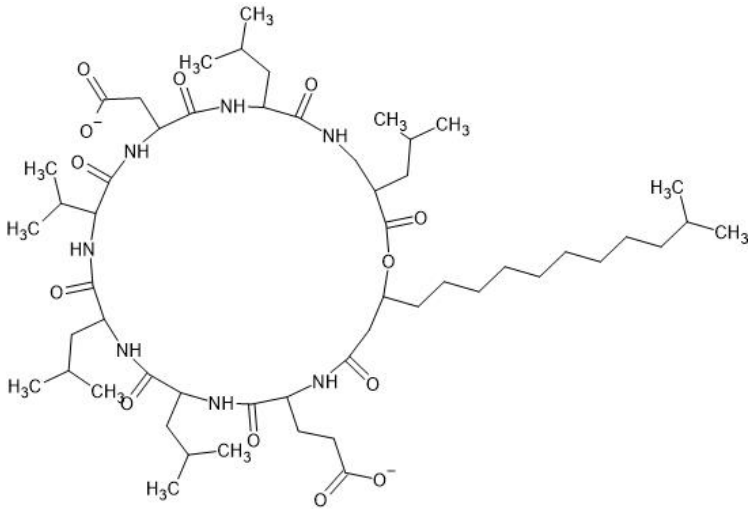

Figure 5: The chemical structure of a homologue of surfactin. Redrawn from (Liu et al., 2015) using ChemSketch.

It has been proposed that the peptide ring of surfactin has a saddle-shaped conformation. Because of this shape, the two anionic residues, Glu[1] and Asp[5], are on the same side of the molecule and form a polar "claw" structure (Kowall et al., 1998). These carboxylic groups that form the "claw" (Glu[1] and Asp[5]), together with the cyclic peptide backbone, form the hydrophilic moiety of the surfactin molecule. This "claw" hydrophilic moiety may allow surfactin to chelate metals, and potentially cause preferential adsorption onto pyrite in a coal desulphurisation system. The hydrophobic moiety is the long fatty acid chain and some lipophilic amino acids, namely: Leu[2], Leu[3], Val[4], Leu[6], Leu[7]. This results in a neutral hydrophobic molecule with a small negatively charged hydrophilic patch (Bonmatin et al., 1994; Liu et al., 2015; Tsan et al., 2007). The hydrophobic moiety will allow surfactin to effectively increase the hydrophobicity of the mineral it attaches to, allowing greater attachment to bubbles in a froth flotation process.

2.7.2 Effect of pH on the structure of surfactin

The pH plays an important role in flotation. Thus, the effect of pH on surfactin needs to be reviewed to understand how it will react to different pH conditions.

The pH of the subphase has an effect on the peptide ring of surfactin. More specifically, the Glu[1] and Asp[5] residues that make up the "claw". These residues have carboxylic groups with a pK_a of 5.4, above which they become ionised (Arutchelvi et al., 2014). Below this pK_a value, in most of the acidic pH range (3-5), the residues are protonated. In the alkaline pH range (8-9), the residues become fully ionised (Song et al., 2007). Thus above pH 5, more than 90% of surfactin in solution has a di-anionic form (Gang et al., 2015). The ionisation leads to an increased interaction between a surfactin molecule and water, making the surfactin molecule more hydrophilic. Subsequently protonation of the residues in the acidic pH range, causes the surfactin molecule to become more hydrophobic and reduce its solubility (Maget-Dana and Ptak, 1992; Shen et al., 2011). No matter the pH, surfactin keeps its compact ball-like structure (Shen et al., 2011). The ionisation of the surfactin molecule will allow it to electrostatically interact with mineral

surfaces. With respect to a flotation system, operating the flotation system in the alkaline pH may make surfactin a more effective collector due to the ionisation of the surfactin molecule.

Literature shows that at pH values higher than 9.5, the peptide ring is sometimes cleaved to form linear surfactin (Osman et al., 1998; Shen et al., 2011). A study by Knoblich et al.(1995), using Fourier transform infrared spectroscopy, suggests that formation of linear surfactin by opening of the lactone group is only at very high pH of 12-14. This would indicate that surfactin may act differently at high values, and that care should be taken when using surfactin to float at very high pH values.

At low pH values, of less than 5, surfactin starts to precipitate out of solution (Abdel-Mawgoud et al., 2008; Wei and Chu, 1998). To recover surfactin from culture broth, a pH of less than 3 is used for acid precipitation. (Arima et al., 1968; de Faria et al., 2011; Long et al., 2017). This indicates that below pH 5 surfactin starts to precipitate and is completely precipitated at pH 3. Thus, when using surfactin at low pH in a flotation process may be ineffective as surfactin forms a precipitate.

2.7.3 Effect of counter ions on surfactin

The ionisation of the Glu^1 and Asp^5 in the alkaline pH range, forms a bidentate group that could provide a potential binding site for divalent cations (Arutchelvi et al., 2014; Shen et al., 2011). Certain divalent cations such as Ca^{2+}, have been found to form a bridge between the ionised Glu^1 and Asp^5 residues, resulting in a surfactin-calcium 1:1 complex (Maget-Dana and Ptak, 1992) Thus, it is proposed that this shows that surfactin could have some chelating action (Bonmatin et al., 1994; Ferré et al., 1997). A Ca^{2+} bridge can also be formed between the acidic residues of adjacent surfactin molecules (Maget-Dana and Ptak, 1992).

The addition of an electrolyte to ionised surfactin in solution neutralises the Glu^1 and Asp^5 residues. The addition of divalent cations (Ca^{2+}) causes complete neutralisation, however, the addition of monovalent cations (K^+, Na^+) causes incomplete neutralisation. Neutralisation of the negative charges increases the hydrophobicity of surfactin (Maget-Dana and Ptak, 1992; Shen et al., 2011). Surfactin seems to have a higher affinity for divalent cations opposed to monovalent cations (Li et al., 2009; Thimon et al., 1992). Surfactin seems to prefer binding with counterions that have a smaller radius and a higher valence. There seems to be a higher counterion binding affinity for the Glu^1 carboxylic group. There also seems to be an affinity for the Glu^1 and Asp^5 carboxylic groups to each bind to a different counterion separately, rather than form a salt bridge. Thus, surfactin seems to prefer forming intermolecular salt bridges compared to intramolecular salt bridges (Gang et al., 2015).

The fact that surfactin interacts and chelates cations shows promise that this interaction will translate to the metal ions on the surface of pyrite, allowing surfactin to act as a collector for pyrite in a coal desulphurisation process using froth flotation.

2.7.4 Surfactin micelle formation and critical micelle concentration

When a surfactant is added to an interface in increasing concentrations, the surface tension is reduced up to a critical level, above which the attraction of the hydrophobic moieties of the surfactant molecules causes the monomers to form into supramolecular cluster-like structures called micelles. This critical level

is known as the critical micelle concentration (CMC) (Desai and Banat, 1997). Below the CMC, surfactant molecules exist as loose monomers (Mnif and Ghribi, 2015).

The CMC of surfactin is reported as 7.8 - 13 mg/L (Bognolo, 1999; Carrillo et al., 2003; Deleu et al., 1999; Heerklotz and Seelig, 2001; Ishigami et al., 1995; Sen and Swaminathan, 2005). The surfactin CMC value changes with the constituents (buffers and pH adjusting solutions used) and the pH of the solution (Knoblich et al., 1995). Surfactin forms core-shell type micelles. The micelle core is formed by the hydrocarbon tail and the four lipophilic leucine amino acids (Li et al., 2009). Surfactin micelles are formed by inter-micelle hydrogen bonding and either β-sheet or rod-like β-turn structures are formed (Bastrzyk et al., 2019; Ishigami et al., 1995). Micelles may form intermicellar aggregates via hydrogen bonds at larger concentrations (Jauregi et al., 2013). The pH and the addition of ions, has an effect on the size and shape of surfactin micelles (Li et al., 2009). Counterion concentration and pH has a big influence on the size and type of surfactin micelle formed.

The formation of micelles will allow surfactin to overcome electrostatic repulsive forces by forming micelles and intermicellar aggregates that have a stronger combined adsorption force, making adsorption onto mineral surfaces more effective.

2.7.5 Effect of pH on surfactin micelle formation

At a pH of 7.5, 8.5 and 9.5, surfactin in solution, forms spherical micelles. As the pH is decreased to 6.5 and 5.5, the number of lamellar micelles increase. As pH is increased from 5.5 to 9.5, the micelle shape changes from lamellar to rod-like to spherical micelles. Additionally, surfactin forms large unstable aggregates at neutral pH (Bonmatin et al., 1994) and at lower pH values (Shen et al., 2011). When the pH is decreased, the two carboxylate groups are neutralized, causing conformational changes, and a different aggregation of surfactin molecules. A surfactin solution at high pH, causes the formation of low aggregation number micellar structures. At low pH values, surfactin forms rod-like or lamellar micelles (Shen et al., 2011).

It is clear that surfactin micelles change as pH changes. This may affect how surfactin micelles adsorb onto minerals and has implications for flotation at higher surfactin concentrations above the critical micelle concentration.

2.7.6 Effect of counterions on surfactin micelle formation

The addition of monovalent and divalent cations favours the formation of surfactin micelles (Thimon et al., 1992). Thus, increasing the counterion concentration, decreases the CMC of surfactin (Li et al., 2009). This is due to the salting out effect. An increase in the aggregation number of micelles is seen with the addition of counterions (electrolytes) to the surfactin solution. This has been attributed to the charge screening effect, which is hypothesised to reduce the substantial surface area of the head groups in the micelles (Knoblich et al., 1995). The binding of counterions to the anionic residues of a surfactin molecule causes an electrostatic shielding effect, reducing the repulsive forces between surfactin monomers. This compresses the electrical double layer, allowing micelles to form at lower surfactin concentrations (Bastrzyk et al., 2019; Li et al., 2009).

The radius of micelles is larger in the presence of counterions. This is attributed to the counterions facilitating the formation of large aggregates and stabilising the β-sheet micelle conformation. This stabilisation is enhanced when surfactin molecules are fully ionised (Bastrzyk et al., 2019).

The addition of monovalent cations to a surfactin solution, causes the formation of low aggregation number micellar structures. The addition of divalent cations to a surfactin solution, causes the formation of rod-like or lamellar micelles (Shen et al., 2011).

Monovalent cations, of up to ten times surfactin concentration, have no effect on the bulk structure of surfactin micelles. The micelles remain spherical at pH 7.5, and there is no change in the aggregation number. Divalent ions, however, have a significant effect. The first thing noticed is that surfactin is nonselective when binding to monovalent cations, but more effective in binding Ba^{2+}, than Ca^{2+}. The addition of Ca^{2+} cations at a pH of 7.5, show a similar profile to surfactin micelles at pH 6.5. This suggests that the two negative charges of surfactin are neutralised by the addition of Ca^{2+}. Ba^{2+} has a stronger interaction with surfactin, probably due to its larger radius, and shows a stronger tendency to cause surfactin to form lamellar micelle structures (Shen et al., 2011).

In a coal desulphurisation flotation system, a vast number of potential counterions are present. As shown, counterions affect the concentration at which micelles form and the shape and size of surfactin micelles. This could have implications on the adsorption of surfactin and the formation of hemicelles and aggregate structures on the surface of minerals when using surfactin as a collector.

2.7.7 Surface and interfacial tension of surfactin in solution

The effect of surfactin on surface tension links to how the critical micelle concentration is determined (discussed in the Methods section) and can be used to verify the purity of surfactin by comparing literature to experimental values.

Surfactin is capable of decreasing the surface tension of water from 72 to 25 – 32.37 mN/m (Ishigami et al., 1995; Lang, 2002; Nitschke and Pastore, 2006; Rosenberg and Ron, 1999; Zdziennicka et al., 2018) and decreasing the interfacial tension between water and hexadecane from 43 to 0.97 – 1 mN/m (Lang, 2002; Nitschke and Pastore, 2006; Rosenberg and Ron, 1999). Surface tension remains fairly constant from pH 5 – 11, however below pH 5, the surface tension increases as pH decreases. This is due to the protonation of surfactin and the precipitation of surfactin (Nitschke and Pastore, 2006).

The strong effect of surfactin at the interfaces hints that surfactin will be very active at the mineral interfaces and thus if adsorbed, have a significant effect on the hydrophobicity of that mineral.

2.7.8 Surfactin and zeta potential

The zeta potential has been discussed previously as a method to determine if surfactant adsorption occurred and what type of adsorption mechanism is responsible. Literature on the effect of surfactin on zeta potential is limited. This section will discuss the available literature on the effect of surfactin on the zeta potential of minerals.

Didyk-Mucha et al.(2019) looked at the effect of surfactin on the zeta potential of serpentine, magnesite and silica. The addition of surfactin biosurfactant mixture caused a more negative zeta potential and shifted the iso-electric point (IEP) of serpentinite from pH 4.4 to 1.7. The adsorption is attributed to the interaction of anionic surfactin with positive ions on the metal lattice of the mineral surface. Magnesite is described as a sparingly soluble mineral salt. Partially dissolved mineral ions (Mg^{2+}, $MgOH^{+}$, $Mg(OH)_2$) determine the surface charge. Magnesite has a negative zeta potential across all pH values and no IEP. Addition of surfactin biosurfactant mixture, causes the zeta potential of magnesite to become slightly more negative. The addition of surfactin biosurfactant caused the zeta potential of silica to become more negative and causing the IEP to shift from pH 2.5 to no IEP (Didyk-Mucha et al., 2019).

This study indicates that surfactin interacts with metal ions on the serpentine and magnesite mineral surfaces. A parallel can be drawn to the surface of pyrite which indicate that surfactin has the potential to adsorb onto the surface of pyrite, allowing surfactin to perform as a collector in a flotation system. However, it was also shown that surfactin interacts with the surface of silica, which could mean that surfactin will interact with quartz in the coal fraction. It is unknown which mineral surfactin will prefer to interact with, and further research is needed in terms of the selectivity of surfactin in a coal desulphurisation system.

2.7.9 Surfactin interaction with mineral surfaces

Few people have studied the interaction between surfactin and mineral surfaces, although this is an important parameter for flotation.

Shen et al.(2011) showed that surfactin does not adsorb onto silica as silica carries a negative surface charge (negative when pH > 2), which repels the negatively charged surfactin. This is contrary to the results found in the zeta potential studies done by Didyk-Mucha et al.(2019) and would require further investigation to clarify. The Shen et al.(2011) study further indicated that there was strong, irreversible adsorption between surfactin and a hydrophobic perdeuterated octadecyl trichlorosilane (OTS) layer. This indicates that surfactin may preferably adsorb onto the hydrophobic surface of coal. Further studies are needed to determine if the hydrophobic adsorption translates to adsorption onto the surface of coal. Shen et al.(2011) concluded that surfactin adsorption is dominated by hydrophobic interactions, but electrostatic interaction partly plays a role. This could indicate that surfactin has a preference for hydrophobic surfaces, but would need further research to confirm.

Didyk-Mucha et al.(2019) tested the adsorption of a biosurfactant made up of mostly surfactin, onto mineral surfaces at pH 8. The adsorption of surfactin onto serpentinite was attributed to the electrostatic interactions between the positive metal cations on the mineral surface (Ni^{2+}, Mg^{2+}, Ca^{2+}, Al^{3+} and Fe^{3+}), and the negatively charged surfactin. The adsorption of surfactin onto magnesite was also attributed to the electrostatic interactions between the positive structural ions on the mineral surface (Ca^{2+}, Mg^{2+}, $MgHCO_3^{+}$), and the anionic surfactin, forming a surfactin salt. This research strongly suggests that surfactin should be able to adsorb onto the surface of pyrite and allow surfactin to act as a pyrite collector in a coal desulphurisation froth flotation process.

2.8 New application for surfactin

This literature review indicated that acid mine drainage (AMD) is a common problem with severe and lasting effects on the environment and health. The need to mitigate the formation of AMD is clear and is viable through the desulphurisation of coal tailings using froth flotation. However, the xanthate collectors currently used in the desulphurisation process are associated with their own set of negative impacts on the environmental and human health. Thus, the opportunity exists to replace these synthetic collectors with more environmentally friendly, less toxic and more sustainable microbial biosurfactants.

Surfactin has been identified as a candidate for the substitution of xanthate collectors in the coal desulphurisation process using froth flotation. Surfactin has the typical amphiphilic structure of a collector and has carboxylic and amide functional groups that show promise for the chelation of pyrite. There is a lack of research into the adsorption of surfactin onto mineral surfaces, but the research that exists indicates that surfactin shows promise in adsorbing onto pyrite, but also indicates potentially adsorbing onto coal. To determine if surfactin can be used as a desulphurisation agent, further research needs to be done.

The purpose of this project will be to investigate a novel application for surfactin, namely as a replacement for synthetic surfactant collectors in the desulphurisation of ultrafine coal tailings, to prevent acid mine drainage.

3 HYPOTHESIS, AIM AND OBJECTIVES

3.1 Hypothesis

Surfactin can be used as a replacement for synthetic surfactants, as a desulphurisation agent for coal tailings, because:

1. Surfactin as a molecule will behave as a collector, based on its structure.
2. Surfactin will preferentially chelate with pyrite, based on the positive charge of pyrite and the negative charges on surfactin functional groups.

3.2 Aim

Determine the effectiveness of surfactin as a collector in desulphurisation of coal through froth flotation of coal and pyrite as a mitigation strategy for the formation of acid mine drainage.

3.2.1 Objectives

The following objectives have been crafted as stepping stones to achieve the above aim.

1. Determine a surfactin concentration range for further experimentation.
2. Evaluate the effect of the coal and pyrite surface charge on the adsorption of surfactin.
3. Evaluate the attachment mechanism of surfactin to the surface of coal and pyrite.
4. Evaluate the effect of surfactin on the hydrophobicity of coal and pyrite.
5. Determine the potential desulphurisation operating conditions.

3.2.2 Key Questions

The key questions identified for each objective

1. At what surfactin concentration should coal and pyrite be floated?
2. Does surfactin attach to the surface of coal and pyrite?
3. To which coal and pyrite surface sites does surfactin attach?
4. Does surfactin float coal and pyrite?
5. Is it possible to separate coal and pyrite using surfactin as a collector?

4 METHODOLOGY

4.1 Experimental plan

The experimental plan centred around the aim, which is to determine if surfactin would be an effective collector in the desulphurisation of coal through froth flotation. In order to accomplish the aim, the interactions between surfactin and coal and the interactions between surfactin and pyrite needed to be understood, as no literature on these interactions were found. The aim has been broken down into the accompanying objectives which are interrogated using surface tension, zeta potential, FTIR and microflotation analyses to characterise the interactions between coal and surfactin, and pyrite and surfactin. These analytical methods, the accompanying objective, and the reasoning behind the method are expanded on in the Methods section (Section 4.3). The preparation of the coal, pyrite and surfactin used in this study, as well as the characterisation of those materials, is given in the Materials section (Section 4.2). Characterisation of the materials was done to aid the interpretation of the experimental results.

4.2 Materials

4.2.1 Sample preparation and characterisation

This section aims to provide clarity on the origin of materials, preparation methods and characterisation of the materials used.

4.2.1.1 Coal

A 1 kg sub-bituminous coal sample was obtained from the Emalahleni region of South Africa through the Department of Earth Science of Stellenbosch University.

a) *Coal sample preparation*

The whole 1 kg coal sample was sequentially processed through a jaw-crusher and a cone-crusher resulting in ± 0.5 cm particles. A small amount of the crushed coal sample was loaded into a swing mill pulveriser. The pulveriser makes use of hardened steel concentric rings and an orbital vibrating motion to pulverise samples. The coal sample was pulverised for 5 seconds. The pulverised sample was placed into a sieve shaker and sieved for 30 seconds using a 75 µm sieve. The +75 µm oversized material left was placed back into the pulveriser and pulverised for a further 3 seconds. This procedure was followed until ± 90% of the sample was passing -75 µm. The remaining oversized fraction was discarded. Short pulverising times were used to prevent an overly small size fraction from forming. This process was repeated until the whole original 1 kg coal sample was processed. The pulverised coal sample was split by way of a rotatory splitter into representative samples of ± 100 g. These 100 g coal samples were rotary split again into 3 g sample as needed. The rotary splitter makes use of a rotary motion to split a sample into 10 equal representative samples, which in theory are of equal size distribution and mineral composition. All the split coal samples were stored under nitrogen atmosphere, at 0 °C, in the presence of a desiccant (Silica gel) to prevent oxidation of the samples.

b) *Coal sample characterization*

The analyses that follow have been conducted in order to characterize the coal sample used in the experiments. This would assist in the interpretation of the results of the experiments.

Proximate analysis of coal sample

Proximate analysis is made up of a group of tests that provide the gross composition of the coal, making it popular for coal characterization in connection with coal usage. The tests are done by heating the coal sample under various temperature conditions and for variable amounts of time to determine the moisture, volatile matter, and ash content. The fixed carbon can then be determined from the mass balance difference. The calorific value is determined using the bomb calorimetric method. The proximate analysis was carried out by Bureau Veritas in Pretoria, South Africa. The testing standards used and the results of the proximate analysis done are provided in Table 1. The typical raw South African coal has an ash content of 25 – 35 % ash, 22 – 24 % volatile matter, and 44 – 50 % fixed carbon (Lloyd, 2000). When comparing typical raw coal with the coal sample, it is observed that the coal sample has a much lower ash content and a much higher fixed carbon content. This is due to the sample being hand-picked coal nuggets, where nuggets that showed ash mineral inclusions were avoided.

Table 1: The analyses that form part of the Proximate analysis with the corresponding testing standard used and result obtained.

Proximate analysis	Testing standard	Result
Moisture content (wt%)	ISO 11722: 1999	2.25
Volatile matter content (wt%)	ISO 562: 2010	20.65
Ash Content (wt%)	ISO 1171: 2010	14.15
Fixed carbon (wt%)	Calculated by difference	62.80
Calorific value (kJ/kg)	ISO 1928: 2009	27.53

Ultimate analysis of coal sample

To provide an indication of the major elemental composition of the coal sample, ultimate analysis was conducted by Bureau Veritas in Pretoria, South Africa. The coal sample is combusted in a furnace where infrared detection determines the weight percent carbon, hydrogen and sulphur, and thermal conductivity detection determines the weight percent nitrogen. The weight percentage oxygen can then be determined from the mass balance difference. The results of the ultimate analysis done is provided in Table 2 together with the corresponding testing standard.

Table 2: The analyses that form part of the Ultimate analysis with the corresponding testing standard used and result obtained.

Ultimate analysis	Testing standard	Result
Carbon content (wt%)	ISO 12902	70.80
Hydrogen content (wt%)	ISO 12902	3.53
Nitrogen content (wt%)	ISO 12902	1.80
Oxygen content (wt%)	Calculated by difference	6.13
Total sulphur (wt%)	ISO 19579: 2006	1.35

Form of sulphur analysis of coal sample

The form of sulphur analysis provides an indication of the of the types of sulphur present in the coal sample which aids the design and evaluation of coal desulphurisation operations. The form of sulphur analysis was carried out by Bureau Veritas in Pretoria, South Africa, using wet chemistry methods and results are given in Table 3.

Table 3: The analyses that form part of the form of sulfur analysis with the result obtained.

Form of sulphur analysis	Result
Pyritical sulphur (wt%)	0.72
Sulphatic sulphur (wt%)	0.01
Organic sulphur (wt%)	0.61

XRD analysis of coal sample

XRD analysis was used to determine the mineral groups that make up the coal forming ash fraction. Knowing the composition of the coal mineral matter would aid in the interpretation of the experimental results. XRD analysis was done on a prepared representative sample, thoroughly mixed and split using a rotary sampler to obtain relevant sample size for XRD analysis, by XRD Analytical and Consulting cc in Pretoria, South Africa, and the results are presented in Table 4. The material was prepared for XRD analysis using a back loading preparation method. Diffractograms were obtained using a Malvern Panalytical Aeris diffractometer with PIXcel detector and fixed slits with Fe filtered Co-Kα radiation. The phases were identified using X'Pert Highscore plus software. The relative phase amounts (weight %) were estimated using the Rietveld method. The diffractograms are provided in Appendix A.

Table 4: XRD analysis of the coal sample, indicating the mineral group and respective weight percentage of the coal ash fraction.

Mineral Group	Weight percentage (%)
Pyrite	2.9
Kaolinite	24.7
Calcite	4.4
Dolomite	2.6
Astrophyllite	2.2
Quartz	1.3
Carbon	61.9

Particle size distribution of coal sample

The particle size distribution (PSD) of a 3 g representative coal sample was determined using a Micromeritics Saturn DigiSizer 5200 and distilled water as a carrier. The PSD is determined by laser diffraction and the Mie theory for data processing. The PSD analysis was done by the analytical facility at the Department of Process Engineering of Stellenbosch University. The particle size distribution of a representative coal sample is provided in Figure 6. The P_{80} value, the size where 80% of particles pass and which was determined graphically, is approximately 44 μm, with 95% passing -75 μm. The PSD follows the conventional sigmoidal curve. The P_{80} value is as expected due to the sample preparation aiming for -75 μm, which has been achieved as 95% passes 75 μm.

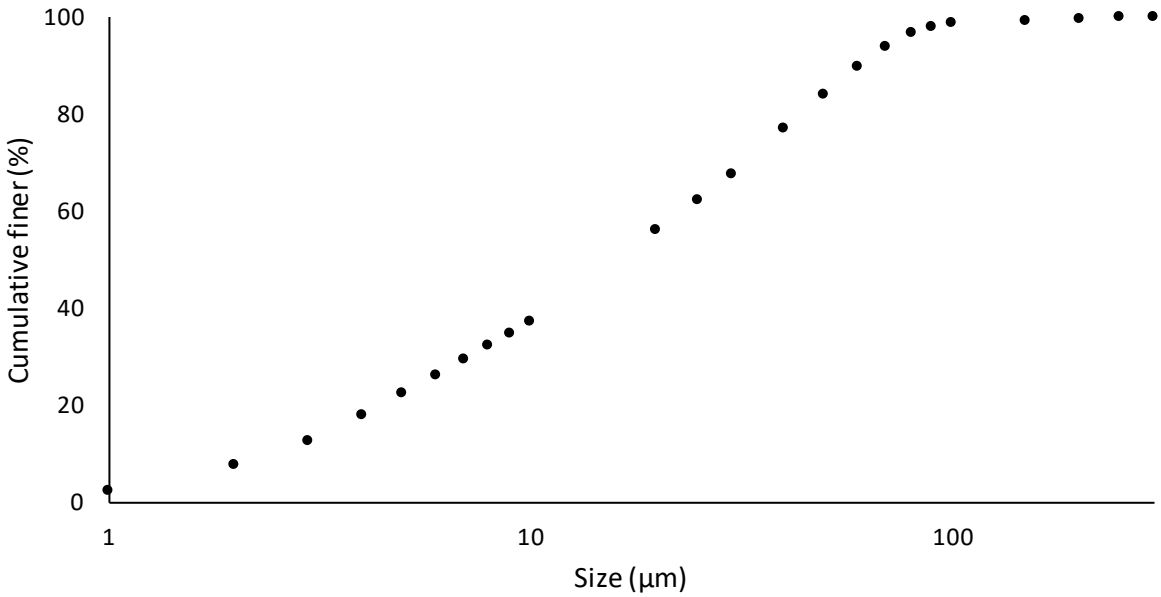

Figure 6: Particle size distribution of a representative coal sample used in the experiments.

4.2.1.2 Pyrite

A 1 kg high grade pyrite crystal sample was obtained through Ward's Science from Huanzala, Peru.

a) *Pyrite sample preparation*

The 1 kg sample pyrite was crushed using a hammer to ± 2 cm samples. These ± 2 cm samples were stored under nitrogen atmosphere, at 0 °C, in the presence of a desiccant (Silica gel). Pyrite samples were prepared as needed by weighing the appropriate amount from the ± 2cm samples. This weighed sample was then crushed using a hammer to 100% passing 0.5 cm. The crushed sample was loaded into a swing mill pulveriser. The pulveriser makes use of hardened steel concentric rings and an orbital vibrating motion to pulverise samples. The sample was pulverised for 5 seconds. The pulverised sample was placed into a sieve shaker and sieved for 30 seconds using a 75 µm sieve. The +75 µm oversized material left was placed back into the pulveriser and pulverised for a further 3 seconds. This procedure was followed until ± 90% of the sample was passing -75 µm. The remaining oversized fraction was discarded. Short pulverising times were used to prevent a disproportionately overly small size fraction from forming. The pulverised pyrite sample was split by way of a rotatory splitter into representative samples of 3 g. The rotary splitter makes use of a rotary motion to split a sample into 10 equal representative samples, which in theory, are of equal size distribution and mineral composition. The split samples were stored under nitrogen atmosphere, at 0 °C, in the presence of a desiccant (Silica gel) to prevent oxidation of the samples. Any remaining prepared pyrite samples that were not used after 72 hours were discarded, as it was deemed, that even though every precaution was taken to prevent oxidation of the pyrite, the likelihood of some oxidation was high after 72 hours.

b) *Pyrite sample characterization*

The analyses that follow have been conducted in order to characterize the pyrite sample used in the experiments. This would assist in the interpretation of the results of the experiments.

XRD analysis of pyrite sample

To determine the purity of the pyrite sample, XRD analysis was done on a prepared representative sample by XRD Analytical and Consulting cc in Pretoria, South Africa. The results are presented in Table 5. Due to the high grade of the sample, repeats were not done and the results were judged to sufficiently represent the whole pyrite sample. The material was prepared for XRD analysis using a back loading preparation method. Diffractograms were obtained using a Malvern Panalytical Aeris diffractometer with PIXcel detector and fixed slits with Fe filtered Co-Kα radiation. The phases were identified using X'Pert Highscore plus software. The relative phase amounts (weight %) were estimated using the Rietveld method. The diffractograms are provided in Appendix A. It can be observed from the results that the pyrite sample had a high purity and there were no significant additional mineral groups that would influence any of the experimental results.

Table 5: XRD analysis of the pyrite sample, indicating the mineral groups and the respective weight percentages.

Mineral Group	Weight percentage (%)
Pyrite	99.3
Anhydrite	0.7

Particle size distribution of pyrite sample

The particle size distribution (PSD) of a 3 g representative pyrite sample was determined using a Micromeritics Saturn DigiSizer 5200. The PSD is determined by laser diffraction and the Mie theory for data processing. The PSD analysis was done by the analytical facility at the Department of Process Engineering of Stellenbosch University. The particle size distribution of a representative pyrite sample is provided in Figure 7. The P_{80} value, which is determined graphically, is approximately 55 μm, with 91% passing -75 μm. The PSD follows the conventional sigmoidal curve. The P_{80} value is as expected due to the sample preparation aiming for -75 μm, which has been achieved as 91% passes 75 μm.

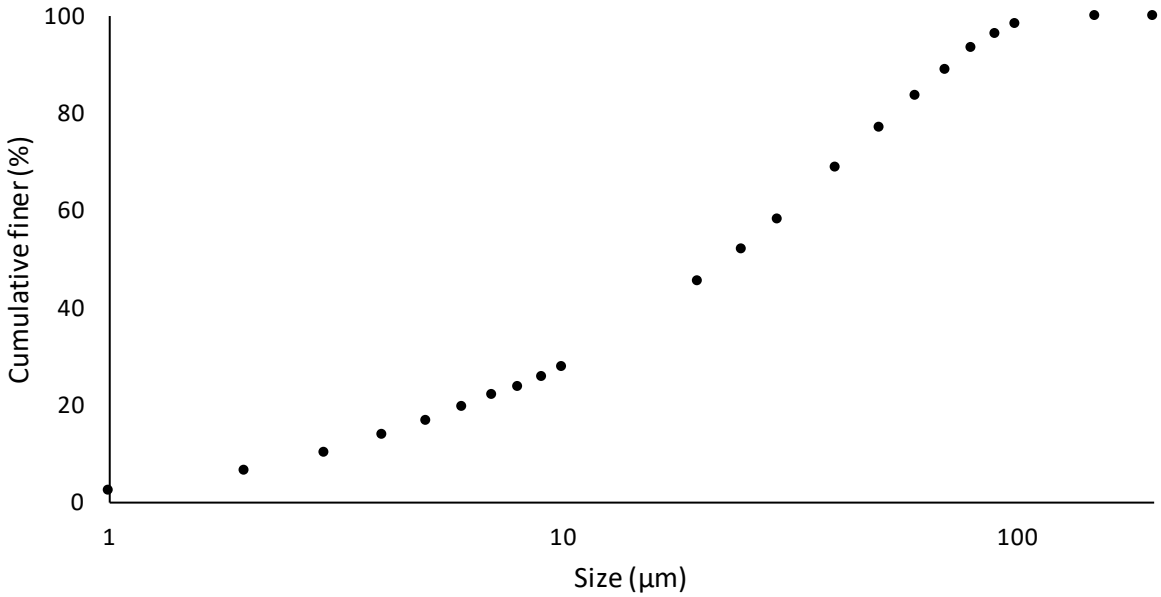

Figure 7: Particle size distribution of a representative pyrite sample used in the experiments.

4.2.1.3 Surfactin lipopeptide

A 100 g, extra pure grade sodium surfactin sample was obtained from Kaneka Corporation, Japan. The surfactin had a documented purity of more than 90 %, with moisture content making up the difference.

a) *Surfactin sample characterization*

High performance liquid chromatography

High performance liquid chromatography (HPLC) analysis was used to determine the purity of the surfactin sample. The surfactin sample was tested against a surfactin standard obtained from Merck.

Surfactin samples were prepared at 150 mg/L surfactin concentration, by mixing 15 mg surfactin with 100 mL of demineralized water. 500 µL of the surfactin sample was mixed with 500 µL of acetonitrile and filtered using a 0.22 µm syringe filter before being injected into the HPLC column. The HPLC specifications used are given in Table 6. Duplicate repeats were performed.

It was found that the surfactin sample has a purity of 79% compared to the reference standard. The purity difference between the HPLC purity result and the documented sample purity was attributed to additional moisture content, as no evidence of lipopeptide contamination was seen. To verify that there was no lipopeptide contamination, the surfactin sample was analysed using liquid chromatography-mass spectroscopy, which is discussed in the following section.

Table 6: HPLC specification used to determine the surfactin sample purity.

HPLC specifications	
Column	Phenomenex Luna 3µm C18 column (250 x 4.6 mm)
Detector	Dionex Ultimate 3000 Diode array detector
Mobile Phase A	0.05% (v/v) Trifluoroacetic acid (Fluka®) in water
Mobile Phase B	0.05% (v/v) Trifluoroacetic acid in acetonitrile (High purity UV grade, Burdick and Jackson)
Mobile Phase Gradient	Start at 35% B, increase to 40% B during the next 2 minutes, isocratic at 40% B for the next 5 minutes, increase to 63% B during the next 43 minutes, increase to 80% B during the next 10 minutes, increase to 87% B during the next 35 minutes, return to 35% B during the next 10 minutes and isocratic stabilisation at 35% B for the next 5 minutes.
Flow rate	0.9 ml/min
Absorbance	210 nm

Liquid chromatography-mass spectroscopy

Liquid chromatography-mass spectroscopy (LC-MS) was used to determine the composition of the surfactin lipopeptide mixture and establish if the sample contains any other lipopeptides such as iturins or fengycins. As the study focuses on the use of surfactin, contamination by other lipopeptides would require further purification of the surfactin sample. The LC-MS analysis was conducted by the Central analytical facility of Stellenbosch University. The LC-MS specifications used for the lipopeptide analysis are given in Table 7.

Table 7: LC -MS specifications for lipopeptide composition analysis.

Column	Waters BEH C18, 2.1x100mm, 1.7um.
Detector	Waters Synapt G2, ESI probe, ESI Pos, Cone Voltage 15 V
Mobile phase A	0.1% formic acid in water
Mobile phase B	0.1% formic acid in acetonitrile
Mobile phase gradient	Start at 40% B, increase to 95% B after 11 min, decrease to 40 % B after 5 min, keep stable at 40% B for 2 min.
Flow rate	0.3 mL/min

The LC-MS analysis results are given in Figure 8. It can be seen that the only peaks detected were peaks associated with C_{13} , C_{14} and C_{15} surfactin homologues (Pecci et al., 2010). Thus, the surfactin sample does not contain any other lipopeptide contamination and further purification of the surfactin sample is not needed.

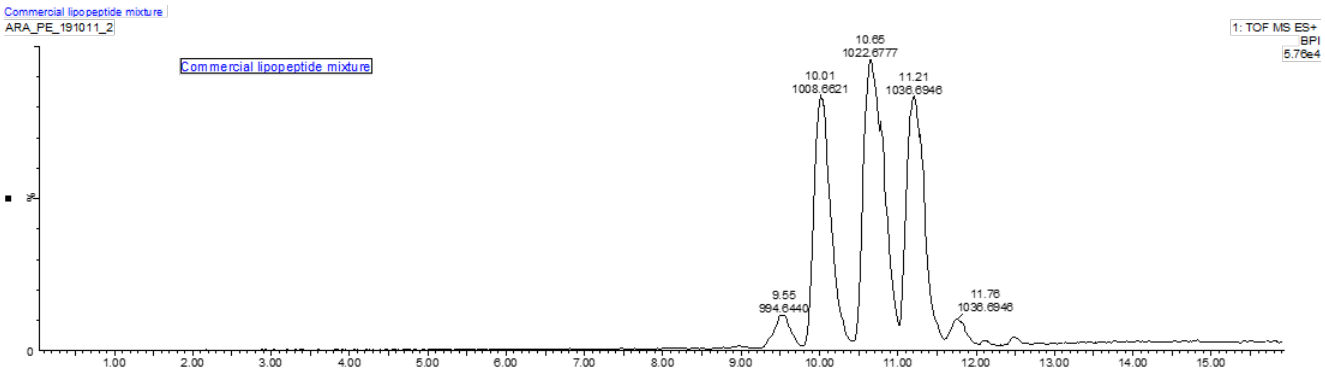

Figure 8: LC-MS chromatogram for the surfactin sample.

b) *Surfactin stock solution preparation*

A fresh surfactin stock solution was prepared weekly to be used in that week's experimentation. A 100 mg/L surfactin stock solution was prepared using 127 mg surfactin sample (considering 79% purity of the surfactin sample) into 1000 mL of demineralised water. The resulting surfactin stock solution had a surfactin concentration of 100 mg/L. The surfactin stock solution was stored at 4 °C and any unused surfactin stock solution was discarded at the end of the week.

4.3 Methods

4.3.1 Surfactin surface activity and critical micelle concentration

The first objective of this study was to determine a practical surfactin concentration range for further experimentation. Due to the novel use of surfactin in the flotation of coal and pyrite, no literature exists on the surfactin concentration ranges that should be used for flotation of coal or pyrite. To determine a starting range, the concentration at which surfactin starts to form micelles was used as an indication. The concentration at which surfactin forms micelles, called the critical micelle concentration (CMC), can be indirectly determined from the surface tension of water at various surfactin concentrations. The

following sections will clarify the methodology used to determine the surface tension of water at various surfactin concentrations and the process of determining the surfactin CMC from the surface tension results.

4.3.1.1 Surface tension

The surface tension was measured using a KSV Sigma 702 Tensiometer employing the du Noüy ring methodology (Bodour and Miller-Maier, 1998). The du Noüy ring methodology measures the surface tension as follows: first a platinum ring is brought into contact with and submerged in the liquid that is being tested (which can be seen in Figure 9 #1-2). The ring is then slowly lifted up, forming a meniscus between the ring and the liquid (the meniscus formation can be seen in Figure 9 # 3). This meniscus exerts a pulling force on the ring that is measured with an electronic balance attached to the ring. As the ring is pulled further, the pulling force from the meniscus becomes larger until a maximum force is reached. Thereafter the meniscus volume drops and eventually the meniscus tears and contact between the ring and the liquid is broken. The maximum force exerted, the characteristics of the ring (weight and radius) and a correction factor are used to determine the surface tension, which is calculated automatically by the tensiometer. For this study the Huh-Mason correction was used as it covers a wide range of liquids.

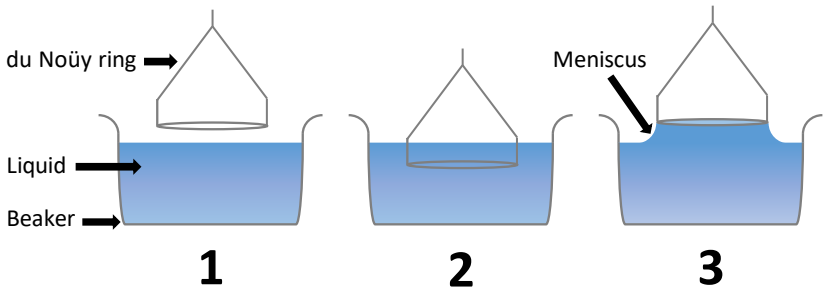

Figure 9: Graphical illustration of the du Noüy ring methodology. #1 shows the ring before contact with the liquid. #2 shows the ring after being submerged in the liquid. #3 shows the formation of the meniscus between the ring and the liquid as the ring is lifted.

a) *Tensiometer validation*

Now that the du Noüy ring methodology is clear, the tensiometer measurements need to be validated to ensure accurate measurements. This is done by measuring the surface tension of known pure liquids and comparing the results to literature. For this validation, a high surface tension liquid, namely distilled water, and a low surface tension liquid, namely methanol, were used. The results for the validation experiments are presented in Table 8, for an ambient temperature of 23 °C. The literature surface tension values of distilled water and methanol at 20 °C are 72.75 mN/m^{-1} and 22.95 mN/m^{-1} respectively (Vazquez et al., 1995). The experimental values are relatively similar to the literature value and thus the tensiometer and the methodology are validated.

Table 8: The surface tension of distilled water and methanol at an ambient temperature of 20 °C.

Water (H_20)	Surface Tension (mNm^{-1})		Methanol (CH_3OH)	Surface Tension (mNm^{-1})
1	72.67		1	22.39
2	72.72		2	22.38
3	72.47		3	22.38
Average	**72.62**		**Average**	**22.38**
Standard deviation	**0.13**		**Standard deviation**	**0.01**

b) *Procedure to determine the surface tension of water in the presence of surfactin*

To establish a surface tension versus surfactin concentration curve, needed to determine the critical micelle concentration, the surface tension of surfactin dilutions at regular surfactin concentration intervals needed to be determined.

The surfactin stock solution was prepared as described in the Materials section (section 4.2.1.3). The surfactin stock solution and demineralized water was used to make a series of surfactin dilutions, from 0 - 100 mg/L, in increments of 10 mg/L (0, 10, 20, 30, 40, 50, 60, 70, 80, 90, 100 mg/L). Repeats were also prepared for the 0, 10, 40, 60 and 90 mg/L dilutions in order to have triplicate repeats at these dilutions. Repeats of approximately every second surfactin dilution was deemed sufficient to provide a measure of the variability. The same procedure was followed for the next batch of surfactin dilutions from 0 – 10 mg/L, at 1 mg/L intervals (0, 1, 2, 3, 4, 5, 6, 7, 8, 9, 10 mg/L). Repeats were done for 1, 4, 6 and 9 mg/L surfactin dilutions. Lastly, to provide a more complete curve, surfactin dilutions from 1.5 - 4.5 mg/L at 1 mg/L intervals (1.5, 2.5, 3, 3.5, 4.5) were prepared using the same dilution preparation procedure as described for the other surfactin dilutions. Dilutions were prepared without any pH buffers and no attempt was made to adjust the pH value. The reason for this was discussed in detail in the results section (section 5.1). The pH of the surfactin dilutions were 6.2.

Before starting each batch of measurements, the tensiometer was calibrated using a calibration weight. After calibration and before each subsequent measurement, the sample cup was rinsed 3 times using demineralised water and then 3 times using acetone, before leaving to dry. The same rinsing procedure was used for the platinum ring. Additionally, the platinum ring was flamed to redness using a Bunsen burner, to remove any impurities stuck to the ring, and left to cool. After the cleaning procedure, 30 mL of the surfactin dilution which is to be tested, is placed into a newly cleaned 50 mL sample cup 50 mL (tensiometer specific sample cup) and placed onto the tensiometer platform. The platinum ring was attached to the tensiometer and the automatic surface tension measuring sequence was initiated. The platinum wire ring is submerged into the solution and slowly pulled through the air-liquid interface. The resistance encountered by the ring as it is pulled through the air-liquid interface is measured by the tensiometer. From the measured resistance force, the tensiometer automatically calculates the surface tension and displays it. After the measurement, the sample was discarded and the sample cup and ring were cleaned using the previously described method. The next surfactin dilution is placed into the sample cup and the testing procedure is repeated.

4.3.1.2 Critical micelle concentration

After determining the surface tension for various surfactin dilutions, the surfactin sample critical micelle concentration (CMC) can be determined. The concentration at which surfactin in solution starts to form micelles, the CMC, was used as a starting point to determine a surfactin concentration range for the experiments to follow.

To determine the CMC, a graphical method was used, as used in previous studies with biosurfactants (Abdel-Mawgoud et al., 2008; Khoshdast et al., 2011). The CMC procedure firstly required plotting the surface tension values against surfactin concentration as seen in Figure 10: A. Then a horizontal line was fitted, using the "LINEST" Microsoft Excel 2016 function, to the minimum surface tension value achieved within the dilution series as shown by the blue dotted line in Figure 10: B. This line was called the concentration-independent line, as this was the minimum surface tension a surfactin dilution could reach, no matter how much the surfactin concentration was increased, essentially making the surface tension independent of surfactin concentration. The third step was using the "LINEST" Microsoft Excel 2016 function to fit a second line to the steepest part of the surface tension vs surfactin concentration plot as show by the red dashed line in Figure 10: C. This line is called the concentration-dependent line as it describes the area in which the surface tension of the surfactin dilution is most dependent on the surfactin concentration. When extrapolated, these two lines intersect, as shown by the red circle in Figure 10: D. The intersection point of the concentration-dependent and concentration-independent lines, is at a certain surfactin concentration, and this concentration is known as the CMC value of the surfactin sample.

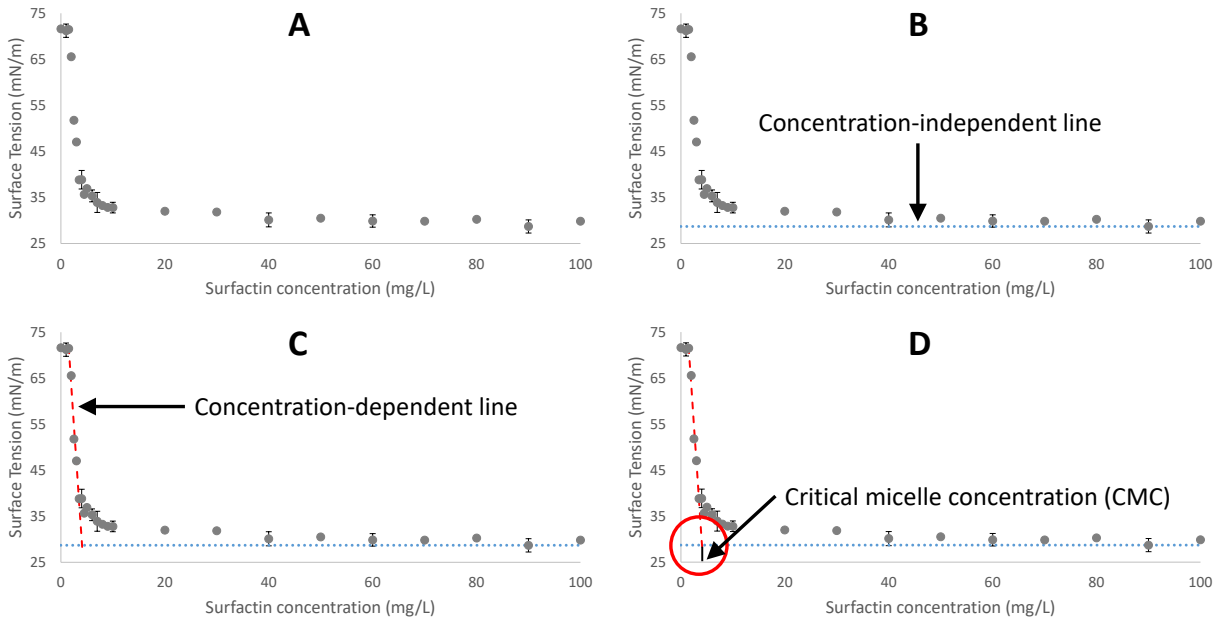

Figure 10: Sequential demonstration of the steps used to determine the critical micelle concentration of surfactin using the tangent method.

4.3.2 Zeta potential analysis

Zeta potential analysis was conducted in order to evaluate the effect of the coal and pyrite surface charge on the adsorption of surfactin. This would indicate if surfactin adsorbed onto the surface of coal or pyrite and provide a greater understanding of the mechanisms involved in the adsorption. The surfactin concentrations 2, 4 and 15 mg/L were used as these values would provide zeta potential data below, at and above the CMC value.

A Malvern Zetasizer Nano-ZS90 was used for the zeta potential analysis. This machine applies an electric field to the sample solution and uses laser Doppler electrophoresis to measures the velocity of the particles in response to the electric field. The speed of movement is the converted to zeta potential using the Smoluchowski's equation.

The volumes and concentrations needed to prepare a sample for zeta potential analysis is dependent on the desired surfactin concentration. The respective volumes and concentrations needed for each desired surfactin concentration are given in Table 9. Preparation of the 15 mg/L surfactin concentration sample will be used as an example. A 1 L NaCl electrolyte solution was prepared by mixing 69 mg of NaCl with 1 L of demineralized water. The molarity of the prepared NaCl solution is higher than 0.001 M to compensate for the surfactin solution addition. The final sample before zeta potential testing will have a 0.001 M NaCl concentration. A 100 mg/L surfactin stock solution is prepared as described earlier in the Materials section (section 4.2.1.3). The NaCl electrolyte solution is adjusted to the desired pH of 2, 3, 4, 5, 6 ,7, 8, 9 or 10 respectively, using hydrochloric acid or sodium hydroxide solution, and 8.5 mL of the NaCl solution at each pH is placed into a 15 mL centrifuge tube (volume of NaCl solution would be different for the other desired surfactin concentrations). The actual pH of the NaCl electrolyte solution was overshot or undershot to account for the pH change when coal or pyrite was added. For example, to achieve a pH of 6 after the addition of pyrite, the pH of the NaCl electrolyte solution needed to be 5.4 before pyrite addition. The amount of overshoot or undershoot was determined by trial and error in earlier scoping experiments. Once the nine different, 10 mL samples, each at the appropriate pH value needed, were prepared, 100 mg of either coal or pyrite was added to each of the samples. The samples were each capped and mixed and the pH measured, and if needed, the pH corrected. To each sample, 1.5 mL of surfactin stock solution was added (other desired surfactin concentrations would need a different volume of surfactin stock solution as shown in Table 9). Each sample was capped and vigorously shaken for 10 seconds. Before each sample was tested, the sample was lightly shaken and the pH confirmed to be within 0.1 of the desired value. The sample was then allowed to settle for 2 min. After settling, the upper portion of supernatant was drawn off with a syringe (as to only include fine particles, as particles should not be settling as well as moving due to electrophoretic mobility) and transferred to a zetasizer cell. The zetasizer cell was in turn transferred to the zetasizer and tested. Each sample was measured 3 times, with each measurement being tested 10 - 100 times, depending on the deviation (determined automatically by the machine). After testing the sample was discarded. The same procedure was used for each of the desired

surfactin concentrations for both coal and pyrite. Two independent duplicate repeats of each measurement were done to determine variability.

Table 9: Concentrations and volumes of solutions needed for each zeta potential sample

Desired sample surfactin concentration (mg/L)	0	2	4	15
Volume surfactin stock solution needed (ml)	0	0.2	0.4	1.5
Volume electrolyte solution needed (ml)	10	9.8	9.6	8.5
Concentration of electrolyte solution (M)	0.001	0.00102	0.001042	0.001176
Mass NaCl (mg)	58	60	61	69

4.3.3 Fourier Transform Infrared (FTIR) Spectroscopy analysis – Surfactin adsorption onto the mineral surface

First, zeta potential indicates whether surfactin adsorption took place and what type of adsorption is most likely responsible. Subsequently, Fourier Transform Infrared Spectroscopy (FTIR) analysis would provide confirmation of surfactin adsorption and provide greater insight into the adsorption/attachment mechanism by indicating with which coal or pyrite surface functional groups surfactin interacts. As a result, FTIR analysis was used to meet the objective to evaluate the attachment mechanism of surfactin to the surface of coal and pyrite.

FTIR analysis was done using a Thermo Scientific Nicolet iS10 6700 spectrometer using a deuterated triglycine sulfate detector (DTGS/KBr) and equipped with an Attenuated Total Reflection (ATR) attachment with a diamond crystal plate. Samples spectra were recorded over the 4000 – 650 cm^{-1} spectral range at 8 cm^{-1} spectral resolution, taking 64 scans per sample/background recording. Spectral data was recorded and processed using Thermos Scientific OMNIC 9.2 computer software. Automatic baseline correction was used to correct for atmospheric H_2O and CO_2.

Samples were prepared by mixing 3 g pyrite or coal sample (coal or pyrite sample preparation described in the Materials section) with the appropriate volume demineralized water. The volume of demineralized water needed at each desired surfactin concentration is given in Table 10. The pH of the mixture was adjusted to pH 3, 6, 8 or 10 using dilute HCl or NaOH solutions and allowed to stabilize over a 10 min period. After stabilization, the relevant amount of a 100 mg/L surfactin stock solution (prepared as discussed in the material section) was added to the pH adjusted mixture to achieve the desired surfactin concentration. Surfactin concentrations of 0, 5 and 15 mg/L were used and the volume of surfactin stock solution needed to achieve these desired surfactin concentrations are given in Table 10. The final 360 mL mixture, after the addition of surfactin stock solution, was conditioned for 10 min using a magnetic stirrer-bar and -plate, keeping the pH within ±0.1 of the desired pH value. Thereafter, the sample was vacuum filtered using a Büchner funnel and filter paper, and dried overnight in an oven at 60 °C. Experiments were conducted at pH 3, 6, 8 and 10 for 0, 5 and 15 mg/L surfactin concentration, using the sample procedure, and repeated independently in duplicate to quantify variability.

Table 10: Volume demineralized water and surfactin stock solution used for the FTIR sample preparation.

Desired surfactin concentration (mg/L)	0	5	15
Volume demineralized water (mL)	360	342	306
Volume surfactin stock solution (mL)	0	18	54

The FTIR Spectroscopy analysis was conducted on the dried, powdered mineral samples. A small amount of sample was added to the crystal plate of the FTIR machine, enough to completely cover the crystal. The ATR attachment was tightened and the spectrum collection was initiated on the FTIR machine. Once the sample spectrum was collected, the sample was discarded and the crystal cleaned with ethanol before the next sample was analysed.

4.3.4 Microflotation – Mineral recovery and kinetics

Microflotation analysis had two goals. The first was to analyse the total recovery of either coal or pyrite in the presence or absence of surfactin achieved by microflotation, and the second was to evaluate the flotation kinetics during the same microflotation. The aim of microflotation analysis was to meet the objective to evaluate the effect of surfactin on the hydrophobicity of coal and pyrite. Analysing various pH and surfactin conditions would also contribute to the final objective of determining the potential desulphurisation operating conditions.

4.3.4.1 Microflotation cell

To conduct microflotation analysis, a microflotation cell setup was used. The setup used is illustrated in Figure 11. Compressed air from a compressed air cylinder is fed into a pressure stabilization burette setup. This pressure stabilization burette system stabilizes the air pressure and indicates when a stable pressure has been reached. From the pressure stabilization burette system air flows to a micro-syringe with a 100 µl SGE™ needle. Using the left most burettes, the air flowrate through the needle can be measured. The air flowrate is measured by partially filling the burettes with water and inserting the needle into the indicated needle port for testing the air flowrate. When the valve on one of the burettes is closed, the bubbles from the needle displace water downwards and into the adjoining burette. The volumetric air flowrate can then be determined from the volume of displaced water and the time taken to displace that water volume. The air flowrate can then be adjusted using the two needle values. The micro-syringe needle is then transferred to the microflotation cell. The microflotation cell has a volume of 360 mL. A peristaltic pump is used to recirculate the pulp. A pH probe is connected to the recirculation line to allow the pH of the pulp to be monitored. The operation of the microflotation cell is discussed in more detail below.

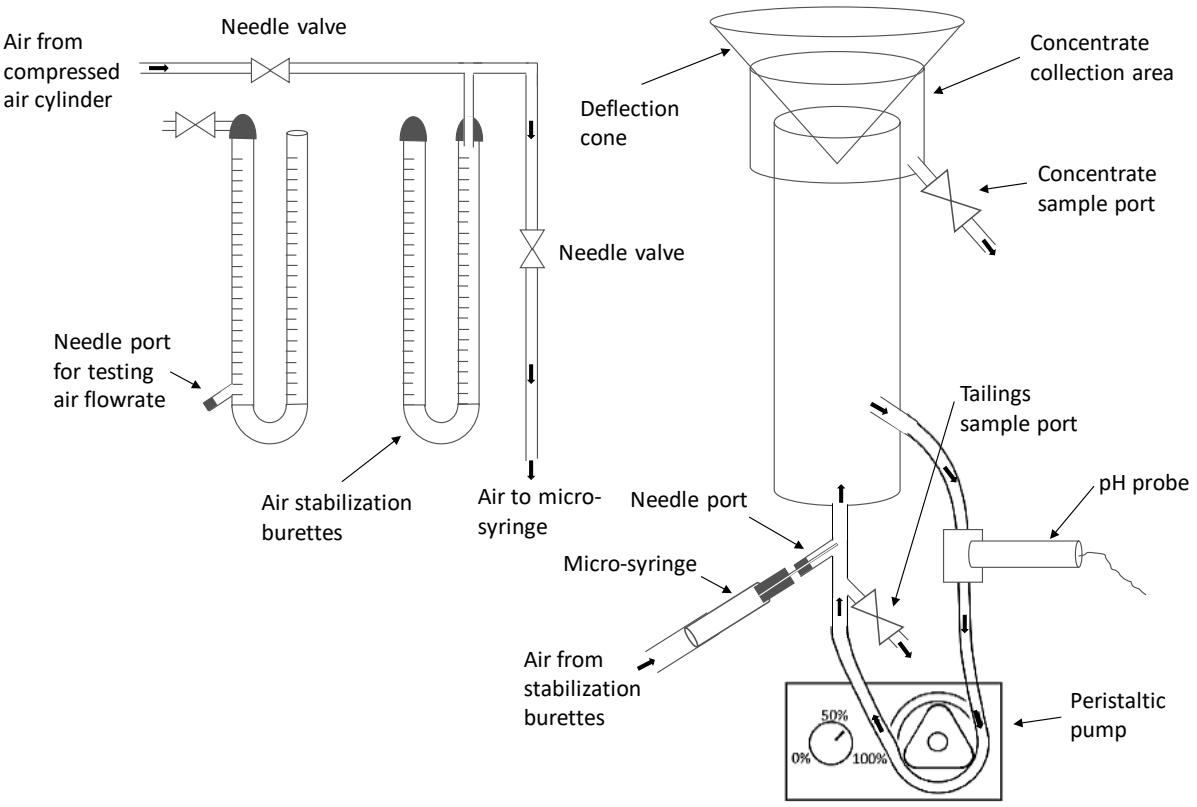

Figure 11: Illustration of the microflotation cell setup used for experimentation. It is made up of a set of air flowrate testing burettes, a set of air pressure stabilization burettes, a micro-syringe needle, the microflotation cell, the deflection cone, a peristaltic pump and a pH probe connected to the recirculation line.

The microflotation cell is filled with the mineral mixture to be floated. The peristaltic pump is turned on and set to the recirculation speed required and the pulp is recirculated. The micro-syringe needle is inserted into the needle port as indicated by #1 in Figure 12. Bubbles float upwards from the needle and enter the microflotation cell at #2. Mineral attachment to the bubbles, if likely, happens mostly in the first half of the cell between #1 and #3. Bubbles, with or without mineral attachment then rise to the deflector cone at #4 and are deflected to the side of the collection cup at #5. At #5 the bubble pops and the attached mineral falls down into the collection cup at #6. The collected mineral can then be recovered through the concentrate sample port. Once flotation is complete, the microflotation cell is drained and the tailings are collected through the tailings sample port.

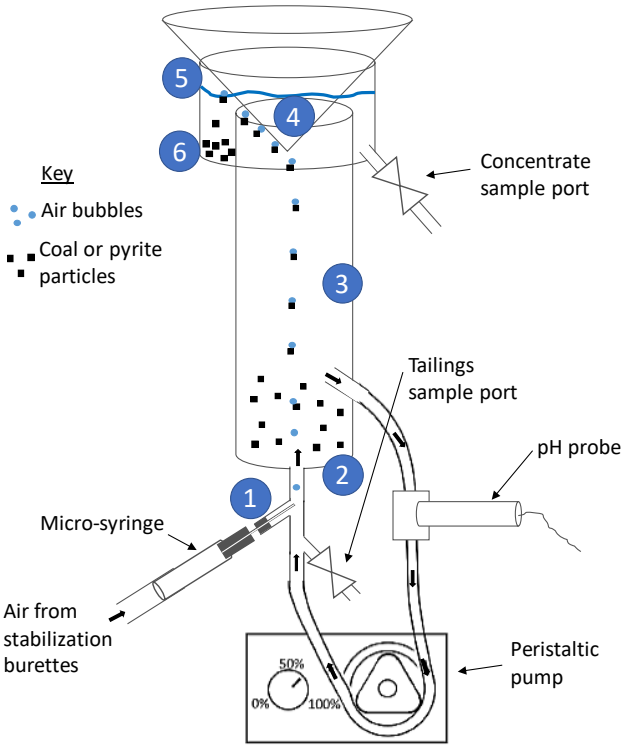

Figure 12: Illustration of the bubble and mineral path during microflotation.

4.3.4.2 Microflotation procedure for the total mineral recovery

A 100 mg/L surfactin stock solution was prepared as described in the Materials section (section 4.2.1.3). Coal or pyrite samples were prepare as described in the Materials section (section 4.2.1.1 for coal and section 4.2.1.2 for pyrite). Enough filter paper for each sample, that was dried in an oven at 60 °C overnight, was weighed.

The compressed air valve was opened and the pressure allowed to stabilize. Afterwards the air flowrate was verified to be 10 mL/min and adjusted if necessary, as described previously. 3 g coal or pyrite sample was added to 300 mL of demineralized water in a beaker. The pH was adjusted to the desired value (pH 3, 6 ,8 or 10) and allowed to stabilize for 10 min. After pH stabilization, the appropriate amount of surfactin stock solution was added to achieve a surfactin concentration of 0, 5 or 15 mg/L and the mixture was conditioned for 10 min using a magnetic stirrer-bar and plate, keeping the pH within ±0.1 of the desired pH value. After conditioning, the mixture was added to the microflotation cell and the peristaltic recirculation pump speed was set to 50% which equals 300 mL/min. Finally, the microflotation cell was topped up with demineralized water at the same pH as the mixture and the deflection cone place on top of the column. The micro-syringe needle was inserted into the needle port and the timer started.

Concentrate samples were taken at 2, 6, 12, and 20 min from the start of the experiment (when the micro-syringe needle was inserted into the needle port). When a concentrate sample was taken, the needle was removed, stopping the air flowrate. The concentrate sample valve was opened and the concentrate collection cup was washed out. The concentrate sample valve was then closed and the collection cup refilled with demineralized water at the same pH of the pulp. If the pH needed to be

corrected, it was done at this point with HCl or NaOH solutions. Then needle was then reinserted and the timing resumed. This was repeated at each sampling time. After the last concentrate sample was collected (at 20 min), the tailings sample was drained through the tailings sample port. Care was taken to wash out all remaining material from the cell and piping.

The concentrate and tailings samples were each vacuum filtered using a Büchner funnel and the appropriate, previously weighed, filter paper. The filtered samples were then dried overnight in an oven at 60 °C and weighed again. The recovery in each section could then be calculated using the before and after masses. The total recovery was the sum of all the masses from each concentration section.

4.3.4.3 Flotation kinetics and rate constant procedure

The flotation kinetics and rate constant provided information on if a maximum flotation recovery is reached and how fast and effective surfactin is at floating coal or pyrite. To determine the rate constant, the cumulative coal or pyrite recovery and the cumulative flotation time data, found during the microflotation experiments, was used.

The pyrite or coal recovery in batch flotation is described by the first order kinetic model as shown in equation [1]. Where R is the cumulative pyrite or coal recovery at the cumulative flotation time, t, in min, and *k* is the flotation rate constant in min^{-1}.

$$R = 1 - exp(-kt) \qquad [\,1\,]$$

Rewriting equation [1] as equation [2], allows solving for the flotation rate constant (*k*), which is the gradient of the *– ln (1 - R)* vs. *t* line.

$$-\ln(1 - R) = kt \qquad [\,2\,]$$

To determine the gradient (the rate constant, *k*), the “LINEST” Microsoft Excel 2016 function was used over the cumulative recovery of coal or pyrite over the cumulative flotation time of 0 – 6 min. The “LINEST” function outputs the gradient, which is the flotation rate constant. The flotation rate constants at different flotation conditions can be compared to determine which operating conditions provide better flotation.

5 RESULTS AND DISCUSSION

The Results and Discussion section presents and discusses the results obtained through the surface tension, zeta potential, FTIR and microflotation analysis experimentation, which was done as presented in the Methods section (section 4.3). The aim of the Results and Discussion section is to answer the five project objectives, which are as follows:

1. Determine a surfactin concentration range for further experimentation.
2. Evaluate the effect of the coal and pyrite surface charge on the adsorption of surfactin.
3. Evaluate the attachment mechanism of surfactin to the surface of coal and pyrite.
4. Evaluate the effect of surfactin on the hydrophobicity of coal and pyrite.
5. Determine the potential desulphurisation operating conditions.

Each experimental analysis will be discussed within the context of these objectives, in a bid to achieve the project aim, which is to determine the effectiveness of surfactin as a collector in the desulphurisation of coal through froth flotation of coal and pyrite as a mitigation strategy for the formation of acid mine drainage.

5.1 Surface tension and critical micelle concentration of surfactin

The critical micelle concentration (CMC) of surfactin was used as a starting point to determine the concentration range that should be used for flotation of coal and pyrite using surfactin. The CMC is the concentration at which surfactin monomers start to form into micelles. Surfactin micelles may have a different way of interacting with coal or pyrite compared to surfactin monomers. The CMC was determined using the surface tension of surfactin in demineralized water.

The plot of the surface tension as a function of surfactin concentration is given in Figure 13. Surfactin lowered the surface tension of demineralized water from 71.87 $mN \cdot m^{-1}$ to a minimum of 28.71 $mN \cdot m^{-1}$. The experimental minimum surface tension of 28.71 mNm^{-1} is comparable to literature values of 27 - 30 $mN \cdot m^{-1}$ for the minimum surface tension of water in the presence of surfactin (Arima et al., 1968; Ishigami et al., 1995; Lang, 2002; Sen and Swaminathan, 2005). The LC-MS analysis on the surfactin used in this study, showed that it was a mixture of surfactin homologues and included no other lipopeptides. The surface tension results provide a second confirmation that indicates that the surfactin used in this study is relatively pure and comparable to surfactin used in literature, in terms of minimum surface tension. Surfactin contaminated with other biosurfactants would produce a different minimum surface tension in water. For example, iturin, a lipopeptide that *Bacillus subtilis* produces in conjunction with surfactin, reduces the surface tension of water to a minimum of 39.0 $mN \cdot m^{-1}$ (Habe et al., 2019). Thus, if the surfactin sample was contaminated with iturin, it would have a larger minimum surface tension than pure surfactin.

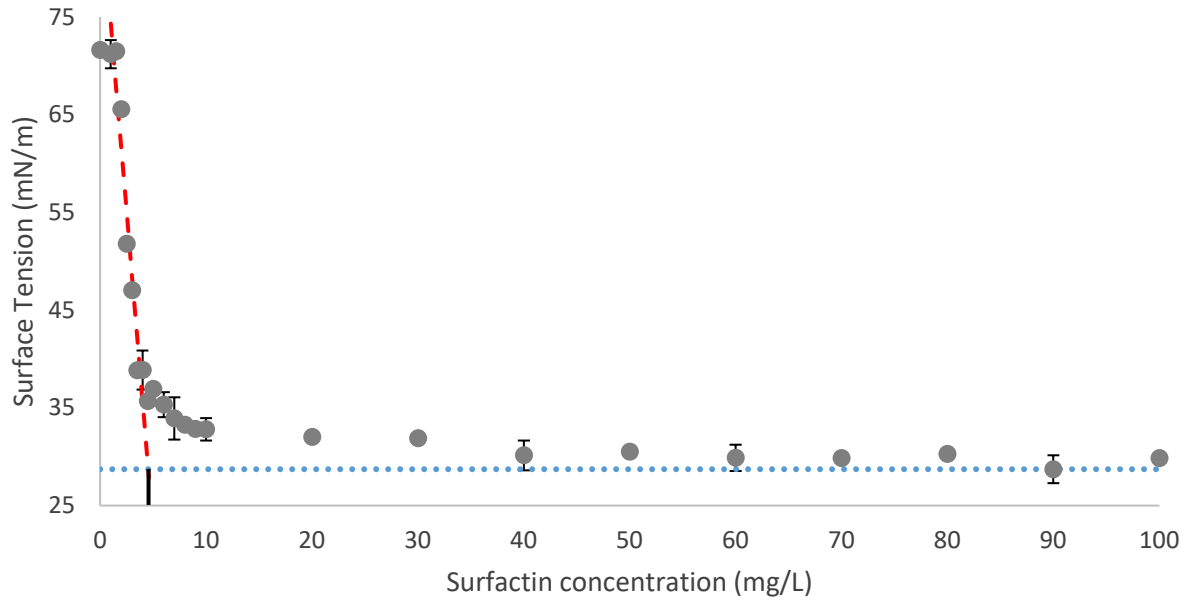

Figure 13: Surface tension of demineralized water as a function of surfactin concentration. The data points (●) indicate the average surface tension values found using the du Noüy ring methodology and the error bars represent the standard deviation of the independent triplicate repeats. The two lines used to determine the CMC are represented by the concentration-dependent line in red (- - -), the concentration-independent line in blue (·····) and the CMC indicator line in black (——).

The experimental CMC was found by fitting a line to the part of the surface tension vs surfactin concentration curve that has the largest gradient. This line is called the concentration-dependent line, as this is where the surface tension is dependent on surfactin concentration. The second line needed to determine the CMC is drawn on a horizontal tangent to the lowest surface tension value found. This second line is called the concentration-independent line, as this is where the surface tension has reached a minimum and is no longer dependent on surfactin concentration. The surfactin concentration where the concentration-dependent and concentration-independent lines cross, is the CMC value. The CMC for the surfactin lipopeptide mixture used in this study, was found to be approximately 4.5 mg/L.

Comparing the CMC found with literature values of 7.8 - 13 mg/L (Bognolo, 1999; Carrillo et al., 2003; Deleu et al., 1999; Heerklotz and Seelig, 2001; Ishigami et al., 1995; Sen and Swaminathan, 2005), indicates that the experimental CMC is lower. The literature CMC values for surfactin, were determined in the alkaline pH range (pH 7.4 – 8.7) and with pH buffers ($NaHCO_3$, Tris, NaCl), whereas this study determined the CMC of surfactin at the natural pH of 6 of demineralized water, with no buffer. The surface tension for surfactin in solution is significantly lower at a pH of 6, than at a pH of 8 (Abdel-Mawgoud et al., 2008). The formation of micelles of ionic surfactants, such as surfactin, are governed by two opposing forces: The hydrophobic force caused by the fatty acid chain, which favours micellization, and an electrostatic repulsion force between the ionic moiety groups, which hinders micellization (Arutchelvi et al., 2014). At a pH of 6, the two anionic residues (Glu_1 and Asp_5) of surfactin are partially protonated, having pK_a of 5.4 (Arutchelvi et al., 2014). Thus, reducing the repulsion forces between

surfactin molecules, allowing micellization at lower concentrations, resulting in a lower CMC value for surfactin at pH 6. Thus, the respective experimental CMC value would be lower. The lower experimental CMC value could not be due to impurities as the surfactin used was shown to be a pure mixture of homologues of surfactin. The mixture of homologues could introduce some variability in the surfactin CMC, but that was considered to be insignificant.

Previous studies have performed the CMC evaluation with buffers, as this provides a more stable and repeatable measurement when adjusting the pH value, and in the alkaline range, as this is where surfactin is fully ionised. The addition of electrolyte has an effect on the CMC of surfactin in an aqueous solution and thus so would pH buffers (Knoblich et al., 1995). The use of a surface tension methodology at a lower pH opens up an opportunity for a greater understanding of the chemistry and micellization behaviour of surfactin, particularly at lower pH values, without the influence of pH buffers.

Since surfactin is more active around the neutral pH range (Abdel-Mawgoud et al., 2008), the pH range from 6 – 8 will have the biggest influence on surfactin adsorption. The experimental CMC combined with the literature CMC provides a CMC range of between 4 – 13 mg/L for pH 6 - 9. This provides a starting range for the evaluation of surfactin concentration on the flotation of coal and pyrite. Using 5 mg/L surfactin concentration as a low surfactin concentration provides a concentration below or close to the surfactin CMC value for most pH values. It was decided to initially use surfactin concentrations at 2 mg/L and 4 mg/L (instead of 5 mg/L), to provide surfactin concentrations below and at the CMC respectively. If zeta potential analysis indicated no significant difference between these concentrations (2 and 4 mg/L), a 5 mg/L surfactin concentration will be used thereafter, as 5 mg/L is closer to the CMC over a range of pH values, while providing a high enough concentration to make any effect of surfactin noticeable. Using 15 mg/L surfactin concentration as the high surfactin concentration provides a concentration above the CMC for most pH values. These surfactin concentrations (2, 4 and 15 mg/L) allow the influence of surfactin concentration below the CMC, at the CMC and above the CMC to be evaluated, and gives a surfactin concentration starting range for the flotation of coal and pyrite.

5.2 The effect of surfactin on coal hydrophobicity

A surfactin concentration range for the flotation of coal and pyrite was established in the previous section using the CMC value of surfactin. In order to determine if coal and pyrite can be separated using surfactin, further investigations needed to be done. In this section the following objectives will be explored for the interaction between coal and surfactin:

1. Evaluate the effect of the coal surface charge on the adsorption of surfactin.
2. Evaluate the attachment mechanism of surfactin to the surface of coal.
3. Evaluate the effect of surfactin on the hydrophobicity of coal.

5.2.1 Zeta potential of coal with surfactin adsorption

Zeta potential provides an indication of the surface charge. Zeta potential analysis was used to establish if surfactin adsorption onto the surface of coal occurred. This would be indicated by a neutralisation of

the coal surface charge, an increase in the coal surface charge or a shift in the isoelectric point (IEP), subject to the adsorption mechanism, with the addition of surfactin. The possible adsorption mechanism can also be determined from the response of the zeta potential curve to the addition of a surfactant (Fuerstenau and Pradip, 2019).

The 2, 4 and 15 mg/L surfactin concentrations, determined in the surfactin CMC section previously, were used to evaluate the adsorption of surfactin below the CMC, at the CMC and above the CMC. The 2 mg/L and 4 mg/L concentrations will be evaluated to see if there would be significant differences in the effect of surfactin between these concentrations and if the chosen surfactin concentration should be changed for the FTIR and microflotation analysis experimentation. The zeta potential of coal as a function of pH is given in Figure 14. The standard deviation for the independent duplicate repeats of each data point is shown by the error bars. The isoelectric point (IEP) is the pH value at which the coal surface has a neutral net surface charge which is a zeta potential of zero. The IEP is considered important as moving above and below this pH reverses the net surface charge. The IEP for coal with the addition of 0, 2, 4 and 15 mg/L surfactin, was found to be pH 4.3, 3.8, 3.6 and 2.7 respectively. It can be seen that the IEP decreases as the surfactin concentration increases. The coal surface charge becomes more negative, with the addition of surfactin, in both the positive zeta potential region, above the IEP, and the negative zeta potential region, below the IEP. The addition of low surfactin concentration (2 & 4 mg/L) had a greater effect on the zeta potential in the region from pH 4 – 7.

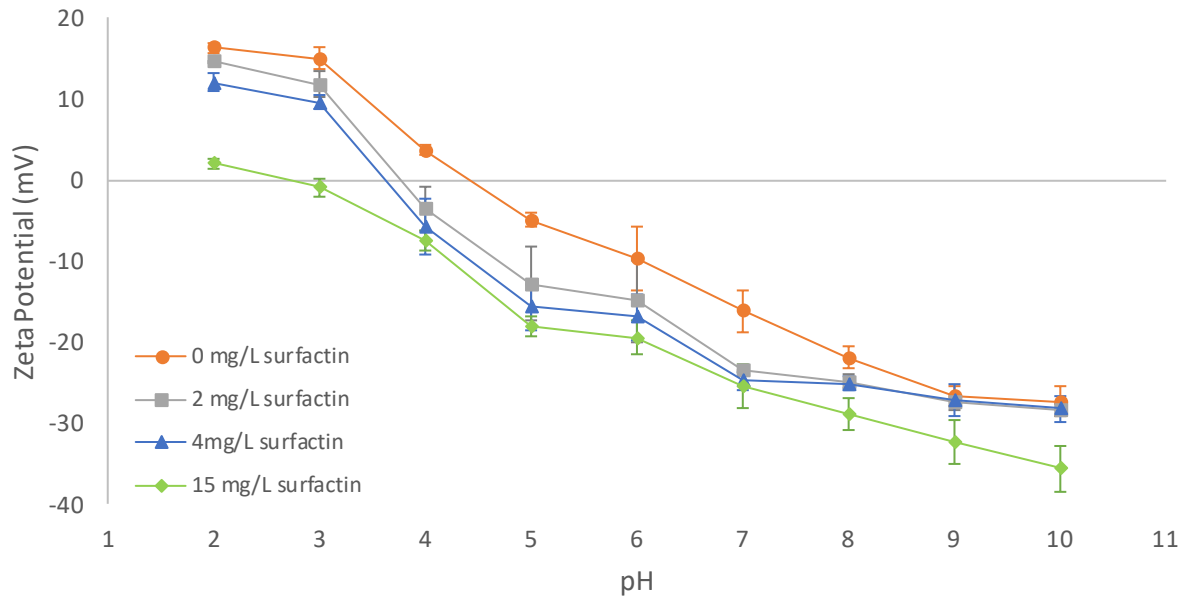

Figure 14: Zeta potential of coal as a function of pH and surfactin concentration. The orange (—●—), grey (—■—), blue (—▲—) and green (—◆—) data points represent the zeta potential of coal with the addition of 0, 2, 4 and 15 mg/L surfactin concentration respectively, across the pH range of 2 – 10. Data points have been connected linearly to better illustrate the resulting trends. The error bars represent the standard deviation for the independent duplicate repeats of each data point.

The potential-determining ions (also known as the charge-determining ions) for both non-oxidized and oxidized coal are hydroxyl (OH^-) and hydronium (H_3O^+) ions. The addition of hydroxyl ions makes the coal surface more negative, whereas the addition of hydronium ions neutralizes the negative charges and makes the coal surface less negative. The dissociation of weakly acidic functional groups causes the surface charge of coal (Dey, 2012). Any deviation from this behaviour would indicate interaction between the surfactin and the coal surface.

The literature gives the IEP of unoxidized coal as pH 4.2 and the IEP of oxidized coal, that was oxidized in an oven at 200 °C for 4 hours, at pH 2.8 (Sarikaya and Özbayoğlu, 1995). The experimental IEP was found to be 4.3 without surfactin addition. Compared to the literature IEP values for unoxidized and oxidized coal, the experimental IEP indicates that the coal used is unoxidized, as expected for coal freshly milled and kept under nitrogen atmosphere. The close comparison between the literature and experimental IEP validates the zeta potential analysis methodology to an extent. The zeta potential profile is negative from pH 4.3 to pH 10 and becomes more negative as pH increases, due to the increased dissociation of the phenolic and carboxylic surface functional groups which become negatively charged (Crawford and Mainwaring, 2001). The positive net surface charge from pH 4.3 to 2 is attributed to the protonated carboxylic and phenolic hydroxyl groups and the formation of carbocations from chromene and pyrone-type structures (Abotsi et al., 1992; Garten et al., 1957).

The shift in the IEP towards lower pH values with the addition of surfactin shows that there is adsorption of surfactin onto the coal surface. The coal surface consists of a mixture of carbonaceous hydrophobic areas and oxygenated functional group areas (phenolic, carbonyl, carboxyl and ester groups). Surfactants interact with these areas via two main mechanisms: through polar groups of the surfactant interacting with the oxygenated functional groups through hydrogen bonding; and through the non-polar chain of the surfactant interacting with the carbonaceous areas on the coal surface (Dey, 2012). Surfactin likely adsorbs onto the coal surface by van der Waals interactions between the aliphatic chain of surfactin and the carbonaceous sites on the coal surface. As surfactin carries anionic residues, its adsorption onto the coal surface by the proposed van der Waals interactions, make the coal surface more negatively charged as indicated by the decrease seen in the zeta potential with the addition of surfactin. The ionised anionic surfactin residues might also adsorb electrostatically to the positive sites on the coal surface. This would also decrease the zeta potential by neutralizing positive surface charges and thus increasing the net negative surface charge. However, positive coal surface sites are few, except in the extreme acidic range. The main surface charge altering mechanism, and thus the main adsorption mechanism, is resultantly attributed to van der Waals interactions between the surfactin aliphatic groups and the coal surface.

The higher deviation of the zeta potential of coal with the addition of low surfactin concentration (2 & 4 mg/L) from no surfactin addition, from pH 4 to 7, is attributed to the lower electrostatic repulsion forces between a slightly negative coal surface and a protonated/partially protonated (neutral/slightly negative) surfactin molecule (pK_a of 5.4), allowing more van der Waals interactions. Above a pH of 7 the electrostatic repulsion forces hinder van der Waals interactions, and below a pH of 4 surfactin tends to precipitate. At pH 9 and above, the repulsive force between the similarly charged coal surface and

surfactin molecule are greater than the hydrophobic interaction forces and thus no adsorption occurs (Fuerstenau and Pradip, 2019).

The zeta potential response of coal, to the addition of surfactin, was an IEP shifts to a lower pH value and the zeta potential becoming more negative. As the pH increases, the zeta potential difference between coal without surfactin addition and coal with surfactin addition, becomes gradually less. Ultimately at high pH values there is no difference between the zeta potential with or without the addition of surfactin. This description of the zeta potential response is distinct to physisorbed anionic surfactants on a hydrophobic surface (Fuerstenau and Pradip, 2019).

Thus, it can be hypothesized that the adsorption mechanism of surfactin onto the surface of coal is physisorption, most probably due to hydrophobic interactions between the hydrophobic aliphatic chains of surfactin and the hydrophobic carbonaceous material on the coal surface, as suggested previously.

Increasing the surfactin concentration from 2 mg/L to 4 mg/L seems to have little to no additional effect on the zeta potential. The zeta potential becomes slightly more negative from pH 2 to 7, with no significant effect from pH 8 – 10, as surfactin concentration is increased. The reason for this is unclear, but suggests that no more adsorption sites are available. Further increasing the surfactin concentration to 15 mg/L has significant effects on the zeta potential at extreme pH conditions, but little effect around neutral conditions. The zeta potential becomes slightly more negative from pH 4 to 7 and significantly more negative from pH 2 - 4 and 8 – 10. The fact that there is only a slight change in zeta potential from pH 4 -7 with a significant increase in surfactin concentration further strengthens the proposal that near maximum coverage has been reached and that no additional adsorption sites are available within this pH range, and further adsorption is most probably hindered by repulsion forces between surfactin molecules. The significant decrease seen in the zeta potential at 15 mg/L surfactin concentration, at pH 2 - 4 and pH 8 – 10 could be due to the formation of surfactin aggregate structures which are able to overcome the adsorption inhibiting forces. However, further study is needed to confirm this.

In summary, comparing the experimental and literature IEP of coal indicated that the coal used was unoxidized and validated the zeta potential methodology. Surfactin addition showed significant effect on the zeta potential of coal in the pH 4 – 7 range at low surfactin concentration (2 and 4 mg/L), but little effect in the extreme pH range of pH 2 – 3, due to surfactin precipitation, and no effect in the pH range 8 – 10, due to electrostatic repulsion overcoming hydrophilic interaction forces. High surfactin concentration (15 mg/L) showed little additional effect on the zeta potential of coal, in the pH 4 - 7 range, above the effect of low surfactin concentration, due to lack of additional adsorption sites. There was however a significant effect in the extreme pH ranges (pH 2 – 3 and 8 – 10) as the high surfactin concentration overcomes previous inhibiting factors, probably due to the formation of aggregate surfactin structures. The zeta potential response to the addition of surfactin suggested that the adsorption mechanism of surfactin onto the surface of coal is physisorption through hydrophobic interactions.

FTIR analysis, presented in the next section, will provide an additional analysis method to clarify and verify the proposed adsorption mechanism of surfactin onto the surface of coal by revealing with which coal surface functional group the surfactin molecules interact.

5.2.2 FTIR analysis on the adsorption of surfactin on coal

5.2.2.1 Surfactin spectrum peak assignment

In order to use FTIR analysis and determine if surfactin molecules are seen on the surface of minerals, the spectrum peaks associated with surfactin need to be identified and assigned to the most likely functional group bonds that produce the respective peak response. This allows differentiation between the peaks associated with the functional groups of surfactin and the functional groups associated with either coal or pyrite.

The FTIR spectrum of surfactin used for this study is shown in Figure 15. The functional groups of surfactin can be divided into two main groups, namely: the functional groups associated with the peptide moiety and the functional groups associated with the hydrophobic moiety of surfactin.

The FTIR spectrum peaks associated with the peptide moiety functional groups of surfactin occur at the 3291 cm^{-1} peak associated with the N-H stretching mode, the 1736 cm^{-1} peak associated with the ester carbonyl group, the peak at 1647 cm^{-1} associated with the CO-N bond stretching mode, and the peak at 1530 cm^{-1} associated with the deformation mode of the N-H bond combined with the stretching mode of the C-N bond (Bastrzyk et al., 2019; de Faria et al., 2011; Joshi et al., 2008). The FTIR spectrum peaks associated with the hydrophobic moiety functional groups of surfactin are the peaks found at 2955 cm^{-1}, 2870 cm^{-1}, 1467 cm^{-1}, 1398 cm^{-1} , and 1368 cm^{-1} which are all associated with $-CH_3$ and $-CH_2$ modes of aliphatic chains (de Faria et al., 2011; Joshi et al., 2008).

When these peaks, that have been associated with the functional groups of surfactin, are seen on the FTIR spectra of either coal or pyrite with the addition of surfactin, the peaks would indicate that surfactin is present on the surface of that mineral and that adsorption has probably taken place.

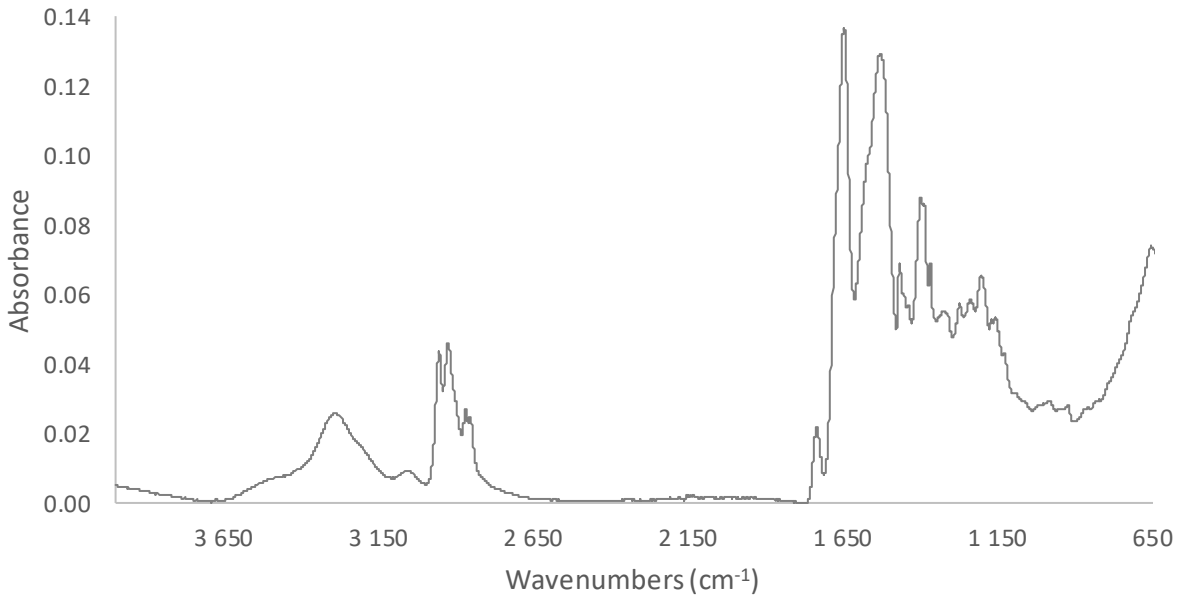

Figure 15: FTIR spectrum of surfactin from 4000 – 650 cm^{-1}. The spectrum shown in the figure above is the average spectrum of independent triplicate repeats, baseline corrected for atmospheric H_2O and CO_2.

5.2.2.2 Coal spectra peak assignment

In order to use FTIR spectra, the spectrum peaks of coal need to be identified and assigned to the most likely functional group bonds that produce the respective peak response. This allows differentiation between peaks associated with coal functional groups and the functional groups associated with surfactin.

The FTIR spectrum of the coal sample used is given in Figure 16. The broad region, 3700 – 3100 cm^{-1} was assigned to the -OH stretching vibrations associated with the oxygen functional groups, indicating the presence of alcohols, phenols and carboxylic acid. The peaks in the 3750 – 3550 cm^{-1} range are assigned to crystal H_2O in clay minerals. The region, 3100 – 3000 cm^{-1}, was assigned to aromatic C-H stretching vibrations and the region, 3000 – 2800 cm^{-1}, was assigned to aliphatic C-H stretching modes. The peak, 1700 cm^{-1}, was assigned to aliphatic C=O and COOH stretching vibrations due to the presence of acids, ketones and aldehydes. The region, 1680 – 1500 cm^{-1}, was assigned to aromatic stretching modes. The peak, 1432 cm^{-1}, was assigned to aliphatic bending vibrations due to CH_2 and CH_3. The peak at 1452 cm^{-1}, was assigned to aromatic C=C stretching modes. The peak, 1374 cm^{-1}, was assigned to aliphatic CH_3 groups. The peak, 1312 cm^{-1}, was assigned to aliphatic CH in-plane bending vibrations. The region, 1280 – 1000 cm^{-1}, was assigned to saturated aliphatic skeletal C-C vibration, C-O stretching vibration of ether groups, and O-H bending vibrations in phenolic, phenoxy and hydroxybenzene structures. The region, 900 – 700 cm^{-1}, was assigned to out-of-plane aromatic C-H bending vibrations indicating the presence of substituted aromatic species in aromatic rings, and trans- and cis-CH_2 in long saturated aromatic -CH-CH chains. The region, 720 – 680 cm^{-1}, was assigned to long aromatic alkanes ($(CH_2)_n$, n>4) side rings (Geng et al., 2009; Okolo et al., 2015; Van Niekerk et al., 2008).

The peaks below 1200 cm^{-1} are generally assigned to the clay minerals kaolinite and quartz. Kaolinite minerals and quartz have distinct peaks assigned to 1010 cm^{-1} and 1160 cm^{-1} respectively. The peaks at 1112 cm^{-1}, 1029 cm^{-1} and 1010 cm^{-1} are assigned to the Si-O stretching and bending vibrations. The peaks 939 cm^{-1} and 913 cm^{-1} are assigned to the Al-OH bending vibrations. The peak at 689 cm^{-1} is assigned to the Si-O stretching vibrations. The peaks at 799 cm^{-1} and 746 cm^{-1} are assigned to the Si-O-Al^{iv} compounded vibrations. Peaks at 1141 cm^{-1}, 1073 cm^{-1}, 1000 cm^{-1}, 882 cm^{-1} and 1219 cm^{-1} could indicate the presence of pyrite, however these peaks are not present or visible in this sample (Abdel-Khalek and El-Midany, 2013; Saikia et al., 2007a, 2007b; Suraj et al., 1997).

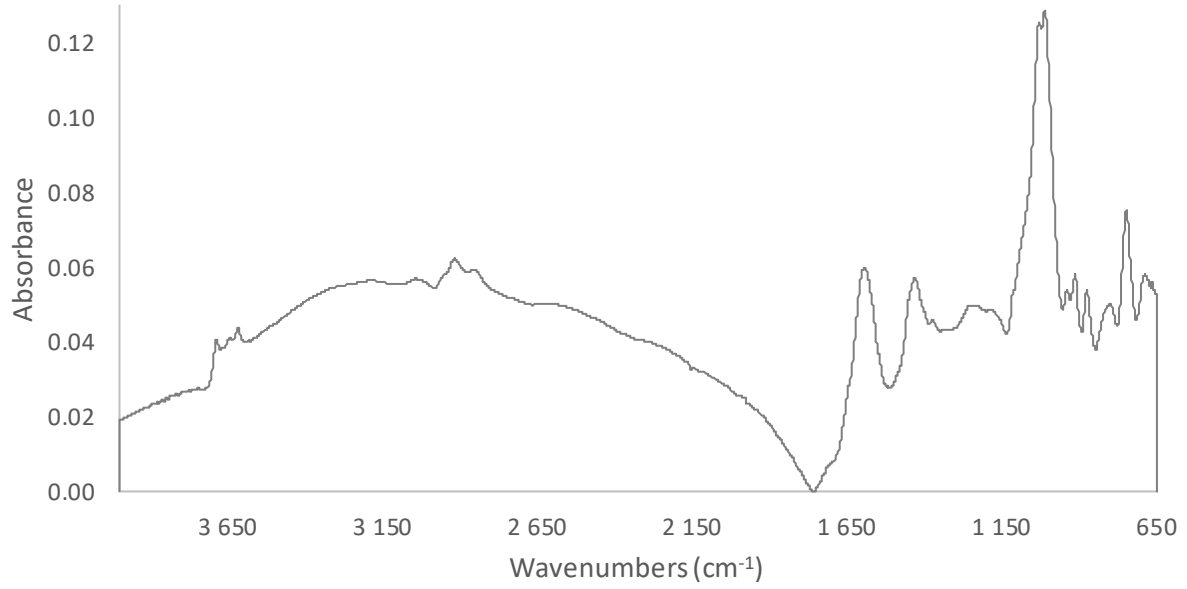

Figure 16: FTIR spectrum of dry coal from 4000 – 650 cm^{-1}. The spectrum shown in the figure above is the average spectrum of independent duplicate repeats, baseline corrected for atmospheric H_2O and CO_2.

5.2.2.3 Effect of pH on the FTIR spectrum of coal

It is important to explore the effect of pH on the coal surface as it will have a significant effect on the coal surface functional groups which in turn will determine the interaction between the coal surface and surfactin. Additionally, it would allow differentiation between the effect of pH and the effect of surfactin concentration on the coal surface. The spectra of coal conditioned at various pH conditions are given in Figure 17. The corresponding peak areas for the major coal FTIR peaks are given in Table 11.

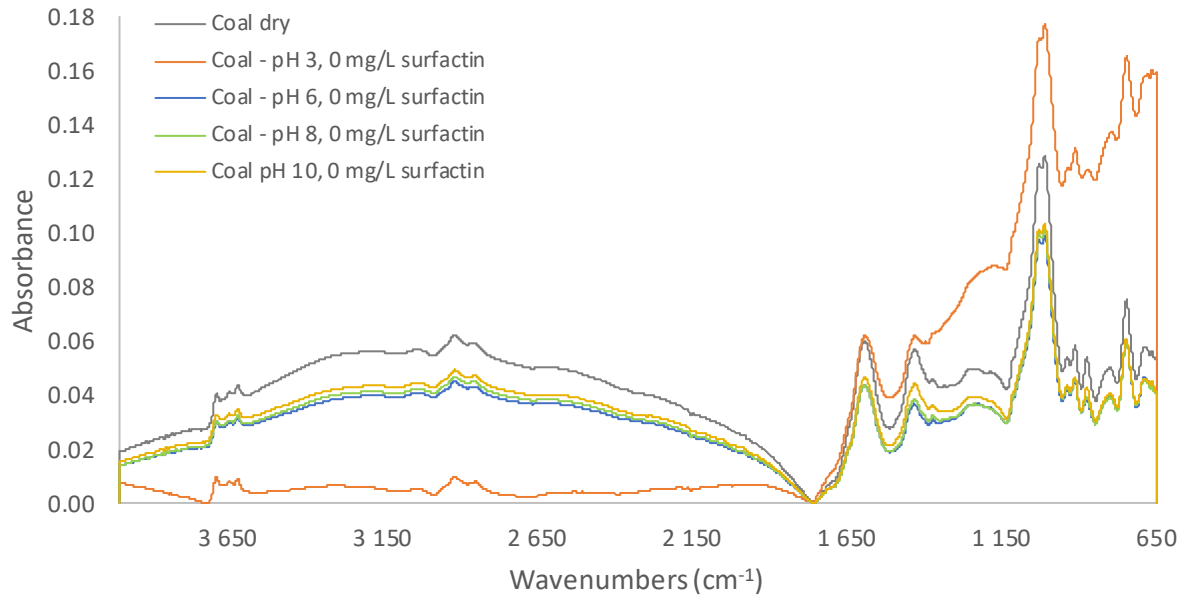

Figure 17: FTIR spectra from 4000 – 650 cm^{-1} of coal conditioned at various pH conditions. The grey, orange, blue, green and red spectra represent the spectra of dry coal and coal conditioned at pH 3, 6, 8 and 10 respectively. The spectra shown in the figure above are the average spectrums of independent duplicate repeats, baseline corrected for atmospheric H_2O and CO_2.

Table 11: Major FTIR peak areas of coal for various pH conditions. The same peak ranges were used, with the baseline drawn through the lowest data points on either side of the peak, eliminating the absorbance offset and allowing areas to be comparable.

Peak range	Dry coal – Peak area	pH 3 – Peak area	pH 6 – Peak area	pH 8 – Peak areal	pH 10 – Peak area
3700 - 3600 cm^{-1}	0.3021	0.266	0.228	0.234	0.249
3080 - 3000 cm^{-1}	0.0748	0.068	0.061	0.061	0.065
2970 - 2800 cm^{-1}	0.6335	0.503	0.457	0.495	0.511
1660 -1550 cm^{-1}	1.748	1.402	1.231	1.241	1.301
1460 - 1410 cm^{-1}	0.317	0.206	0.21	0.226	0.246
1060 - 980 cm^{-1}	2.364	2.011	1.853	1.883	1.915
939 cm^{-1} (950 - 930)	0.04	0.034	0.031	0.031	0.032
913 cm^{-1} (920 – 900)	0.086	0.073	0.066	0.067	0.068
875 cm^{-1} (890 – 860)	0.174	0.04	0.086	0.101	0.132
799 cm^{-1} (820 - 780)	0.098	0.102	0.09	0.085	0.097
747 cm^{-1} (760 - 730)	0.293	0.266	0.237	0.233	0.24
689 cm^{-1} (700 - 675)	0.052	0.046	0.053	0.046	0.042

It is noted that at a pH of 3, the absorbance is significantly lower across the 4000 – 1800 cm^{-1} wavenumber range compared to the dry, unconditioned coal. This is due to the removal of -OH functional groups on the coal surface at low pH. The addition of H^+ ions causes the removal of -OH from the coal surface. This

is supported by each successive increase in absorbance with each successive pH increases from pH 3 to 6 to 8 to 10. Increasing the pH increases the OH- ions available to interact with the coal surface, effectively increasing the -OH functional groups on the surface and consequently the absorbance response in the 4000 – 1800 cm^{-1} range. Thus, at pH 10, the -OH ion concentration would be highest, allowing the greatest interaction with the coal surface, producing the correspondingly biggest absorbance response across the 4000 – 1800 cm^{-1} range. The higher levels of absorbance for pH 3 compared to the other conditioning pH values in the 1750 – 650 cm^{-1} range could be due to the removal of -OH from the coal surface causing a greater exposure of aliphatic and aromatic groups, increasing the absorbance response. However, this might not be the case as the second highest absorbance response is from pH 10, followed by pH 8 and then pH 6. The reason for this is unclear. The exposure of coal surface aliphatic and aromatic groups would have a significant effect on the adsorption of surfactin, as the zeta potential analysis indicated that the main adsorption mechanism of surfactin is hydrophobic physisorption between the aliphatic surfactin functional groups and the hydrophobic coal functional groups, which are aliphatic and aromatic groups.

There is no significant difference in the peak area for the clay mineral peaks in the 3700 – 3600 cm^{-1} range, or for the peaks associated with aromatic and aliphatic C-H stretching vibrations in the 3100 – 2800 cm^{-1} range, for the coal conditioned at pH 3 to 10.

There is however a difference in the 1029 cm^{-1} and 1010 cm^{-1} peak shape and area for pH 3, compared to the other pH conditions. The peaks at pH 3 are sharper and have a larger comparable peak area, indicating a more significant presence of Si-O bonds at the surface. This could indicate an enhanced Si-O bond surface exposure due to the removal of -OH from the surface of the clay minerals.

The 875 cm^{-1} peak shows significant difference in peak shape and area across the pH conditions. The flattest and smallest peak is at pH 3, with pH 6 and 8 having comparable middle peaks, and pH 10 having the sharpest and biggest peak. The 875 cm^{-1} peak is assigned to low intensity aromatic -CH bending bands and thus indicates that as pH rises there is a greater presence of substituted aromatic species on the coal surface.

5.2.2.4 FTIR analysis of adsorption of surfactin onto coal

Zeta potential analysis was used to establish that there is interaction between the coal surface and surfactin. After determining the effect of pH on the coal surface, the peak shapes and areas of the FTIR spectra of coal at different surfactin concentrations and pH values will be compared to develop a greater understanding with which coal surface functional groups and surfactin molecules interact and provide confirmation or more clarity on the surfactin adsorption mechanism.

The FTIR spectra of coal conditioned at pH 3, with various surfactin concentrations, are given in Figure 18. The corresponding peak areas for the major peaks are given in Table 12. As surfactin concentration increases, the absorbance across the 4000 – 1800 cm^{-1} range increases. This is most probably due to the exposed -OH groups on the surfactin molecule after hydrophobic adsorption between the coal surface and the surfactin hydrophobic groups. This could also indicate that surfactin has an oxidizing effect on the surface of coal, but this would need further investigation.

There is also a reduction in the peak area for the clay mineral peaks in the 3700 – 3600 cm^{-1} range as surfactin concentration increases from 0 to 5 mg/L to 15 mg/L. This indicates some interaction between surfactin and the clay minerals. This is further confirmed by reductions in the 1029 cm^{-1} and 1010 cm^{-1} peak areas associated with the Si-O bonds and the 799 cm^{-1} and 746 cm^{-1} peak areas associated with the Si-O-Al^{iv} bonds, as surfactin concentration increases. Thus, it is clear that surfactin interacts with the mineral component of coal at a pH of 3.

There is a decrease in the 3100 – 2800 cm^{-1}, 1680 – 1500 cm^{-1}, 1432 cm^{-1} and 1452 cm^{-1} peak areas, associated with the aliphatic and aromatic functional groups, as surfactin concentration increases. There is also a decrease in the level of absorbance in the 1750 – 650 cm^{-1} range as surfactin concentration increases. The decrease in peak areas combined with the reduction in absorbance response could be due to the hydrophobic interactions between surfactin and the coal surface aliphatic and aromatic groups, with the surfactin peptide moiety shielding these aliphatic and aromatic functional groups on the coal surface.

Although no clear indication of the surfactin molecule itself was seen on the surface of coal, it was clear that surfactin had an effect on the clay mineral peaks and the aliphatic and aromatic functional groups on the coal surface.

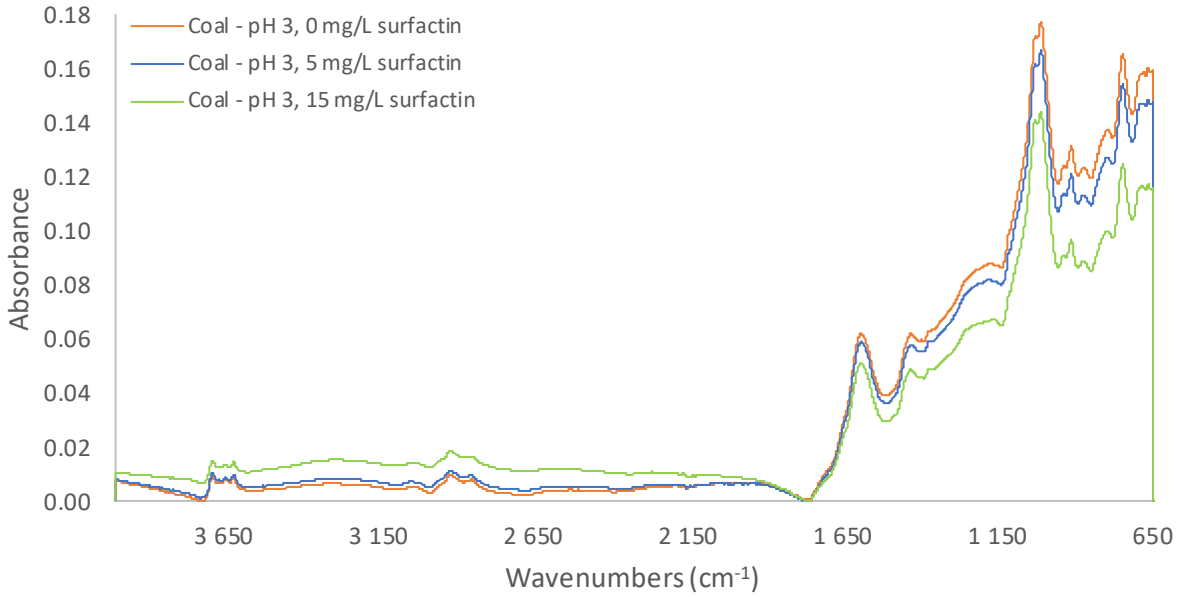

Figure 18: FTIR spectra from 4000 – 650 cm^{-1} of coal conditioned for various surfactin concentrations at pH 3. The orange, blue and green spectra represent the spectra of coal conditioned at pH 3 with a concentration of 0, 5 and 15 mg/L surfactin respectively. The spectra shown in the figure above are the average spectrums of independent duplicate repeats, baseline corrected for atmospheric H_2O and CO_2.

Table 12: Major peak areas for coal conditioned at pH 3 for various surfactin concentrations. The same peak ranges were used, with the baseline drawn through the lowest data points on either side of the peak, eliminating the absorbance offset and allowing areas to be comparable.

Peak range	0 mg/L surfactin - Peak area	5 mg/L surfactin- Peak area	15 mg/L surfactin- Peak area
3700 - 3600 cm^{-1}	0.2656	0.2537	0.2486
3080 - 3000 cm^{-1}	0.068	0.0641	0.0545
2970 - 2800 cm^{-1}	0.5027	0.4825	0.4727
1660 -1550 cm^{-1}	1.402	1.358	1.193
1460 - 1410 cm^{-1}	0.206	0.196	0.186
1060 - 980 cm^{-1}	2.011	1.968	1.839
939 cm^{-1} (950 - 930)	0.034	0.033	0.028
913 cm^{-1} (920 – 900)	0.073	0.072	0.063
875 cm^{-1} (890 – 860)	0.04	0.043	0.041
799 cm^{-1} (820 - 780)	0.102	0.096	0.096
747 cm^{-1} (760 - 730)	0.266	0.255	0.242
689 cm^{-1} (700 - 675)	0.046	0.047	0.04

The FTIR spectra of coal conditioned at pH 6, with various surfactin concentrations, are given in Figure 19. The corresponding peak areas for the major peaks are given in Table 13. As surfactin concentration increases, the absorbance across the 4000 – 1800 cm^{-1} range increases, indicating an increase in -OH species. Again, this is probably due to the surfactin molecule hydrophobically interacting with the coal surface and increasing the -OH concentration as the surfactin peptide moiety contains -OH groups. There is also a slight increase in the peak area for the clay mineral peaks in the 3700 – 3600 cm^{-1} range as surfactin concentration increases. This indicates some interaction between surfactin and the clay minerals causing greater exposure of the clay mineral bonds. There is a further increase in the peak area of the peaks assigned to Si-O at 1029 cm^{-1} and 1010 cm^{-1}, as well as a slight increase in the peak areas of the peaks assigned to the Si-O-Al^{iv} bonds at 799 cm^{-1} and 746 cm^{-1}, as the surfactin concentration is increased. Surfactin might have a cleaning effect and play a role in exposing these mineral bonds. However, this would need further investigation to clarify and confirm.

The peak area for the peaks associated with aliphatic C-H stretching vibrations in the 3000 – 2800 cm^{-1} range increases as surfactin concentration increases. This could indicate the presence of the aliphatic chains of surfactin on the coal surface. The aromatic functional group peak area at 1680 – 1500 cm^{-1} and the peak areas at 1432 cm^{-1} and 1452 cm^{-1}, associated with aliphatic and aromatic surface functional groups, increases as surfactin concentration increases. This shows that surfactin again has some cleaning effect and has some role in exposing more aromatic functional groups. This could indicate a greater concentration of surface aliphatic groups, which include the aliphatic groups of surfactin, and aromatic functional groups that could lead to greater coal surface hydrophobicity, leading to better flotation of coal.

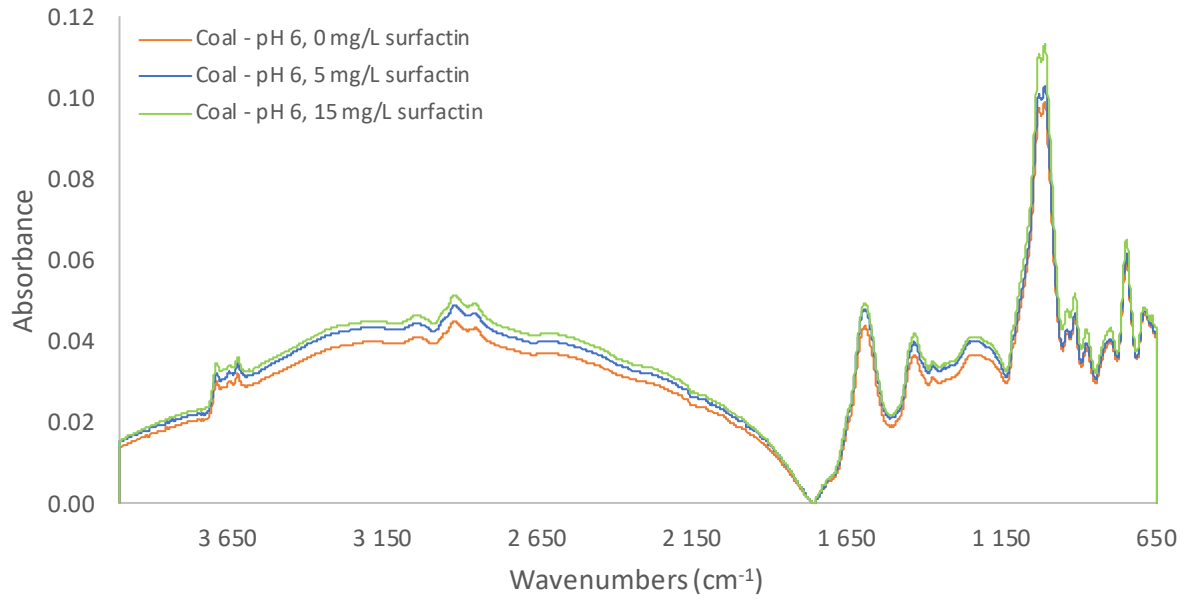

Figure 19: FTIR spectra from 4000 – 650 cm^{-1} of coal conditioned for various surfactin concentrations at pH 6. The orange, blue and green spectra represent the spectra of coal conditioned at pH 6 with a concentration of 0, 5 and 15 mg/L surfactin respectively. The spectra shown in the figure above are the average spectrums of independent duplicate repeats, baseline corrected for atmospheric H_2O and CO_2.

Table 13: Major peak areas for coal conditioned at pH 6 for various surfactin concentrations. The same peak ranges were used, with the baseline drawn through the lowest data points on either side of the peak, eliminating the absorbance offset and allowing areas to be comparable.

Peak range	0 mg/L surfactin-Peak area	5 mg/L surfactin-Peak area	15 mg/L surfactin-Peak area
3700 - 3600 cm^{-1}	0.2278	0.2285	0.2753
3080 - 3000 cm^{-1}	0.061	0.0628	0.0692
2970 - 2800 cm^{-1}	0.4574	0.516	0.5563
1660 -1550 cm^{-1}	1.231	1.355	1.35
1460 - 1410 cm^{-1}	0.21	0.223	0.241
1060 - 980 cm^{-1}	1.853	1.94	2.124
939 cm^{-1} (950 - 930)	0.031	0.033	0.036
913 cm^{-1} (920 – 900)	0.066	0.068	0.074
875 cm^{-1} (890 – 860)	0.086	0.088	0.095
799 cm^{-1} (820 - 780)	0.09	0.088	0.106
747 cm^{-1} (760 - 730)	0.237	0.247	0.271
689 cm^{-1} (700 - 675)	0.053	0.056	0.051

The FTIR spectra of coal conditioned at pH 8, with various surfactin concentrations, are given in Figure 20. The corresponding peak areas for the major peaks are given in Table 14. The absorbance across the 4000 - 1800 cm^{-1} range increases as surfactin concentration increases to 5 mg/L, but decreases to below

the 0 mg/L absorbance when the surfactin concentration is further increased to 15 mg/L. This shows that surfactin increases the surface -OH functional groups at low concentration (5 mg/L), but reduces the surface -OH functional groups at high surfactin concentration (15 mg/L). The same trend is seen when the peak areas associated with clay minerals and Si-O-Al^{iv} in the 3700 – 3600 cm^{-1} range and 799 cm^{-1} and 746 cm^{-1} peaks are first increased at 5 mg/L surfactin and then decreased at 15 mg/L surfactin. It seems as if surfactin removes positive ions from the clay mineral surface at low surfactin concentrations (5mg/L) and as concentration increases to 15 mg/L, surfactin interacts further with those cleared sites to reduce the clay mineral surface functional groups. The Si-O bond peak areas at 1029 cm^{-1} and 1010 cm^{-1}, however, show only a reduction as the surfactin concentration increases. This might indicate that some of the complexes formed by surfactin during the cleaning effect interact with the Si-O sites on the coal surface at low concentration.

There is an increased peak area for the peaks associated with the aliphatic C-H bonds in the 3000 - 2800 cm^{-1} range at 5 mg/L surfactin concentration. As the surfactin concentration increases to 15 mg/L there is a decrease in the peak area compared to 0 mg/L. The same trend is seen for the 1680 – 1500 cm^{-1} peak areas. This shows an increase in the aliphatic and aromatic surface group at low surfactin concentration, but a decrease in those groups at higher surfactin concentration. The reason for this is not clear and would require further investigation.

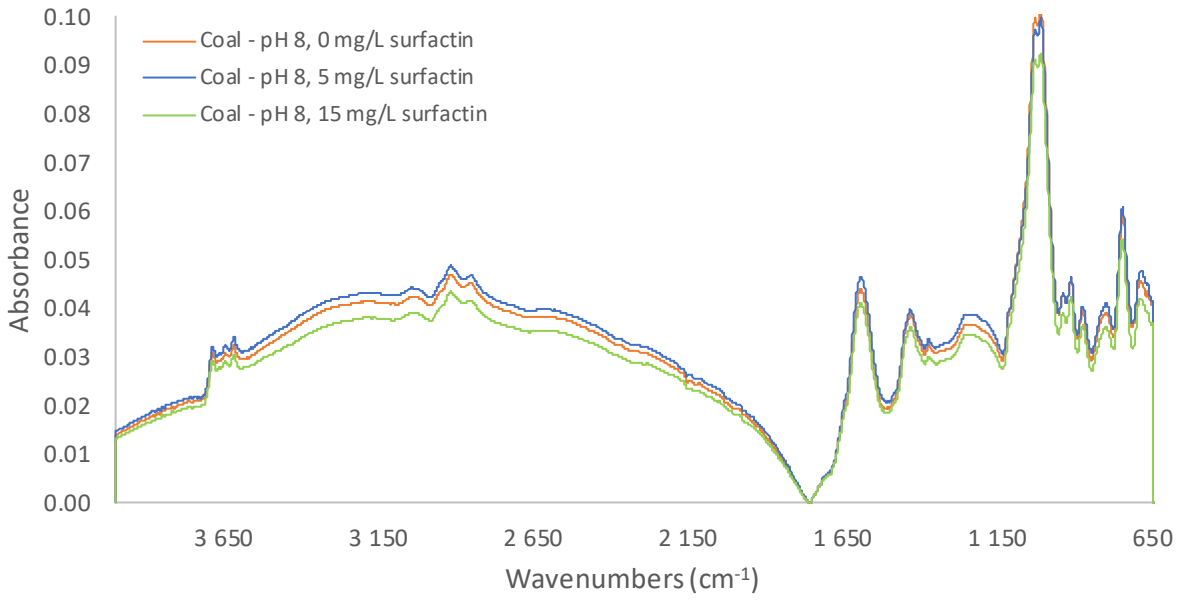

Figure 20: FTIR spectra from 4000 – 650 cm^{-1} of coal conditioned for various surfactin concentrations at pH 8. The orange, blue and green spectra represent the spectra of coal conditioned at pH 8 with a concentration of 0, 5 and 15 mg/L surfactin respectively. The spectra shown in the figure above are the average spectrums of independent duplicate repeats, baseline corrected for atmospheric H_2O and CO_2.

Table 14: Major peak areas for coal conditioned at pH 8 for various surfactin concentrations. The same peak ranges were used, with the baseline drawn through the lowest data points on either side of the peak, eliminating the absorbance offset and allowing areas to be comparable.

Peak range	0 mg/L surfactin - Peak area	5 mg/L surfactin - Peak area	15 mg/L surfactin - Peak area
3700 - 3600 cm^{-1}	0.2335	0.2534	0.2198
3080 - 3000 cm^{-1}	0.0607	0.0611	0.0596
2970 - 2800 cm^{-1}	0.4954	0.5085	0.4647
1660 -1550 cm^{-1}	1.241	1.293	1.126
1460 - 1410 cm^{-1}	0.226	0.224	0.204
1060 - 980 cm^{-1}	1.883	1.827	1.764
939 cm^{-1} (950 - 930)	0.031	0.03	0.031
913 cm^{-1} (920 – 900)	0.067	0.066	0.063
875 cm^{-1} (890 – 860)	0.101	0.095	0.093
799 cm^{-1} (820 - 780)	0.085	0.097	0.085
747 cm^{-1} (760 - 730)	0.233	0.234	0.22
689 cm^{-1} (700 - 675)	0.046	0.05	0.046

The FTIR spectra of coal conditioned at pH 10, with various surfactin concentrations, are given in Figure 21. The corresponding peak areas for the major peaks are given in Table 15. As surfactin concentration increases from 0 mg/L to 5 mg/L, the absorbance across the 4000 - 1800 cm^{-1} range increases as well. However, when the surfactin concentration is further increased to 15 mg/L, the absorbance subsequently decreases to below the 0 mg/L surfactin absorbance. This indicates a reduction in surface -OH functional groups at high surfactin concentration (15 mg/L), but increased surface -OH functional groups at low concentration (5 mg/L). The same trend is seen in the peak areas associated with clay minerals, Si-O bonds and Si-O-Al^{iv} in the 3700 – 3600 cm^{-1} peak range, peak 1029 cm^{-1} and 1010 cm^{-1}, and peaks 799 cm^{-1} and 746 cm^{-1} respectively. Each relative peak area is increased at 5 mg/L compared to 0 mg/L surfactin, and then decreases at 15 mg/L surfactin. It seems as if surfactin removes positive ions from the clay mineral surface at low surfactin concentrations (5 mg/L) and as concentration increases to 15 mg/L surfactin, surfactin interacts further with those cleared sites to reduce the clay mineral surface functional groups.

At 5 mg/L surfactin concentration there is an increased peak area for the peaks associated with the aliphatic C-H bonds in the 3000 - 2800 cm^{-1} range compared to 0 mg/L surfactin concentration. The peak area decreases compared to 0 mg/L as the surfactin concentration increases to 15 mg/L. The same trend is seen for the 1680 – 1500 cm^{-1}, and 1432 cm^{-1} and 1452 cm^{-1} peak areas. This indicates that at a low surfactin concentration of 5 mg/L, there is an increase in the aliphatic and aromatic surface groups, which decreases at high surfactin concentration compared to 0 mg/L. The reason for this is not clear and requires further investigation.

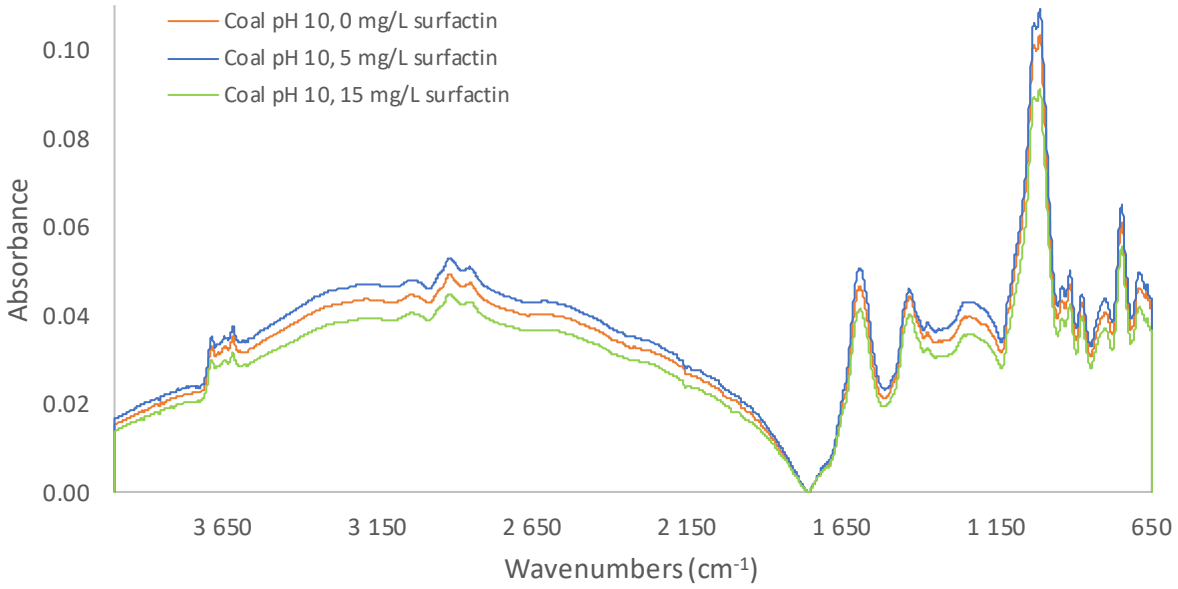

Figure 21: FTIR spectra from 4000 – 650 cm^{-1} of coal conditioned for various surfactin concentrations at pH 10. The orange, blue and green spectra represent the spectra of coal conditioned at pH 3 with a concentration of 0, 5 and 15 mg/L surfactin respectively. The spectra shown in the figure above are the average spectrums of independent duplicate repeats, baseline corrected for atmospheric H_2O and CO_2.

Table 15: Major peak areas for coal conditioned at pH 10 for various surfactin concentrations. The same peak ranges were used, with the baseline drawn through the lowest data points on either side of the peak, eliminating the absorbance offset and allowing areas to be comparable.

Peak range	0 mg/L surfactin - Peak area	5 mg/L surfactin - Peak area	15 mg/L surfactin - Peak area
3700 - 3600 cm^{-1}	0.2486	0.26	0.2255
3080 - 3000 cm^{-1}	0.0645	0.067	0.0595
2970 - 2800 cm^{-1}	0.5113	0.5611	0.4756
1660 -1550 cm^{-1}	1.301	1.409	1.124
1460 - 1410 cm^{-1}	0.246	0.251	0.227
1060 - 980 cm^{-1}	1.915	1.998	1.687
939 cm^{-1} (950 - 930)	0.032	0.033	0.028
913 cm^{-1} (920 – 900)	0.068	0.071	0.059
875 cm^{-1} (890 – 860)	0.132	0.122	0.124
799 cm^{-1} (820 - 780)	0.097	0.101	0.082
747 cm^{-1} (760 - 730)	0.24	0.253	0.221
689 cm^{-1} (700 - 675)	0.042	0.052	0.043

5.2.2.5 Summary of FTIR analysis of adsorption of surfactin onto coal

At a pH of 3 there is a reduction in peak area, as surfactin concentration increases, for the peaks associated with clay minerals, and the associated Si-O and Si-O-Al bonds, as well as for the peaks

associated with the aliphatic and aromatic functional groups. Surfactin forms a precipitate at pH 3 and from zeta potential analysis it was determined that this surfactin precipitate interacts with the coal surface. The FTIR analysis confirms that there is interaction between the surfactin precipitate and the coal surface, reducing the clay mineral, aliphatic and aromatic surface functional groups.

At a pH of 6, as surfactin concentration increases, there is an increase in peak area for the peaks associated with clay minerals, and the associated Si-O and Si-O-Al bonds, as well as for the peaks associated with the aliphatic and aromatic functional groups. Surfactin is probably partially ionised at pH 6 and this could lead to surfactin interacting and removing coal surface ions and thus exposing and subsequently increasing the peak areas of the relative surface functional groups

At a pH of 8 there is an increase in peak area, as surfactin concentration increases from 0 mg/L to 5 mg/L, for the peaks associated with clay minerals, and the associated Si-O-Al bonds, as well as for the peaks associated with the aliphatic and aromatic functional groups. However, there is a reduction in the peak area associated with the Si-O bonds as surfactin concentration increases to 5 mg/L. As the surfactin concentration is increased to 15 mg/L, there is a reduction in the peak area compared to 0 mg/L, for the peaks associated with clay minerals, and the associated Si-O and Si-O-Al bonds, as well as for the peaks associated with the aliphatic and aromatic functional groups. The surfactin molecule is fully ionised at pH 8. This would allow surfactin to interact with and remove coal surface ions at a concentration of 5 mg/L and subsequently produce the observed increase in peak area. As the surfactin concentration increases to 15 mg/L, these surfactin complexes again interact with the coal surface, most probably by hydrophobic interactions, producing the subsequent decrease in peak area seen.

At a pH of 10 the trend is the same as at pH 8, except that there is an increase in the peak area of the peak associated with the Si-O bonds at 5 mg/L surfactin, as opposed to the reduction seen at pH 8. The surfactin molecule is fully ionised at pH 10. This would allow it to interact with and remove coal surface ions at a concentration of 5 mg/L and subsequently produce the observed increase in peak area associated with clay minerals, and the associated Si-O and Si-O-Al bonds, as well as for the peaks associated with the aliphatic and aromatic functional groups. However, the electrostatic repulsion between the coal surface and the ionised surfactin molecule prevents further hydrophobic interaction between the surfactin and the coal surface. As the surfactin concentration increases to 15 mg/L, these surfactin complexes are able to overcome the electrostatic repulsion and again interact with the coal surface, most probably by hydrophobic interactions, producing the subsequent decrease in peak area seen.

There is no clear evidence of the presence of a peptide moiety on the surface of the coal. This could be due the peptide absorption bands being weaker and thus not visible, or could indicate that the adsorption of surfactin is relatively weak (Didyk-Mucha et al., 2019). However, surfactin does seem to change the coal surface, as evidenced by the change in peak areas experienced with the addition of surfactin. There is evidence that surfactin interacts with the coal surface at all pH values. But, the interaction mechanism between surfactin and the coal surface seems to be concentration dependent. At low surfactin concentration (5 mg/L) and particularly in alkaline pH values (pH 8 and 10), surfactin seems to have a

cleaning effect on the coal surface. At high surfactin concentration (15 mg/L), surfactin seems to interact via hydrophobic interactions with the coal surface.

5.2.3 Effect of pH and surfactin concentration on coal recovery

Zeta potential has been used to establish the occurrence and the type of adsorption between surfactin and the coal surface. FTIR analysis has been used to determine which coal surface functional groups interact with surfactin. In this section microflotation analysis will be used to tie all the previous analyses together and determine the effect of surfactin on the hydrophobicity of the coal surface and the subsequent coal recovery. The use of a microflotation cell reduces the hydrodynamic effects associated with flotation and allows greater emphasis on the reagent and mineral interactions. This discussion section aims to separate the effect of surfactin concentration from the effect of pH on surfactin during the recovery of coal through flotation.

5.2.3.1 Effect of surfactin concentration on coal recovery

The coal recovery at each surfactin concentration will be evaluated to determine the effect of surfactin concentration on coal recovery at different pH conditions. Coal flotation recovery as a function of pH for different surfactin concentrations is given in Figure 22.

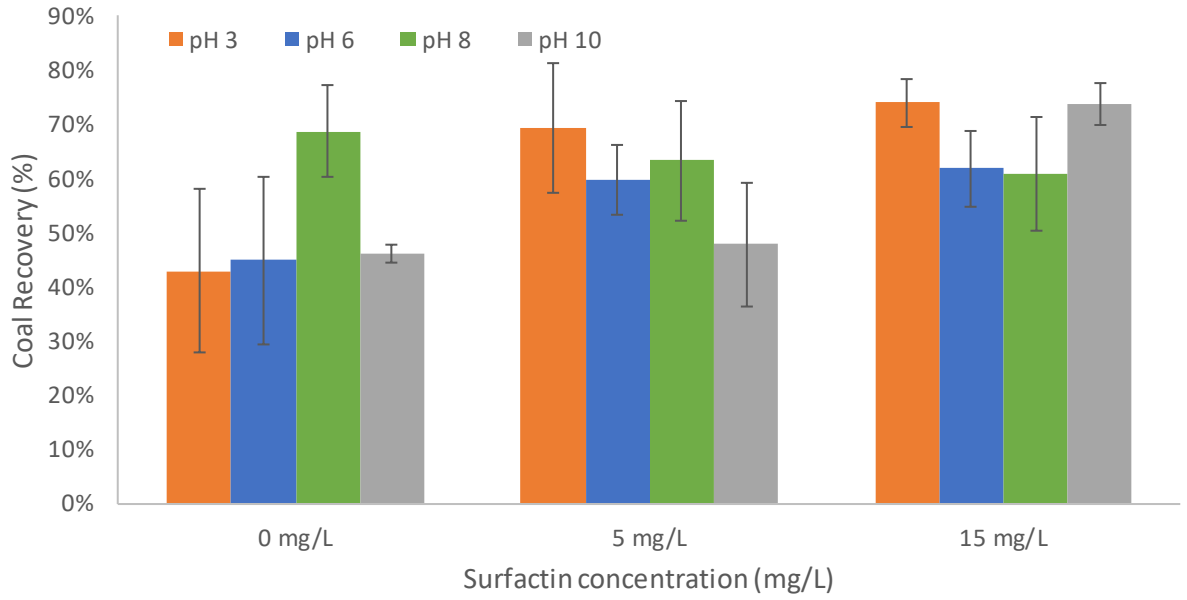

Figure 22: Coal flotation recovery as a function of pH and surfactin concentration. Experiments were conducted by floating 3 g coal in a microflotation cell over a 20 min period. Error bars represent the standard deviation for the duplicate repeats.

With the addition of 5 mg/L surfactin, there is an increase in coal recovery at pH 3, 6 and 10, but at pH 8 a decrease in coal recovery was observed. The largest increase in coal recovery at 5 mg/L surfactin concentration, compared to 0 mg/L surfactin concentration, was observed at pH 3, with the coal recovery increasing from 42.9% to 69.3%, followed by an increase in coal recovery from 44.9% to 59.7% at pH 6. The smallest increase was at pH 10, with the coal recovery increasing insignificantly from 45.9% to 47.8%.

At pH 8 there was a decrease in coal recovery from 68.6% to 63.3% as surfactin concentration was increased from 0 mg/L to 5 mg/L. The addition of 5 mg/L surfactin increased the hydrophobicity of coal insignificantly at pH 10, but significantly at pH 3 and 6, meaning surfactin acted as a coal collector in the acidic pH range (pH 3 and 6), but had no significant effect at pH 10. This follows the trend seen in the zeta potential analysis that showed that at low surfactin concentration (2 and 4 mg/L), surfactin had a noticeable effect on the coal zeta potential in the acidic pH range (pH 3 and 6), but no effect at pH 10.

The lack of effect on the zeta potential at pH 10 was attributed to the electrostatic repulsion force between the ionised surfactin and the coal surface, both negatively charged, being larger than the hydrophobic attraction force between the aliphatic groups of surfactin and the coal surface, and thus preventing adsorption between surfactin and the coal surface.

FTIR analysis indicates that at pH 10 and 5 mg/L, surfactin seems to have a cleaning effect on the coal surface rather than adsorbing onto the coal surface. The cleaning effect of surfactin is the removal of surface species from the coal surface by surfactin. The zeta potential analysis, FTIR analysis and the insignificant increase in coal recovery achieved in flotation at pH 10 at 5 mg/L surfactin concentration supports the theory that surfactin at low concentration (5 mg/L) at a pH of 10, the main interaction mechanism is that surfactin has a cleaning effect on the surface of coal and that no significant adsorption occurs.

At pH 8 and 5 mg/L surfactin concentration, surfactin acts as a depressant and reduces coal hydrophobicity. Zeta potential analysis indicated that there is some adsorption of surfactin onto the coal surface at low surfactin concentrations (2 and 4 mg/L). This is supported by the FTIR analysis that indicates that the surfactin cleaning effect takes place on the surface of coal, but that there is indication of adsorption onto the Si-O sites on the coal surface. Thus, the hypothesis is that at pH 8 surfactin cleans off certain surface species and forms complexes with these species. The nature of these surface species is unknown and would need further investigation. The surfactin complexes then adsorb hydrophobically onto the surface of coal, with the complexed peptide moiety of surfactin in contact with the water. This orientation of the surfactin complex decreases the hydrophobicity of the coal surface and causes the depression of coal in the flotation.

Increasing the surfactin concentration from 5 mg/L to 15 mg/L causes an increase in coal recovery at pH 3, 6 and 10, with pH 8 being the exception once again, where surfactin still depresses the coal recovery. The recovery of coal increases to 74.0%, 61.8% and 73.7% for pH 3, 6 and 10 respectively, but decreases slightly to 60.7% for pH 8. Thus at 15 mg/L surfactin concentration, surfactin acts as a coal collector that significantly increases the hydrophobicity of coal at pH 3, 6 and 10, but remains a coal depressant at pH 8. Considering the zeta potential analysis and FTIR analysis indicate that surfactin adsorption takes place at pH 8 at 15 mg/L surfactin concentration, the decrease in coal recovery is contradictory. However, it could simply be that the maximum possible coal recovery at pH 8 has been reached, as the coal recovery is relatively similar to that of pH 3, 6 and 10. This is supported by the relatively small increase in coal recovery of 2 – 5 % from increasing the surfactin concentration form 5 mg/L to 15 mg/L, compared to the coal recovery increase of 15 – 26% observed from the surfactin

concentration increase from 0 mg/L to 5 mg/L for pH 3 and 6, that suggest that there is a maximum possible coal recovery, even with the addition of a higher surfactin concentration. Zeta potential analysis also suggested that a maximum adsorption had been reached at 15 mg/L from pH 4 – 7, further strengthening the maximum adsorption theory. The flotation kinetics explored in the next section might provide further insight into whether a maximum has been reached. At pH 10 at 15 mg/L surfactin concentration, the repulsive forces between the surfactin molecules and the coal surface are overcome by the formation of surfactin micelle structures. Zeta potential and FTIR analysis at pH 10 with 15 mg/L surfactin also showed that the repulsive forces were overcome, strengthening the argument.

An increase in surfactin concentration has been observed to cause a definite increase in coal recovery by flotation, with the exception of pH 8. Although some experimental conditions have large standard deviations, the general trend is strong enough to provide some degree of confidence. The main interaction mechanism between surfactin and the coal surface seems to be the cleaning effect of surfactin, followed by the hydrophobic adsorption of surfactin complexes onto the surface of coal. Lastly there appears to be a maximum possible coal recovery using surfactin. Surfactin appears to be an effective collector of coal, especially in the acidic pH range and at high surfactin concentrations (15 mg/L). Although surfactin did produce some depression of coal at pH 8, it is not an effective depressant of coal. These coal flotation results answer one of the key questions: Verifying that surfactin does indeed float and to some extent depress coal.

5.2.3.2 Effect of pH on coal recovery with surfactin

The coal recovery at each pH value will be evaluated to determine the effect of pH on coal recovery at different surfactin concentrations. Coal flotation recovery as a function of pH for different surfactin concentrations is given in Figure 22.

Surfactin acts as a coal collector at a pH of 3 for a high (15 mg/L) and a low (5 mg/L) surfactin concentration. The fact that there is a noticeable increase in coal recovery is of interest because surfactin precipitates at a pH of 3 (Long et al., 2017). Thus, the increase in hydrophobicity with the addition of surfactin at pH 3, is thought to be due to the surfactin precipitate interacting with the coal surface. Surfactin molecules either precipitate onto the surface of coal or forms precipitate structures that adsorb onto the surface of coal. This theory is supported by the FTIR analysis and the zeta potential experiments that show a notable interaction between surfactin and the coal surface at pH 3, indicating some type of adsorption occurs.

As the pH increases from 3 towards 6, the coal surfaces become less hydrophobic in the presence of surfactin, for both high (15 mg/L) and low (5 mg/L) surfactin concentrations. However, surfactin remains a collector at both surfactin concentrations. FTIR analysis indicated that surfactin had a cleaning effect at pH 6, which could contribute to the decrease in hydrophobicity compared to pH 3.

Further increasing the flotation pH from 6 to 8, the hydrophobicity of coal remains largely the same at low (5 mg/L) and high surfactin concentration (15 mg/L). This could be the result of the same surfactin cleaning effect seen at both pH 6 and pH 8. However, compared to 0 mg/L surfactin concentration at

pH 8, surfactin acts as a depressant at pH 8. This was speculated to be due to there being a maximum possible coal recovery having been reached at 0 mg/L surfactin and that the addition of surfactin and the accompanying cleaning effect of surfactin, as seen in the FTIR analysis, caused a reduction in the hydrophobicity of coal and the resulting coal recovery was lower.

By increasing the flotation pH from 8 to 10, there is a decrease in coal hydrophobicity at low surfactin concentration (5 mg/L), but an increase in the hydrophobicity of coal at high surfactin concentration (15 mg/L). However, compared to 0mg/L surfactin concentration at pH 10, surfactin has no significant effect on the hydrophobicity of coal at low surfactin concentration (5 mg/L) at pH 10. There is evidence from the zeta potential and FTIR analysis that surfactin may have cleaning effect at 5 mg/L concentration, but the electrostatic repulsion force between the ionised surfactin and the negatively charged coal surface is too high to allow adsorption. Increasing the surfactin concentration to 15 mg/L overcomes these repulsion forces as seen with the large increase in coal recovery and the significant zeta potential response. The repulsion forces are thought to be overcome at high surfactin concentration (15 mg/L) by the formation of surfactin aggregates and micelles, as 15 mg/L is above the CMC value of surfactin.

The effect of pH on the recovery of coal with and without the addition of surfactin was evaluated. There is a decrease in coal recovery as pH is increased at 5 mg/L surfactin concentration. At 15 mg/L surfactin concentration, the pH values closer to neutral (pH 6 and 8) showed reduced coal recovery compared to the pH extremes (pH 3 and 10). Flotation at pH 3 is not practical on an industrial scale and thus the recommended operating pH for using surfactin as a collector for coal is pH 10. Contributing to the recommendation is the fact that coal flotation at pH 10 also provides an excellent coal recovery of 74% at 15 mg/L surfactin concentration. However, if the goal is to have minimal interaction between surfactin and coal, then pH 10 at 5 mg/L surfactin concentration is recommended. At pH 10 and 5 mg/L surfactin concentration, there is an increase in coal recovery of less than 2% compared to 0 mg/L surfactin concentration.

5.2.4 Effect of pH and surfactin concentration on coal flotation rate constant

All unmeasured flotation variables are lumped together using the rate constant, providing an engineering measure of flotation (Wills and Napier-Munn, 2005). At this stage of the research into the flotation abilities of surfactin, where individual variables have not yet been explored sufficiently to elucidate their effects, the lumped constant approach is a sensible way to evaluate floatability. The coal flotation rate constants as a function of surfactin concentration and pH are given in Figure 23. The rate constants were determined by fitting flotation recovery vs time data to a first order kinetics model, which is discussed in greater detail in the Methods section (section 4.3.4.3).

There is a strong correlation between the coal flotation rate constants in Figure 23 and their respective recoveries in Figure 22. The rate constants in the acidic range (pH 3 and 6) are approximately the same at 5 mg/L and 15 mg/L, indicating that the increasing the surfactin concentration above 5 mg/L does not have any additional effect or benefit. This indicates that there are no additional binding sites for surfactin and that the peak surfactin adsorption capacity in the acidic pH range is below 5 mg/L surfactin concentration. This also strengthens the theory that a maximum possible coal recovery has been reached

as discussed in the previous flotation section. The flotation rate constant is observed to be significantly higher at pH 3 than pH 6. Indicating that the surfactin precipitates are much more effective at interacting with the coal surface than a partially ionised soluble surfactin molecule at pH 6.

The two pH values (pH 8 and 10) in the alkaline pH range show opposing flotation rate constant trends. The flotation rate constant at pH 8 decreases with increasing surfactin concentration, whereas the flotation rate constant at pH 10 increases with increasing surfactin concentration. The decrease in flotation rate constant at pH 8 shows that surfactin exhibits clear depressant characteristics at pH 8. This depressant effect is seen much clearer than in the previous flotation recovery section. The only pH value at which surfactin presents any depressant effects is at pH 8. The highest flotation rate constant is found at pH 10 at 15 mg/L, indicating the formation of surfactin aggregates or micelles significantly improves the flotation.

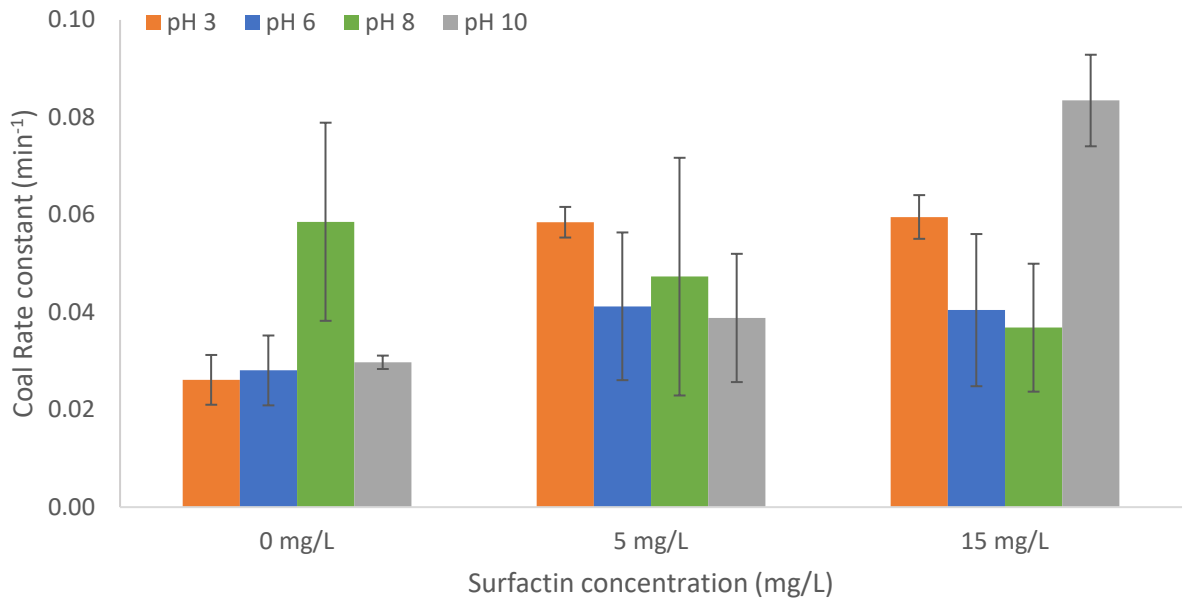

Figure 23: Coal flotation rate constants as a function of pH and surfactin concentration. Experiments were conducted by floating 3 g coal in a microflotation and determining the first-order rate constants over the period of 0 – 6 min.

The coal recovery as a function of flotation time at various surfactin concentrations and pH values are given in Figure 24. Figure 24: A, B, C and D show that at both 5 mg/L and 15 mg/L surfactin concentration, all kinetic first order model curves have a more logarithmic shape than linear, with the exception of 5 mg/L surfactin concentration at pH 10. This logarithmic model indicates that a maximum coal recovery is approached during flotation. It is also observed that there is not much difference between the 5 mg/L and 15 mg/L surfactin concentration kinetic models, with 5 mg/L surfactin at pH 10 being the exception once again. This suggests that at pH 3, 6 and 8, an increase in surfactin concentration above 5 mg/L does not produce a significant effect on the coal recovery. These observations confirm similar findings discussed in the zeta potential, FTIR and flotation sections, that indicate that the adsorption sites for

surfactin on the coal surface are limited and that a maximum adsorption has been reached. Practically, this means that coal flotation using surfactin is rate limited and that adding a surfactin concentration above 5 mg/L, with the exception of pH 10, is an unnecessary excess of reagent which may have cost implications to the process and increase the operating cost. The first order model shows a relatively good fit to the experimental data, indicating the first order model appropriately describes coal flotation using surfactin.

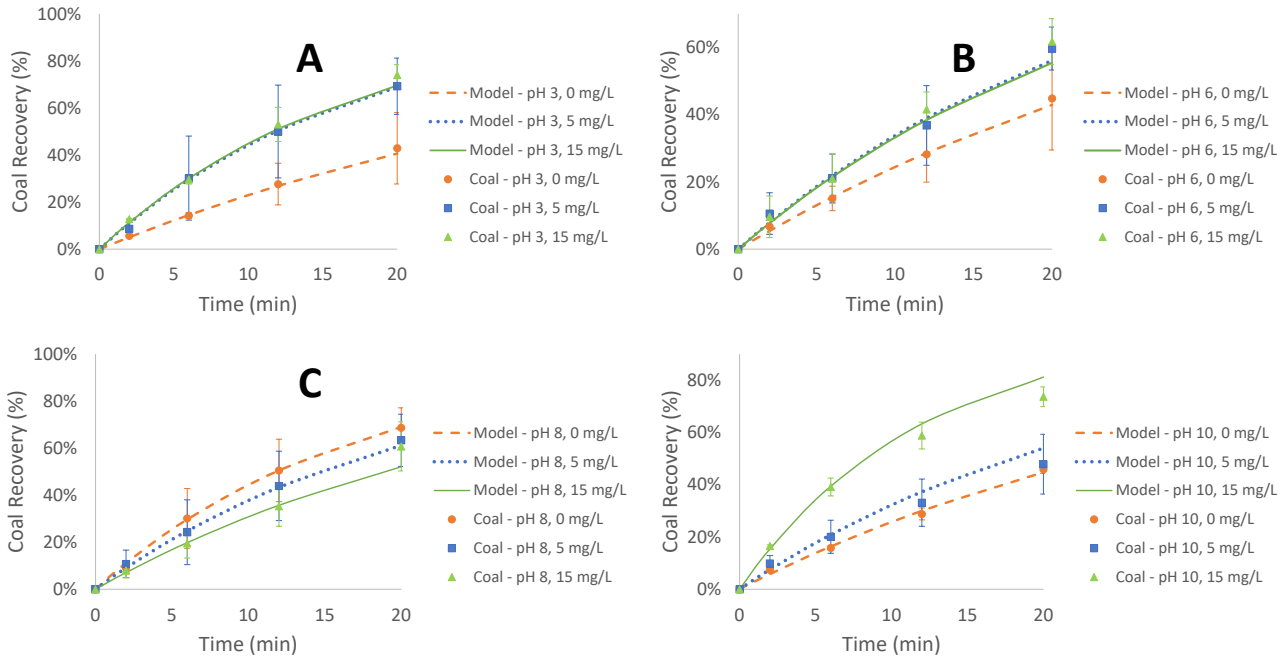

Figure 24: Coal recovery as a function of flotation time at various pH values and surfactin concentrations. Experiments were conducted by floating 3 g coal in a microflotation and collecting concentrate samples at 2-, 6-, 12- and 20-min. Figure A, B, C and D represent flotation at pH 3, 6, 8 and 10 respectively. The experimental flotation recovery values at 0 mg/L (●), 5 mg/L (■) and 15 mg/L (▲) surfactin concentrations are given by the data points. The orange (- - -), blue (·····) and green (——) lines represent first order kinetics models fitted using the rate constants to the corresponding 0, 5 and 15 mg/L surfactin concentration.

5.2.5 Application of surfactin as a coal flotation agent

Surfactin increases the hydrophobicity of coal and acts as a collector of coal in the acidic pH range (pH 3 and 6) at low surfactin concentration (5 mg/L) and high surfactin concentration (15 mg/L). In the alkaline pH range surfactin acted as a depressant of coal at pH 8, although not very well, and had no significant effect on coal recovery at pH 10 for 5 mg/L surfactin concentration, but performed as a very effective collector of coal at 15 mg/L surfactin concentration at pH 10. Thus, to achieve the highest coal recovery, flotation would need to occur at pH 10 and 15 mg/L surfactin concentration and for the lowest coal recovery in the presence of surfactin, flotation of coal would again need to occur at pH 10, but at 5 mg/L surfactin concentration.

When considering the application towards coal desulphurisation, surfactin can be used either to increase the hydrophobicity of coal to float coal while pyrite is depressed, or used as a depressant in reverse coal flotation, where the coal is depressed while pyrite is floated. However, as pyrite is a positive-type semiconductor, the ionisation of the anionic surfactin groups above pH 6 will cause electrostatic attraction between surfactin and pyrite, theoretically increasing the hydrophobicity of pyrite. Thus, to discriminate between the hydrophobicity of pyrite and coal, coal would have to be depressed while pyrite is floated, in order to achieve the desired separation. Adopting a reverse flotation process, using a low surfactin concentration (5 mg/L) should provide the desired separation, causing depression of coal, and flotation of pyrite. This theory will be explored further after the evaluation of the effect of surfactin on pyrite in the next section.

5.3 The effect of surfactin on pyrite hydrophobicity

Following the evaluation of the effect of surfactin on coal hydrophobicity, the same will be done for the effect of surfactin on pyrite hydrophobicity. In this section the following objectives will be explored for the interaction between surfactin and pyrite:

1. Evaluate the effect of the pyrite surface charge on the adsorption of surfactin.
2. Evaluate the attachment mechanism of surfactin to the surface of pyrite.
3. Evaluate the effect of surfactin on the hydrophobicity of pyrite.

5.3.1 Zeta potential of pyrite with surfactin adsorption

Zeta potential analysis would provide an indication if surfactin adsorption on pyrite took place. This would be shown by neutralisation of the pyrite surface charge or by an increased surface charge and shifting isoelectric point (IEP), with the addition of surfactin, depending on the adsorption mechanism. Fuerstenau and Pradip (2019) showed that the response of the zeta potential curve to the addition of a surfactant, provided a hint of the possible adsorption mechanism. This method will be used to determine the adsorption mechanism for surfactin onto pyrite. The zeta potential of pyrite as a function of pH is given in Figure 25. The standard deviation for the independent duplicate (0, 2, 4 & 15 mg/L) repeats of each data point are shown by the error bars. The isoelectric point (IEP) for pyrite with the addition of 0, 2, 4 and 15 mg/L surfactin, was found to be 2.98, 2.55, 2.62 and 2.08 respectively. It can be seen that the IEP decreases as the surfactin concentration increases. The pyrite surface charge becomes more negative, with the addition of surfactin, in both the positive zeta potential region, above the IEP, and the negative zeta potential region, below the IEP.

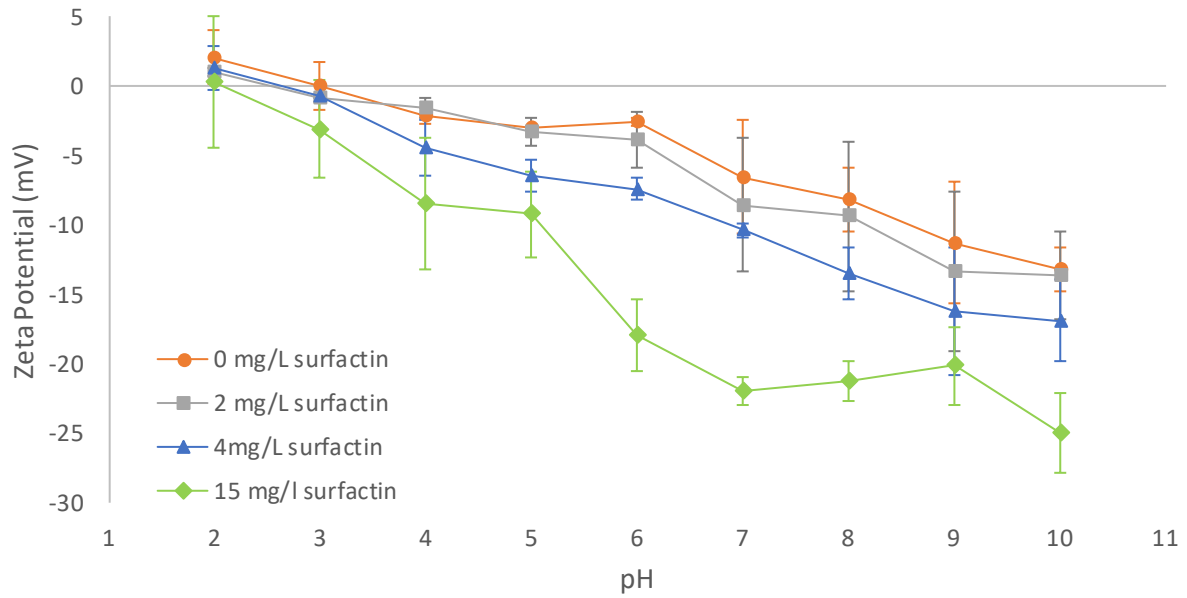

Figure 25: Zeta potential of pyrite as a function of pH and surfactin concentration. The orange (—●—), grey (—■—), blue (—▲—) and green (—◆—) data points represent the zeta potential of pyrite with the addition of 0, 2, 4 and 15 mg/L surfactin concentration respectively, across the pH range of 2 – 10. Data points have been connected linearly to better illustrate the resulting trends. The error bars represent the standard deviation for the independent duplicate repeats of each data point.

Hydronium (H_3O^+) and hydroxyl (OH^-) ions are the potential-determining ions for pyrite. The pyrite surface charge may be caused by ferrous cations and sulphide or polysulphide anions. However, pyrite is unstable in aqueous solutions and thus it is difficult to determine the exact surface conditions. Fornasiero et al. (1992) demonstrated that the IEP of pyrite changes to approximately pH 2 when conditioned for 30 min in an aqueous solution in the presence of air, compared to an IEP of 1.2 for pyrite conditioned for 30 min in an aqueous solution in the presence of argon. The IEP of pyrite increased to an approximate pH of 5.2 after conditioning for 2 hours in an aqueous solution in the presence of air. Thus, the IEP of pyrite can be used to determine the degree of surface oxidation of pyrite, as the IEP of pyrite shifts towards the higher IEP of its respective metal oxides as oxidation occurs (Fornasiero et al., 1992). At an IEP of 2, pyrite is slightly oxidized, compared to an IEP of 5.2, where pyrite is completely oxidized.

The experimental IEP of pyrite, without surfactin addition, was found to be 2.98, and thus can be said to be slightly oxidized. XRD analysis of the pyrite used for these experiments indicate a purity of 99.3% pyrite. Thus, the IEP difference compared to literature is due to oxidation of the pyrite, and not due to impurities in the pyrite sample. The experimental zeta potential of the pyrite surface at 0 mg/L surfactin concentration, is net positive from pH 2 to pH 2.98, as seen in Figure 25. The net positive charge is attributed to the formation of ferric ions on the pyrite surface. The surface becomes more negative as pH increases, and the net negative surface charge from pH 2.98 to pH 10, is due to the specific adsorption of hydrolysed ferric ions, eventually forming a hydroxide or oxide film in the form of hematite, magnetite or goethite on the mineral surface (Fornasiero et al., 1992; Lotter et al., 2016).

The addition of surfactin causes the IEP of pyrite to shift towards lower pH values. This indicates that there is adsorption of surfactin onto the pyrite surface. According to Fuerstenau and Pradip (2019) a distinct shift in the IEP, in the presence of a surfactant, compared to the IEP without surfactant addition, indicates the surfactant chemisorbed onto the mineral surface. Thus, surfactin can be considered to have chemisorbed onto the surface of the pyrite, perhaps through the chelating ability of the carboxylic functional groups of surfactin. Didyk-Mucha et al. (2019) proposed that surfactin analogues may interact with the structural metal ions on the surface of magnesite and serpentinite, forming surfactin salts. A comparison could be drawn to the surface of pyrite, which also has these same structural metal ions. Further studies showed surfactin forming complexes with metal ions such as Ni^{2+}, Zn^{2+}, Cd^{2+}, Cu^{2+}, Mg^{2+} and Pb^{2+} (Arutchelvi et al., 2014; Janek et al., 2019; Mulligan et al., 1999b). Therefore, it can be confidently said that this is the interaction mechanism between surfactin and the pyrite surface.

Increasing the surfactin concentration from 0 mg/L to 2 mg/L has no effect on zeta potential in the acidic range (pH 2 – 6) and little effect in the neutral and alkaline range (pH 6 – 10). This indicates that surfactin only interacts with the pyrite surface, at low concentration (2 mg/L), in the alkaline pH range. This would be due to surfactin becoming ionised at pH 6 and thus being able to electrostatically interact with surface sites.

As the surfactin concentration increases from 2 mg/L to 4 mg/L, there is a more pronounced effect on the zeta potential from pH 4 to 10. The zeta potential becomes more negative indicating that the maximum surfactin adsorption has not yet been reached at 2 mg/L. At pH 2- 3 the increase in surfactin still has no significant effect on zeta potential. This is most likely due to surfactin being a precipitate at pH 2 and 3.

Further increasing the surfactin concentration to 15 mg/L shows that the pyrite zeta potential becomes more negative compared to 4 mg/L, indicating further surfactin interaction. At pH 3 there is a slight but noticeable decrease in the zeta potential of pyrite as the surfactin concentration is increased to 15 mg/L. This would indicate that there is some interaction between the surfactin precipitate and the pyrite surface at pH 3 and 15 mg/L. There is a greater response from pH 6 to pH 10 at 15 mg/L compared to the other surfactin concentrations. As mentioned earlier, the surfactin molecule becomes ionised at pH 6. This combined with the formation of surfactin micelles, or surfactin bilayer or surfactin aggregates through hydrophobic surfactin-surfactin interactions, where the additional negative charge is not reduced, could explain the greater negative zeta potential response.

The experimental IEP of pyrite compared to the literature IEP of pyrite indicates that there was slight oxidation of the pyrite surface. Surfactin addition showed little to no effect on the zeta potential of pyrite in the acidic pH range (pH 2 - 6) at low surfactin concentration (2 and 4 mg/L), due to the formation of a surfactin precipitate. A significant decrease in zeta potential was seen in the pH 6 – 10 range in the presence of 15 mg/L surfactin concentration, which indicates that the ionisation of surfactin at pH 6, and above, plays a significant role in the adsorption of surfactin onto pyrite. The distinct shift in the IEP of pyrite indicates that surfactin chemisorbed onto the surface of pyrite. This is most likely due to chelation between the pyrite surface metal ions and the carboxylic functional groups on surfactin molecules. The

addition of FTIR analysis, discussed in the next section, would allow verification of surfactin adsorption onto the pyrite surface by two different analysis methods, and provide additional insight and clarity into the adsorption mechanism by giving an indication with which pyrite surface functional groups surfactin molecules interact.

5.3.2 FTIR analysis on the adsorption of surfactin on pyrite

5.3.2.1 Pyrite spectra peak assignment.

The spectrum peaks of pyrite need to be identified and assigned to the most likely functional group bonds that produce the respective peak response. This allows differentiation between peaks associated with pyrite functional groups and the functional groups associated with surfactin.

The FTIR spectrum of the pyrite used for this study is shown in Figure 26. The 4000 – 3000 cm^{-1} range was assigned to the OH− vibrations of hydrated Fe-hydroxides. Little response was seen in this range, indicating little oxidation as expected for freshly milled pyrite. This confirms the zeta potential analysis that indicated that the pyrite surface was slightly oxidized. The peaks in the 2400 - 2000 cm^{-1} range were assigned to overtones and combination bands as no literature was found identifying peaks in this range for pyrite spectra. The noise seen around 1650 cm^{-1} and 1400 cm^{-1} is associated with waters of hydration (water incorporated into the crystalline structure of metal complexes) and ferric and ferrous hydroxide species respectively. The broad peak from 1200 – 1050 cm^{-1} was assigned to the S-O bonds in SO_3^{2-} and SO_4^{2-}, and their associated species that occur as a result of surface oxidation in air. The peaks at 795 cm^{-1} and 704 cm^{-1} are associated with ferric oxyhydroxides. The peak at 664 cm^{-1} is assigned to the S-S-O vibrations associated with the oxidation of the disulphide groups. The stretching vibrations associated with the S-S bonds of the sulphide groups are in the 420 - 510 cm^{-1} range, but due to equipment limitations, are not visible in these spectrums (Chernyshova, 2003; Dunn et al., 1993; Güler et al., 2013; Weerasooriya et al., 2010).

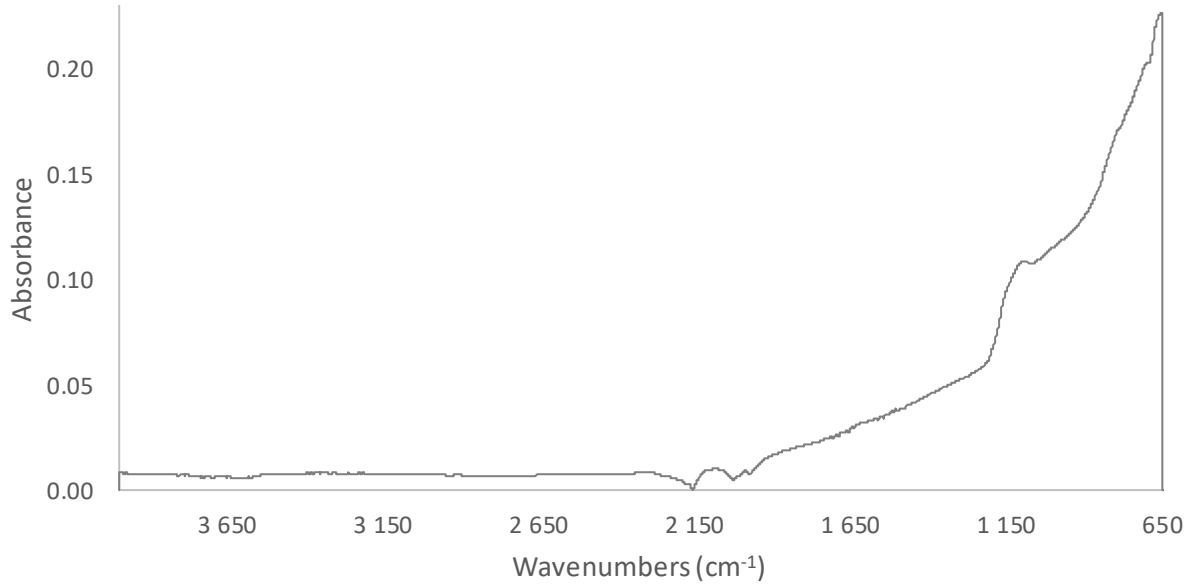

Figure 26: FTIR spectrum of dry pyrite from 4000 – 650 cm^{-1}. The spectrum shown in the figure above is the average spectrum of independent duplicate repeats, baseline corrected for atmospheric H_2O and CO_2.

5.3.2.2 Effect of pH on the FTIR spectrum of pyrite

The effect of pH on the surface of pyrite should be explored in order to differentiate the effect of pH from the effect of surfactin concentration. The spectra of pyrite conditioned at various pH conditions are given in Figure 27. The corresponding peak areas for the major peaks are given in Table 16.

It can be clearly seen that there is a major reduction in the 2077 cm^{-1}, 1990 cm^{-1}, 1200 – 1600 cm^{-1}, 795 cm^{-1} and 704 cm^{-1} peak area compared to dry pyrite. The changes are most probably associated with the hydration effect on the S-O bonds and the associated overtones and combination bands, reducing the peak areas.

The difference in peak areas between different conditioning pH values were subtle. However, a higher peak area for the broad 1200 – 1060 cm^{-1} S-O bond vibration range associated with SO_3^{2-} and SO_4^{2-} was found for pH 6 and 10, compared to pH 3 and 8. The peak areas at 795 cm^{-1} and 704 cm^{-1}, associated with ferric oxyhydroxides, 1475 - 1270 cm^{-1}, associated with Fe-hydroxides, and 1690 – 1580 cm^{-1}, associated with water of hydration, increased slightly at pH increased, as expected due to the higher -OH concentration at higher pH values. Various changes occurred in the peak areas in the 2400 - 2000 cm^{-1} range, but due to this range being combination bands it is difficult to determine the possible causes. There is the formation of new peaks at 2357 cm^{-1} and 2341 cm^{-1} at pH 3 exclusively. This could be a combination band of a sulfur bond visible at low pH. At higher pH values these bonds would be covered and hidden by S-O and hydroxide bonds.

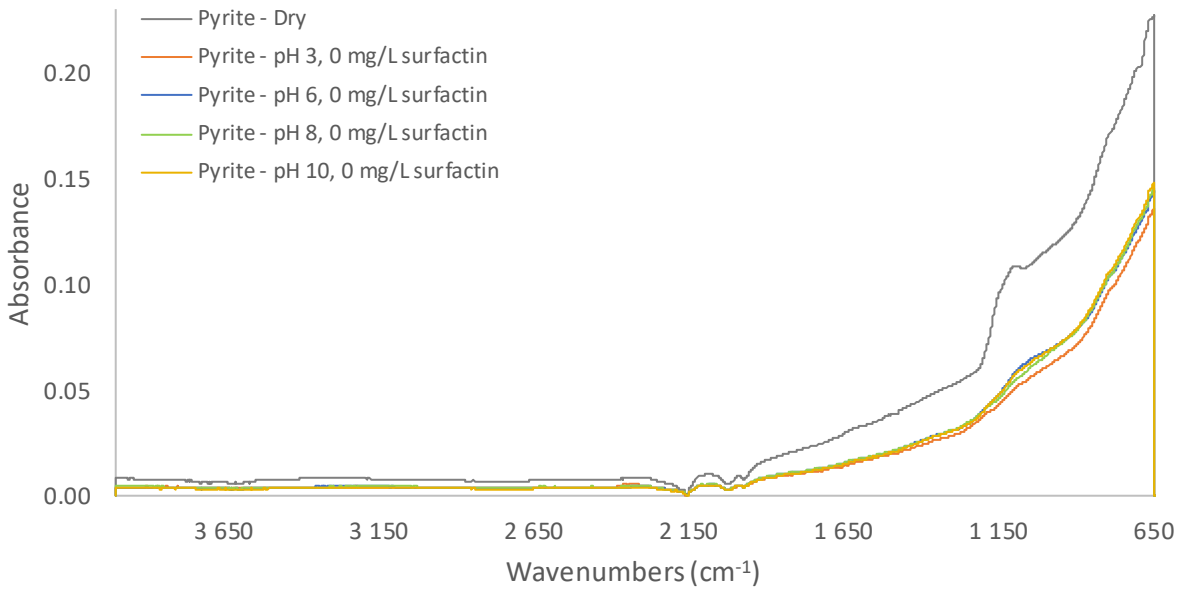

Figure 27: FTIR spectra from 4000 – 650 cm^{-1} of pyrite conditioned at various pH conditions. The grey, orange, blue, green and yellow spectra represent the spectra of dry pyrite and pyrite conditioned at pH 3, 6, 8 and 10 respectively. The spectra shown in the figure above are the average spectrums of independent duplicate repeats, baseline corrected for atmospheric H_2O and CO_2.

Table 16: Major FTIR peak areas of pyrite for various pH conditions. The same peak ranges were used, with the baseline drawn through the lowest data points on either side of the peak, eliminating the absorbance offset and allowing areas to be comparable.

Peak range	Dry coal – Peak area	pH 3 – Peak area	pH 6 – Peak area	pH 8 – Peak area	pH 10 – Peak area
2980 - 2830 cm^{-1}	0.0061	0.0043	-0.0041	0.0028	0.0024
2380 - 2335 cm^{-1}	0.0035	0.0136	-0.0019	-0.0016	-0.0032
2328 cm^{-1} (2335 - 2320)	0.0005	0.0016	0.0020	0.0007	0.0006
2288 cm^{-1} (2320 - 2270)	0.0165	-0.0008	0.0104	0.0136	0.0074
2077 cm^{-1} (2150 - 2030)	0.5312	0.2498	0.2719	0.2880	0.2831
1990 cm^{-1} (2030 1980)	0.0332	0.0099	0.0126	0.0140	0.0097
1690 - 1580 cm^{-1}	0.0551	0.0112	0.0219	0.0296	0.0189
1560 - 1475 cm^{-1}	0.0406	0.0288	0.0022	0.0268	0.0122
1475 - 1270 cm^{-1}	0.0876	0.0312	0.1056	-0.0191	0.0501
1200 - 1060 cm^{-1}	1.335	0.0140	0.0380	0.0110	0.0720
795 cm^{-1} (810 - 785)	0.027	0.0140	0.0150	0.0120	0.0160
704 cm^{-1} (720 - 690)	0.044	0.0120	0.0120	0.0160	0.0180

5.3.2.3 FTIR analysis of adsorption of surfactin onto pyrite

Having established that surfactin adsorbs onto the surface of pyrite, using zeta potential analysis, and establishing the effects of pH on pyrite, the FTIR spectra peak shapes and areas of pyrite with different surfactin concentrations are compared here to try and verify the presence of adsorbed surfactin and with which pyrite functional groups the surfactin molecules interact.

The FTIR spectra of pyrite conditioned at pH 3, with various surfactin concentrations, are given in Figure 28. The corresponding peak areas for the major peaks are given in Table 17. There is a clear increase in the peak area associated with the aliphatic groups in the 2980 -2830 cm^{-1} and 14755 – 1270 cm^{-1} range as surfactin concentration increases. This indicates the presence of surfactin on the surface of the pyrite at pH 3, even though surfactin precipitates at pH 3. Further evidence of surfactin on the pyrite surface is provided by an increase in the 1690 - 1580 cm^{-1} and 1560 – 1475 cm^{-1} range peak areas associated with the CO-N, and C-N and N-H bond vibrations respectively, associated with the peptide moiety of surfactin, as surfactin concentration increases. However, these ranges also contain the water of hydration and Fe-hydroxide bond vibrations respectively, which could also add additional contribution to increases in these associated peak areas.

The disappearance of the suspected sulfur bond formed at the combination peaks of 2360 cm^{-1} and 2328 cm^{-1} indicate possible interaction between surfactin and the suspected sulfur bonds. This could indicate interaction between the pyrite surface sulfur species and the amine groups in the surfactin molecule. Low pH conditions (pH 3) may cause protonation of the amide groups of surfactin, creating a positive site for the chelation of sulfur species on the pyrite surface. Several papers have suggested that the amide groups play a role in the chelation action of the surfactin molecules (Janek et al., 2019; Taira et al., 2015). This would make the amide groups the main collecting functional groups at pH 3. There is also an increase in the S-O bond peak area associated with sulfate and sulfite, but no significant increase in oxyhydroxide peak range area. This indicates that surfactin seems to have a preference for sulfur species at pH 3 and no discernible effect on iron species.

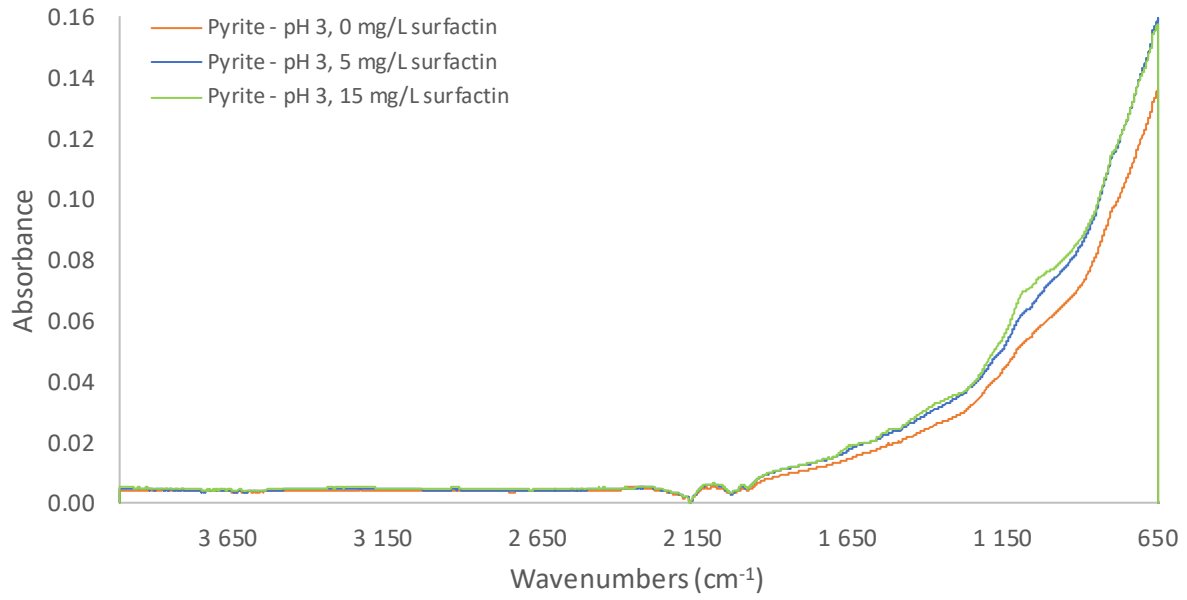

Figure 28: FTIR spectra from 4000 – 650 cm^{-1} of pyrite conditioned for various surfactin concentrations at pH 3. The orange, blue and green spectra represent the spectra of pyrite conditioned at pH 3 with a concentration of 0, 5 and 15 mg/L surfactin respectively. The spectra shown in the figure above are the average spectrums of independent duplicate repeats, baseline corrected for atmospheric H_2O and CO_2.

Table 17: Major peak areas for pyrite conditioned at pH 3 for various surfactin concentrations. The same peak ranges were used, with the baseline drawn through the lowest data points on either side of the peak, eliminating the absorbance offset and allowing areas to be comparable.

Peak range	0 mg/L surfactin - Peak area	5 mg/L surfactin- Peak area	15 mg/L surfactin- Peak area
2980 - 2830 cm^{-1}	0.0043	0.0236	0.0436
2380 - 2335 cm^{-1}	0.0136	-0.0031	-0.0025
2328 cm cm^{-1} (2335 - 2320)	0.0016	0.005	-0.0001
2288 cm^{-1} (2320 - 2270)	-0.0008	0.0086	0.0097
2077 cm^{-1} (2150 - 2030)	0.2498	0.3104	0.3032
1990 cm^{-1} (2030 1980)	0.0099	0.0165	0.0161
1690 - 1580 cm^{-1}	0.0112	0.0365	0.0954
1560 - 1475 cm^{-1}	0.0288	0.0382	0.0667
1475 - 1270 cm^{-1}	0.0312	0.0228	0.1711
1200 - 1060 cm^{-1}	0.014	0.041	0.077
795 cm^{-1} (810 - 785)	0.014	0.021	0.021
704 cm^{-1} (720 - 690)	0.012	0.015	0.015

The FTIR spectra of pyrite conditioned at pH 6, with various surfactin concentrations, are given in Figure 29. The corresponding peak areas for the major peaks are given in Table 18. Again, an increase in the aliphatic group vibration peaks areas in the 2980 – 2830 cm^{-1} range is seen with an increase in surfactin concentration. Increases in the peak areas of both the CO-N peak range at 1690 - 1580 cm^{-1} and the C-N

and N-H peak range at 1560 - 1475 cm^{-1} are seen with the corresponding increase in surfactin concentration. Increases in these peak areas confirm the presence of surfactin molecules on the surface of the pyrite at pH 6. There are no changes in the peak areas associated with the amide functional groups (CO-N, C-N and N-H) that would indicate the amide groups are the main collecting functional groups at pH 6. However, Janek et al. (2019) has suggested that the amide group of surfactin plays a role in the chelating of Cu^{2+} ions. A comparison could be drawn suggesting that amide groups of surfactin would also have a role in the chelation of Fe species on the pyrite surface.

However, the expected corresponding aliphatic peak area increase in the 1475 - 1270 cm^{-1} range was not seen as there was a decrease in that peak area with an increase in surfactin concentration. This would indicate that there is a reduction in the Fe-hydroxide bonds, as they are also associated with the 1475 - 1270 cm^{-1} range. This indicates a probable interaction between a partially ionised surfactin and the Fe-hydroxide sites, reducing the hydroxide sites. The same increase in the peak range areas associated with sulfate and sulfite, at 1200 - 1060 cm^{-1}, with the corresponding increase in surfactin concentration was seen at pH 6 as with pH 3. This would suggest that surfactin has a cleaning function, removing Fe-hydroxide species from the pyrite surface and stimulating the oxidation of sulfur to sulfate and sulfite. In future studies it might prove useful to look at the redox potential and gain insight into the potential redox effect of surfactin.

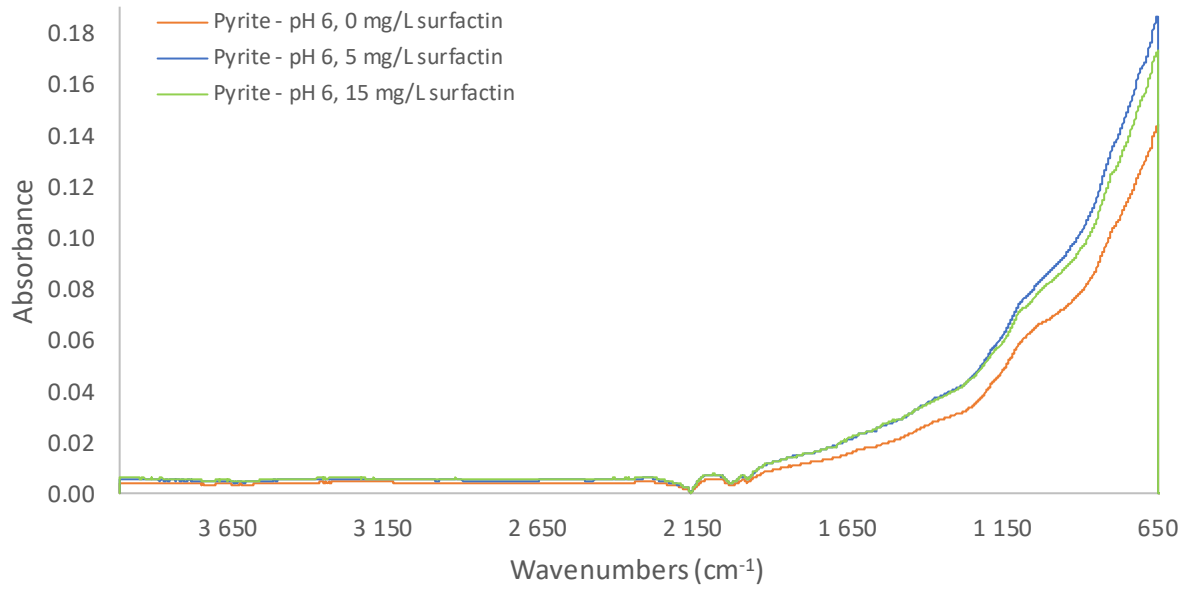

Figure 29: FTIR spectra from 4000 – 650 cm^{-1} of pyrite conditioned for various surfactin concentrations at pH 6. The orange, blue and green spectra represent the spectra of pyrite conditioned at pH 6 with a concentration of 0, 5 and 15 mg/L surfactin respectively. The spectra shown in the figure above are the average spectrums of independent duplicate repeats, baseline corrected for atmospheric H_2O and CO_2.

Table 18: Major peak areas for pyrite conditioned at pH 6 for various surfactin concentrations. The same peak ranges were used, with the baseline drawn through the lowest data points on either side of the peak, eliminating the absorbance offset and allowing areas to be comparable.

Peak range	0 mg/L surfactin - Peak area	5 mg/L surfactin - Peak area	15 mg/L surfactin - Peak area
2980 - 2830 cm^{-1}	-0.0041	0.0157	0.0439
2380 - 2335 cm^{-1}	-0.0019	-0.0019	-0.0012
2328 cm^{-1} (2335 - 2320)	0.002	0.001	0.0017
2288 cm^{-1} (2320 - 2270)	0.0104	0.0138	0.0088
2077 cm^{-1} (2150 - 2030)	0.2719	0.3479	0.39
1990 cm^{-1} (2030 1980)	0.0126	0.019	0.0179
1690 - 1580 cm^{-1}	0.0219	0.0411	0.0813
1560 - 1475 cm^{-1}	0.0022	0.0416	0.0517
1475 - 1270 cm^{-1}	0.1056	0.0895	0.0253
1200 - 1060 cm^{-1}	0.038	0.069	0.051
795 cm^{-1} (810 - 785)	0.015	0.012	0.022
704 cm^{-1} (720 - 690)	0.012	0.029	0.021

The FTIR spectra of pyrite conditioned at pH 8, with various surfactin concentrations, are given in Figure 30. The corresponding peak areas for the major peaks are given in Table 19. There is an increase in the aliphatic groups on the pyrite surface as surfactin concentration is increased, as indicated by the increase in peak areas for the 2980 - 2830 cm^{-1} and 1475 - 1270 cm^{-1} range. There is some change in the other peak areas associated with surfactin, but these are not significant and attributed to noise in the spectra. The strong indication of aliphatic groups however is enough to confirm surfactin presence on the pyrite surface.

Once again surfactin appears to cause the formation of sulphate and sulfite species on the pyrite surface as indicated by the increase in the 1200 - 1060 cm^{-1} peak range area. At 15 mg/L surfactin at pH 8, there was the reappearance of the 2980 - 2830 cm^{-1} peak range, which has previously been seen only at pH 3 with 0 mg/L. This was a combination band attributed to sulfur species, indicating that at 15mg/L at pH 8, the action of surfactin somehow exposes these sulfur species again. The exact mechanism is difficult to determine, and would require further study. As mentioned previously, looking into the potential redox effect of surfactin may lend insight into this mechanism.

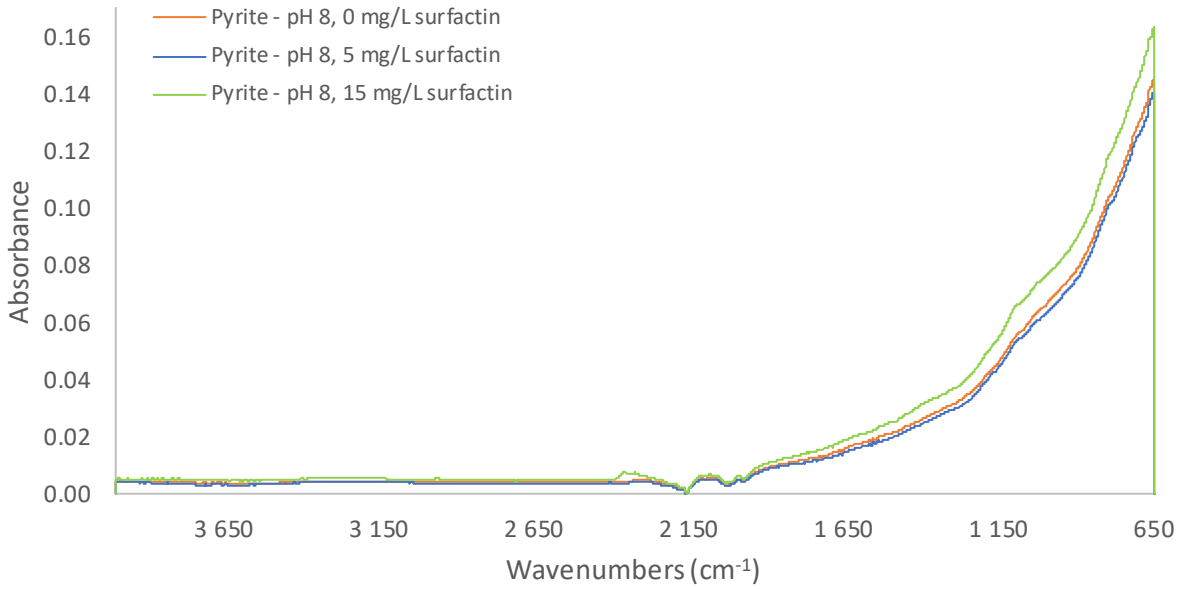

Figure 30: FTIR spectra from 4000 – 650 cm^{-1} of pyrite conditioned for various surfactin concentrations at pH 8. The orange, blue and green spectra represent the spectra of pyrite conditioned at pH 8 with a concentration of 0, 5 and 15 mg/L surfactin respectively. The spectra shown in the figure above are the average spectrums of independent duplicate repeats, baseline corrected for atmospheric H_2O and CO_2.

Table 19: Major peak areas for pyrite conditioned at pH 8 for various surfactin concentrations. The same peak ranges were used, with the baseline drawn through the lowest data points on either side of the peak, eliminating the absorbance offset and allowing areas to be comparable.

Peak range	0 mg/L surfactin - Peak area	5 mg/L surfactin - Peak area	15 mg/L surfactin - Peak area
2980 - 2830 cm^{-1}	0.0028	0.0073	0.0279
2380 - 2335 cm^{-1}	-0.0016	-0.0027	0.0282
2328 cm^{-1} (2335 - 2320)	0.0007	0.0002	0.0014
2288 cm^{-1} (2320 - 2270)	0.0136	0.0061	-0.0072
2077 cm^{-1} (2150 - 2030)	0.288	0.2544	0.3406
1990 cm^{-1} (2030 1980)	0.014	0.0116	0.016
1690 - 1580 cm^{-1}	0.0296	0.0217	0.0369
1560 - 1475 cm^{-1}	0.0268	0.0174	0.0303
1475 - 1270 cm^{-1}	-0.0191	0.0207	0.0708
1200 - 1060 cm^{-1}	0.011	0.024	0.077
795 cm^{-1} (810 - 785)	0.012	0.017	0.017
704 cm^{-1} (720 - 690)	0.016	0.019	0.004

The FTIR spectra of pyrite conditioned at pH 10, with various surfactin concentrations, are given in Figure 31. The corresponding peak areas for the major peaks are given in Table 20. There is a clear increase in the aliphatic group peak area in the 2980 - 2830 cm^{-1} range, when the surfactin concentration is increased to 5 mg/L. However, there is a decrease in the same peak area range compared to the peak area at 5 mg/L

when the surfactin concentration is increased from 5 mg/L to 15 mg/L. This seems to suggest that there is a reduction of surfactin molecules on the pyrite surface as surfactin concentration increases from 5 mg/L to 15 mg/L. However, a significant increase in the 1560 - 1475 cm^{-1} peak area, associated with the peptide moiety of surfactin, at the 15 mg/L surfactin concentration, indicates that the number of surfactin molecules on the surface of pyrite do not decrease as surfactin concentration is increased from 5 mg/L to 15 mg/L as suggested by the previously discussed peak area changes. Further, it is assumed the 1475 - 1270 cm^{-1} range is associated with Fe-hydroxide species, instead of the aliphatic groups, in this case as there is a decrease in peak area with increased surfactin concentration compared to 0 mg/L, which is not possible for aliphatic groups. Thus, from 0 mg/L to 5 mg/L surfactin concentration there is a decrease in the peak area at 1475 - 1270 cm^{-1} associated with the Fe-hydroxide species. This peak area then increases again as surfactin concentration increases from 5 to 15 mg/L. This suggests the removal of Fe-hydroxide species at 5 mg/L surfactin, and a subsequent return of these species as surfactin concentration is increased to 15 mg/L. Once again increasing the surfactin concentration causes the formation of sulphate and sulfite species on the pyrite surface as indicated by the increase in the 1200 - 1060 cm^{-1} peak range area. This again indicates that surfactin may have a cleaning effect on the surface of pyrite that causes the oxidation of sulfur.

These peak area changes suggest that at 5 mg/L surfactin concentration, surfactin interacts with the Fe-hydroxide groups, reducing the peak area of that bond. This interaction is most likely surfactin adsorbing onto the surface of pyrite. The peak area changes as the bulk surfactin concentration changes from 5 mg/L to 15 mg/L suggesting that rather than the surfactin presence on the surface of pyrite decreasing, as indicated by changes in the aliphatic group peak area, the surfactin molecules either change orientation or the formation of a surfactin bilayer or aggregate structure. This bilayer structure would reduce the exposure of aliphatic groups on the surface, as the peptide moiety covers these groups. In addition, the return of Fe-hydroxide species as surfactin concentration was increased from 5 mg/L to 15 mg/L, suggests that the second layer of surfactin molecules in the bilayer is chelated with Fe-hydroxide species. This means that surfactin chelates Fe-hydroxide species in solution, that were removed from the pyrite surface, and then subsequently these chelated surfactin-Fe-hydroxide complexes formed a bilayer with surfactin molecules adsorbed on the surface of pyrite.

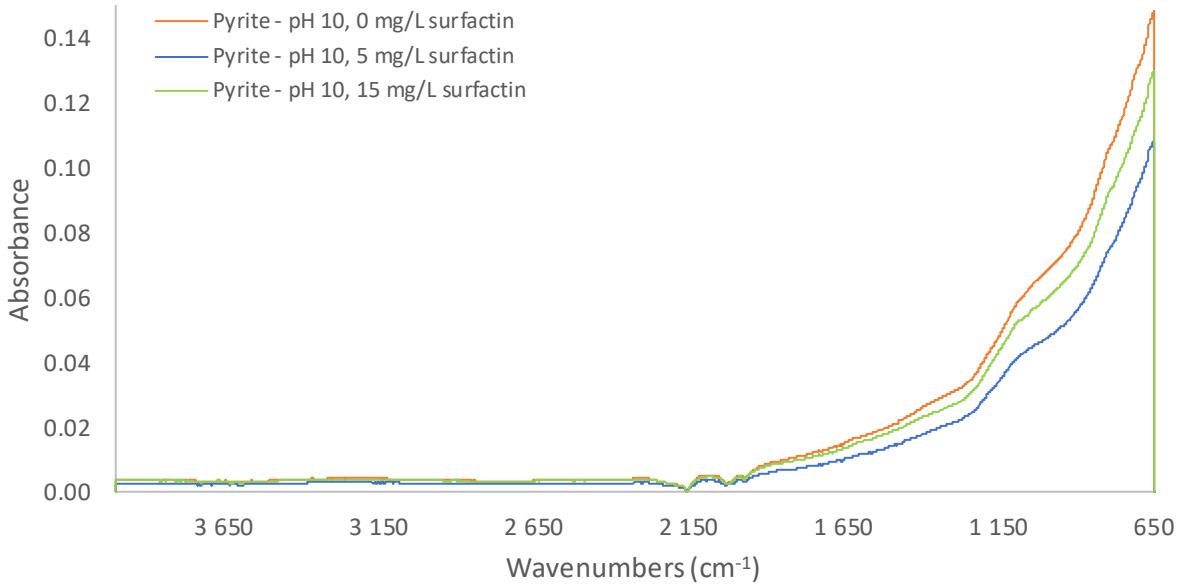

Figure 31: FTIR spectra from 4000 – 650 cm^{-1} of pyrite conditioned for various surfactin concentrations at pH 10. The orange, blue and green spectra represent the spectra of pyrite conditioned at pH 10 with a concentration of 0, 5 and 15 mg/L surfactin respectively. The spectra shown in the figure above are the average spectrums of independent duplicate repeats, baseline corrected for atmospheric H_2O and CO_2.

Table 20: Major peak areas for pyrite conditioned at pH 10 for various surfactin concentrations. The same peak ranges were used, with the baseline drawn through the lowest data points on either side of the peak, eliminating the absorbance offset and allowing areas to be comparable.

Peak range	0 mg/L surfactin - Peak area	5 mg/L surfactin - Peak area	15 mg/L surfactin - Peak area
2980 - 2830 cm^{-1}	0.0024	0.0118	0.0041
2380 - 2335 cm^{-1}	-0.0032	-0.0034	-0.001
2328 cm^{-1} (2335 - 2320)	0.0006	0.0001	0.0001
2288 cm^{-1} (2320 - 2270)	0.0074	0.0018	0.0059
2077 cm^{-1} (2150 - 2030)	0.2831	0.1632	0.2561
1990 cm^{-1} (2030 1980)	0.0097	0.0015	0.0119
1690 - 1580 cm^{-1}	0.0189	0.0032	0.0121
1560 - 1475 cm^{-1}	0.0122	0.0128	0.0285
1475 - 1270 cm^{-1}	0.0501	0.0213	0.0454
1200 - 1060 cm^{-1}	0.072	0.087	0.157
795 cm^{-1} (810 - 785)	0.016	0.008	0.014
704 cm^{-1} (720 - 690)	0.018	0.014	0.01

5.3.2.4 Summary of FTIR analysis of adsorption of surfactin onto pyrite

A short summary of the pyrite FTIR analysis discussed in the previous section will be given to allow a more concise understanding of the interaction between surfactin and certain functional groups on the pyrite surface, before moving on to the microflotation analysis in the next section.

At a pH of 3 there is an increase in the peak areas associated with the aliphatic and peptide moiety of surfactin, as well as the S-O bonds associated with sulfate and sulfite, as the bulk surfactin concentration is increased. There is also the disappearance of a suspected sulfur combination band peak as bulk surfactin concentration increased, indicating that the amide group of surfactin might act as a collecting functional group. These changes in peak area indicate the presence of surfactin on the pyrite surface, even though surfactin is a precipitate at pH 3, and that surfactin facilitates the formation of sulfate and sulfite in some way.

At a pH of 6 there is the same increase in the peak areas associated with the aliphatic and peptide moiety of surfactin, as well as the S-O bonds associated with sulfate and sulfite, as the bulk surfactin concentration is increased, as seen at pH 3. However, there is a reduction in the peak area associated with Fe-hydroxides. These changes in peak areas suggest the presence of surfactin on the pyrite surface, with surfactin molecules binding to Fe-hydroxide sites and facilitating the formation of sulfate or sulfite.

At a pH of 8 the increase in bulk surfactin concentration once again caused an increase in the peak areas associated with the S-O bonds associated with sulfate and sulfite, and the aliphatic functional groups associated with the presence of surfactin on the pyrite surface. However, the presence of a peptide moiety was not seen. At 15 mg/L surfactin at pH 8, there was a reappearance of the sulfur species combination band peak seen at 0 mg/L surfactin at pH 3. These changes in peak area subsequently provide enough evidence of the presence of surfactin on the surface of pyrite and that surfactin may have a cleaning effect that facilitates the exposure of sulfur species on the pyrite surface and the formation of sulfite and sulfate.

The response at pH 10 is different compared to other pH values. Increasing the bulk surfactin concentration to 5 mg/L, increases the peak area associated with aliphatic groups, but decreases the Fe-hydroxide peak area. Increasing the bulk surfactin concentration from 5 mg/L to 15 mg/l causes the reverse to occur, with a decrease in aliphatic peak area, but increase in Fe-hydroxide peak area. However, the peak area associated with sulfate and sulfite increases with both increases of bulk surfactin concentration. These changes in the respective peak areas indicate the presence of surfactin on the surface of the pyrite, with the formation of a bilayer with Fe-hydroxide-surfactin complexes at 15 mg/L surfactin concentration. While surfactin continues to facilitate the formation of sulfate and sulfite.

It is evident that the addition of surfactin causes surfactin to interact with the pyrite surface at all examined pH values. There is a strong suggestion that surfactin does indeed adsorb onto the surface of pyrite, with the most likely adsorption site being the Fe-hydroxide sites. Additionally, there was an indication that the surfactin amide group does play a role in chelation and adsorption. Finally, surfactin seems to have a cleaning effect on the surface of pyrite that leads to the oxidation of sulfur, indicated by the formation of sulfate and sulfite.

5.3.3 Effect of pH and surfactin concentration on pyrite recovery

Zeta potential has been used to establish the occurrence and the type of adsorption between surfactin and the pyrite surface. FTIR analysis has been used in conjunction to determine which pyrite surface functional groups interact with surfactin. In this section microflotation analysis is once again used to link together all the previous analyses and determine the effect of surfactin on the hydrophobicity of the pyrite surface and the subsequent pyrite recovery. As stated in the coal section (section 5.2.3), the use of a microflotation cell reduces the hydrodynamic effects associated with flotation and allows greater emphasis on the reagent and mineral interactions. This discussion section endeavours to separate the effect of surfactin concentration from the effect of pH on surfactin during the recovery of pyrite through flotation.

5.3.3.1 Effect of surfactin concentration on pyrite recovery

The pyrite recovery at each surfactin concentration will be evaluated to determine the effect of surfactin concentration on pyrite recovery at different pH conditions. Pyrite flotation recovery as a function of pH for different surfactin concentrations is given in Figure 32.

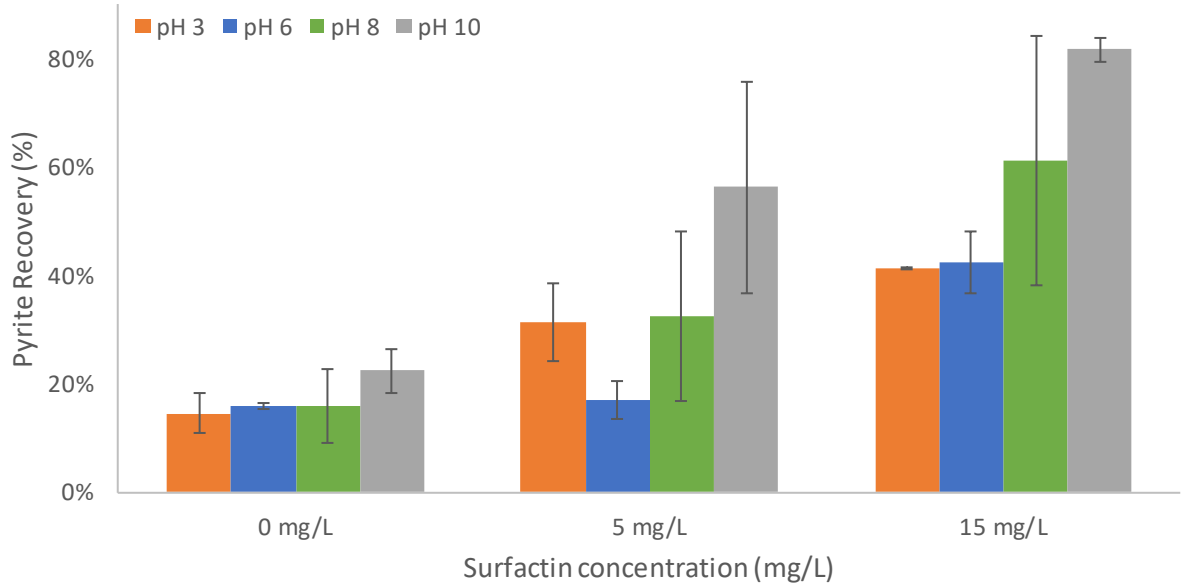

Figure 32: Pyrite flotation recovery as a function of pH and surfactin concentration. Experiments were conducted by floating 3 g pyrite in a microflotation cell over a 20 min period. Error bars represent the standard deviation for the duplicate repeats.

Increasing the bulk surfactin concentration from 0 mg/L to 5 mg/L causes a general increase in pyrite recovery at pH 3, 8 and 10, but not at pH 6. With surfactin concentration increasing from 0 mg/L to 5 mg/L, the biggest increase in recovery was seem at pH 10, with the pyrite recovery increasing from 22.4% to 56.2 %, and pH 8 and 3 showed approximately equal increases in pyrite recovery, from 15.9% to 32.6% and 14.5% to 31.5% respectively. The smallest increase in pyrite recovery was at pH 6 where the pyrite recovery only increased from 15.9% to 17.1% as bulk surfactin concentration increased from 0 mg/L to 5 mg/L. Thus, at a bulk surfactin concentration of 5 mg/L, surfactin acted as a collector and increased the

hydrophobicity at all pH values. During the FTIR analysis it was seen that there is a reduction in the Fe-hydroxide groups on the surface of pyrite at pH 6 when the surfactin concentration is increased from 0 mg/L to 5 mg/L. This could indicate that surfactin initially has a potential cleaning effect on pyrite, whereby surfactin removes Fe-hydroxide species from the pyrite surface. These removed Fe species are replaced by sulfate and sulfite species, supported by FTIR analysis, which do not increase the hydrophobicity of pyrite, resulting in the relatively inconsequential increase in recovery at pH 6 at 5 mg/L surfactin concentration.

The almost equal pyrite recovery at a surfactin concentration of 5 mg/L for pH 3 and 8 was an interesting and unexpected occurrence. At pH 3 surfactin is precipitated and not in solution. At pH 8, surfactin is fully ionised and soluble. Thus, the effect of the surfactin precipitate and the effect of the ionised surfactin molecule, on the hydrophobicity of pyrite, is relatively equal at low surfactin concentration (5 mg/L).

When the bulk surfactin concentration is increased from 5 mg/L to 15 mg/L, there is an increase in pyrite recovery across all pH values. The recovery of pyrite increases to 41.3%, 42.4%, 61.6% and 81.6% for pH 3, 6, 8 and 10 respectively. Thus at 15 mg/L surfactin concentration, surfactin acts as a pyrite collector significantly increasing the hydrophobicity of pyrite at all pH values.

The effect of surfactin concentration on pyrite recovery was evaluated. It is shown that the addition of surfactin acts as an effective collector for the flotation of pyrite at all evaluated surfactin concentrations. An increase in surfactin concentration lead to increased hydrophobicity of pyrite and subsequently the recovery of pyrite, except at a low surfactin concentration (5 mg/L) at pH 6 where an insignificant increase in recovery was seen. The main attachment mechanisms of surfactin is the carboxylic functional groups, due to the higher recovery seen when the carboxylic functional are fully ionised at pH 8 and 10. Although according to the FTIR analysis the amide functional group of surfactin also plays a role in the adsorption of surfactin onto the surface of pyrite, this mechanism is considered to be secondary. This is supported by the increase in pyrite recovery seen with the addition of surfactin in the acidic pH range where the carboxylic functional groups are not ionised. The cleaning effect of surfactin on the mineral surface is seen to be an added advantage.

There is a definite increase in pyrite recovery as surfactin concentration increases, to a high degree of confidence. Although the standard deviation is large at some experimental conditions, the general trend is strong enough to provide a high degree of confidence in the results. Therefore, surfactin is an excellent collector of pyrite, especially in the alkaline pH range, increasing the recovery of pyrite from 22 % - 80% in the case of pH 10 and 15 mg/L. These results answer one of the key questions: Confirming that surfactin does indeed float pyrite.

5.3.3.2 Effect of pH on pyrite recovery with surfactin

The pyrite recovery at each pH value will be evaluated to determine the effect of pH on pyrite recovery at different surfactin concentrations. Pyrite flotation recovery as a function of pH for different surfactin concentrations is given in Figure 32.

At a pH of 3, the recovery of pyrite increases as surfactin concentration increases. Surfactin acts as a collector for pyrite at both 5 and 15 mg/L surfactin. This is interesting as surfactin is a protonated precipitant at pH 3 (Long et al., 2017) and has little effect on the zeta potential as discussed earlier. The increase in pyrite recovery indicates that the surfactin precipitant does interact with the pyrite surface at pH 3. FTIR analysis at pH 3 indicates the presence of sulfur functional groups on the surface of pyrite, that disappear with the addition of surfactin, indicating these sulfur functional groups may provide a site for interaction with the amide group of surfactin. This would explain the increase in pyrite hydrophobicity and subsequent recovery at a pH of 3 in the presence of surfactin.

Increasing the pH from 3 to 6, causes the pyrite surface to become less hydrophobic at 5 mg/L surfactin concentration, but the recovery remains approximately the same at 15 mg/L. Surfactin remains a pyrite collector at 15 mg/L at pH 6, but has no significant collecting ability at 5 mg/L when compared to 0 mg/L at pH 6. The lack of an effect at 5 mg/L pH 6 was attributed to the cleaning effect of surfactin as discussed in an in the FTIR section. When the concentration is increased to 15 mg/L this effect is overcome, indicating that surfactin may initially prefer interacting with Fe-hydroxide on the surface, and a lack of Fe-hydroxide sites at 15 mg/L surfactin cause surfactin to attach to less preferential sites and significantly increase the hydrophobicity of pyrite.

As the pH increases from 6 to 8, there is an increase in the pyrite hydrophobicity at both 5 mg/L and 15 mg/L. Surfactin is still a collector of pyrite at 5 mg/L and 15 mg/L at pH 8. The increase in hydrophobicity is attributed to the complete ionisation of the surfactin molecule at pH 8, allowing greater chelating ability.

Further increasing pH from 8 to 10 causes a further increase in the hydrophobicity of pyrite, as shown by the increased pyrite recovery, at both 5 mg/L and 15 mg/L surfactin concentration. At pH 10, surfactin is still a collector of pyrite and has shown to provide the highest pyrite recoveries at both 5 mg/L and 15 mg/L compared to the other pH values.

The effect of pH on pyrite recovery in the presence of surfactin was evaluated. It is seen that generally there is a greater pyrite recovery at alkaline pH values at both 5 mg/L and 15 mg/L surfactin concentration compared to acidic pH values. The outlier remains at pH 6 at 5 mg/L surfactin concentration, which showed significantly lower pyrite recovery compared to all other pH values. The recommended pH for the flotation of pyrite, using surfactin, is pH 10 which provided an excellent pyrite recovery of 80% at a 15 mg/L surfactin concentration.

5.3.4 Effect of pH and surfactin concentration on pyrite flotation rate constant

As mentioned previously in the coal section (section5.2.4), the rate constant lumps together all the unmeasured variables and provides an engineering measure of floatability (Wills and Napier-Munn, 2005). The rate constant is seen as a sensible way to assess the floatability of pyrite, as the individual variables were not sufficiently explored to do otherwise, at this preliminary stage of research into the flotation of pyrite with surfactin. The pyrite flotation rate constants as a function of pH and surfactin concentrations are provided graphically Figure 33. The rate constants were determined by fitting

flotation recovery vs time data to a first order model, which is discussed in greater detail in the Methods section (section 4.3.4.3).

It can be seen that there is a strong correlation between the flotation rate constants and their respective recoveries when Figure 33 is compared to Figure 32. With the addition of 5 mg/L or 15 mg/L surfactin, the alkaline range (pH 8 and 10) has a higher flotation rate constant than the acidic range (pH 3 and 6). At 5 mg/L surfactin concentration the flotation rate constant is twice as large as any other pH value. At 15 mg/L surfactin concentration, the flotation rate constant at pH 8 and pH 10 is more than double and triple, respectively, the rate constants of the acidic pH values. The larger rate constant values indicate that surfactin produces a greater and faster flotation response in alkaline pH value, and at high surfactin concentrations (15 mg/L). This would indicate that surfactin should be used to float pyrite in the alkaline range, as it would be more effective.

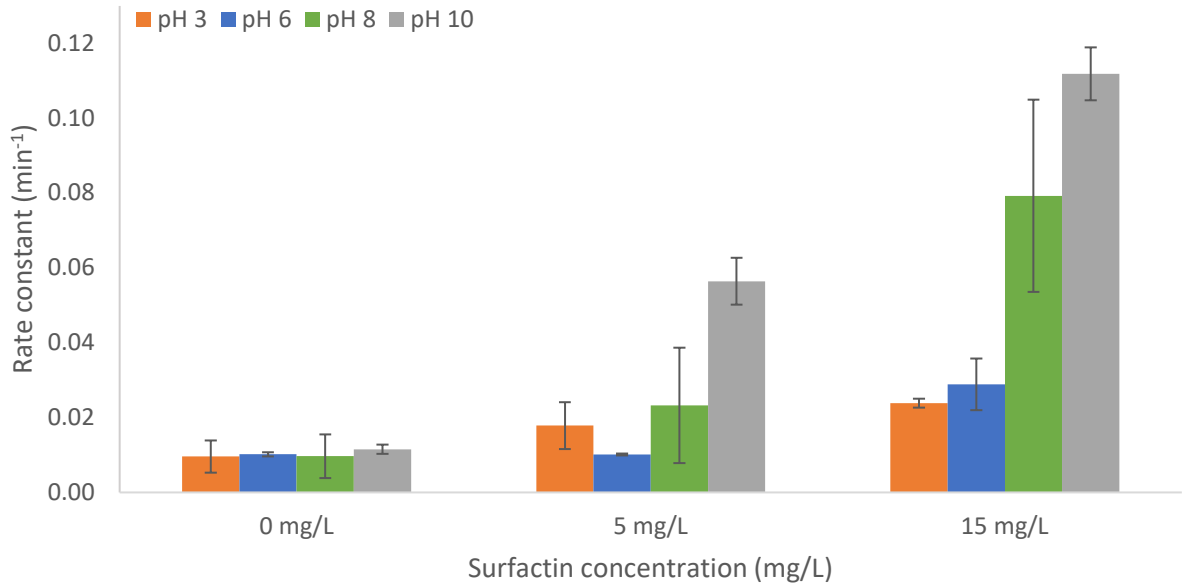

Figure 33: Pyrite flotation rate constants as a function of pH and surfactin concentration. Experiments were conducted by floating 3 g pyrite in a microflotation and determining the first-order rate constants over the period of 0 – 6 min.

Pyrite recovery as a function of flotation time at various pH values and surfactin concentrations are provided in Figure 34. It can be seen in Figure 34: A and B, that in acidic pH ranges (pH 3 and 6), the pyrite recovery remains linear over time and does not reach a maximum at either 5 mg/L or 15 mg/L surfactin concentration within the flotation time period. In the alkaline pH range (pH 8 and 10), as seen Figure 34: C and D, the pyrite recovery has a logarithmic shape and approaches a maximum pyrite recovery at 5 mg/L surfactin concentration at pH 10, and at 15 mg/L surfactin concentration for both pH 8 and 10. This indicates that flotation is not complete in the acidic range, but does approach maximum recovery in the alkaline range within 20 min. Practically, this would mean to achieve effective pyrite flotation in the acidic pH range would require a longer residence time. The first order model shows a relatively good fit

to the experimental data, indicating the first order model is appropriately describing pyrite flotation using surfactin.

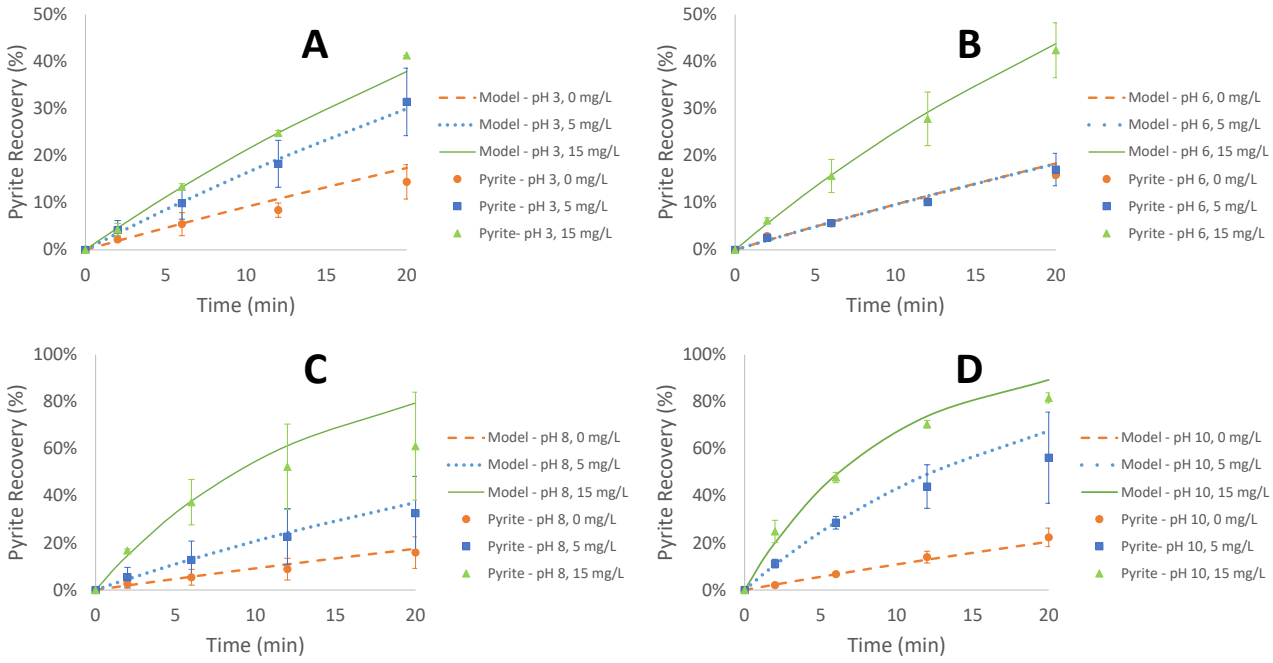

Figure 34: Pyrite recovery as a function of flotation time at various pH values and surfactin concentrations. Experiments were conducted by floating 3 g pyrite in a microflotation and collecting concentrate samples at 2-, 6-, 12- and 20-min. Figure A, B, C and D represent flotation at pH 3, 6, 8 and 10 respectively. The experimental flotation recovery values at 0 mg/L (●), 5 mg/L (■) and 15 mg/L (▲) surfactin concentrations are given by the data points. The orange (- - -), blue (·····) and green (——) lines represent first order models fitted using the rate constants to the corresponding 0, 5 and 15 mg/L surfactin concentration.

5.3.5 Application of surfactin as a pyrite flotation agent

Surfactin increases the hydrophobicity of pyrite and performs as a collector of pyrite at all pH values at low surfactin concentration (5 mg/L) and high surfactin concentration (15 mg/L), except at 5 mg/L surfactin concentration at pH 6, which proved to provide an insignificant increase in recovery. Thus, the choice of flotation parameters would be largely dependent on the surfactin-coal interaction.

Surfactin can only be used as a collector for pyrite and cannot be used to depress pyrite in flotation. Thus, to effectively use surfactin in the desulphurisation of coal, direct flotation of pyrite from coal needs to occur. Meaning the operating pH and surfactin concentration needs to be chosen as to depress coal or at the least have minimal effect on the recovery of coal, in order to provide effective separation of coal and pyrite.

At 15 mg/L surfactin concentration, the recovery of coal is significantly increased and would not achieve the desired coal and pyrite separation, thus 5 mg/L surfactin concentration would need to be used. At 5 mg/L surfactin concentration, the lowest coal recoveries and coal flotation rate constants are seen at

pH 6 and pH 10. Compared to pyrite flotation, at 5 mg/L surfactin concentration, the highest pyrite recovery of either pH 6 or 10, was at pH 10, which consequently also had the largest pyrite flotation rate constant (at 5 mg/L surfactin concentration). Thus, it would be possible to separate coal and pyrite. With this preliminary data, the recommendation would be to desulphurise coal at a pH of 10 with 5 mg/L surfactin concentration. However, this recommendation is based on the flotation of coal and pyrite separately. It is unknown at this stage precisely how surfactin will act in the combined flotation and whether surfactin would have preference for pyrite over coal. However, the zeta potential analysis showed that surfactin chemisorbed onto pyrite, but showed hydrophobic physisorption onto coal, which could indicate a preference for pyrite in a combined system. Further steps to answer these questions will be provided in the recommendation section.

5.4 Repeatability

To quantify the repeatability of the microflotation experimental setup, two centre points were repeated in triplicate for coal flotation, at 10 mg/L surfactin concentration at pH 5 and 9 respectively. Coal was chosen as it was shown to have higher variability compared to pyrite during the microflotation experiments. The results of the triplicate centre point repeats are given in Figure 35.

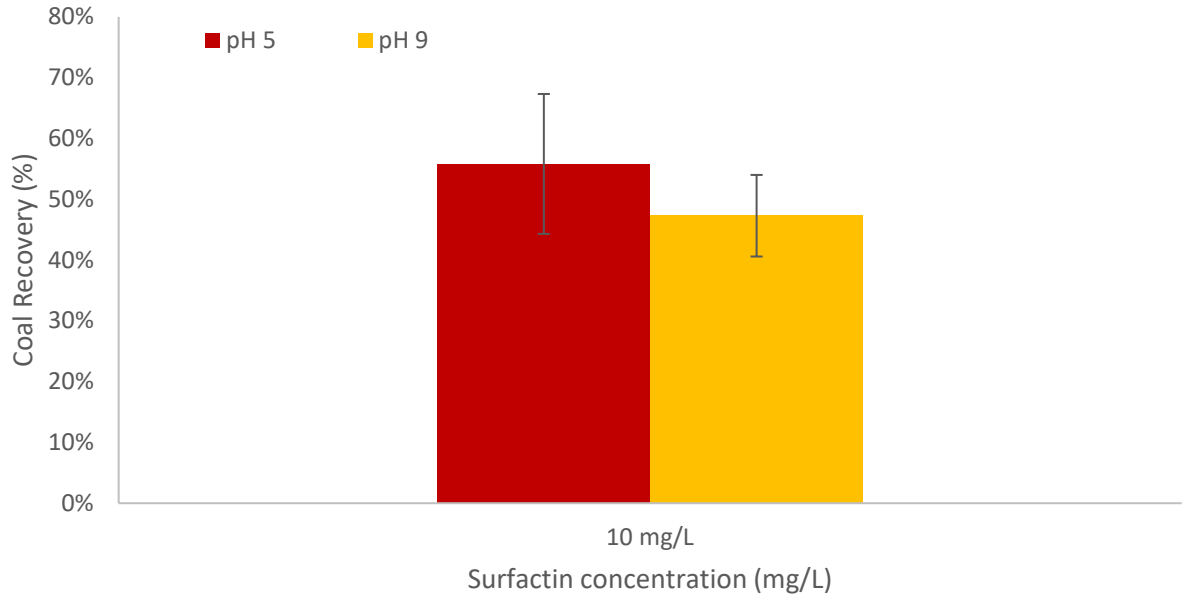

Figure 35: Coal flotation recovery centre points as a function of pH and surfactin concentration. Experiments were conducted by floating 3 g coal in a microflotation cell over a 20 min period. Error bars represent the standard deviation for the triplicate repeats.

The standard deviations of the triplicate results seen above are consistent with the standard deviations of the duplicate results and thus the variability seen in the data presented in this thesis was considered to be largely due to the inherent variability often associated with froth flotation. Although the experiments were conducted only in duplicate, the use of three different experimental methods (Zeta potential, FTIR and microflotation) provided results that confirmed and supported one another, which

provides some degree of confidence in the overall results obtained. As this was an initial investigation into a novel concept, the goal was to explore the general effect of surfactin on coal and pyrite, and to that effect the repeatability was considered adequate.

6 CONCLUSION

This research was initiated with the hypothesis that surfactin can be used as a replacement for synthetic surfactants, as a desulphurisation agent for coal tailings, largely due to the structure and the anionic nature of the surfactin molecule. This led to the overall aim of this study being to determine the effectiveness of surfactin as a collector in desulphurisation of coal, through froth flotation of coal and pyrite, as a mitigation strategy for the formation of acid mine drainage.

The work described in this dissertation indicated that surfactin is an effective collector of both coal and pyrite. However, the collecting ability of surfactin is a function of pH and concentration, and the effectiveness curves are such that a process for preferential flotation of either coal or pyrite is possible. Through the use of pH and surfactin concentration, it was possible to manipulate surfactin to either act as a collector of coal or pyrite, or to have little to no effect on the flotation of coal or pyrite. This preliminary study concluded that, at the right pH and surfactin concentration, surfactin could be an effective collector of pyrite for the desulphurisation of coal, as a mitigation strategy for the formation of acid mine drainage.

Conclusions regarding the specific objectives are detailed below:

1. Determine a surfactin concentration range for further experimentation.

The surface tension was used to determine the critical micelle concentration (CMC) of the surfactin sample. The CMC of the surfactin sample was found to be 4.5 mg/L and this surfactin concentration was used as a starting point from which the surfactin concentration range was determined. The surfactin concentration range was chosen at values below, near equivalent to and above the CMC of the surfactin sample, corresponding to 2 mg/L, 4 mg/L and 15 mg/L respectively. This provided a range of surfactin values that also allowed the evaluation of the formation of micelles on adsorption. Zeta potential analysis revealed that 2 mg/L and 4 mg/L surfactin concentrations provided similar results. Thus, it was decided to consolidate these two concentrations and use a 5 mg/L surfactin concentration, as the low surfactin concentration, as it was closer to the CMC over a larger range of pH values. The low surfactin concentration at 5 mg/L and the high surfactin concentration at 3 times larger, at 15 mg/L, provided a large enough contrast to allow the effect of surfactin concentration to be seen. Finally, the microflotation results indicated that the 5 mg/L and 15 mg/L surfactin concentration provided a useable and practical surfactin concentration range for the evaluation of both the flotation of coal and pyrite.

As a result, the first objective has been achieved. To answer the key question: at what surfactin concentration should coal and pyrite be floated? At low surfactin concentration (5 mg/L), surfactin increases the recovery of both coal and pyrite, but has little effect at pH 8 and 10 for coal, and pH 6 for pyrite. At high surfactin concentration (15 mg/L), surfactin significantly increases the recovery of both coal and pyrite, except at pH 8 for coal where surfactin is a depressant. In conclusion, there is a greater difference in the recovery between coal and pyrite at 5 mg/L surfactin concentration, compared to 15 mg/L surfactin concentration. By implication, to separate coal and pyrite, low surfactin concentration (5 mg/L) would provide a greater opportunity for preferential flotation of either coal or pyrite.

2. Evaluate the effect of the coal and pyrite surface charge on the adsorption of surfactin.

Zeta potential analysis has been used as a method for investigating the effect of coal and pyrite surface charge on the adsorption of surfactin. The response of the zeta potential to the addition of surfactin indicated the adsorption of surfactin and suggested the possible adsorption mechanism involved.

Coal

The isoelectric point (IEP) of coal was used as method verification and a measure of coal surface oxidation. An experimental coal IEP at a pH of 4.3 indicated that the coal used was unoxidized. The zeta potential of coal became more negative with the addition of surfactin, indicating that there was interaction between the coal surface and the surfactin molecules and the zeta potential response curve suggested that the adsorption mechanism of surfactin onto the surface of coal was physisorption through hydrophobic interactions.

It was seen that low surfactin concentrations showed a higher effect on zeta potential around the neutral pH range, with little or no effect at the extreme pH ranges. Little difference was seen in the zeta potential response of 2 mg/L compared to 4 mg/L surfactin concentration, indicating that the concentrations were too close together to make any significant change to zeta potential. High surfactin concentration (15 mg/L) showed little additional effect on zeta potential in the neutral pH range compared to the low surfactin concentrations, but indicated significant effect in the extreme pH ranges (pH 2 - 4 and pH 8 - 10). This indicated that there was most likely a limited amount of surfactin adsorption sites on coal and that a maximum surfactin adsorption was reached in the neutral pH range, while the formation of surfactin micelles and surfactin precipitate adsorption allowed adsorption hinderances to be overcome at extreme pH values.

Pyrite

The experimental isoelectric point (IEP) of pyrite was found to be at pH 2.98 and indicated that there was minor oxidation of the pyrite surface. The effect of the addition of surfactin on the pyrite zeta potential response indicated that there was interaction between the pyrite surface and surfactin molecules which made the surface of the pyrite more negatively charged. The response also suggested that surfactin chemisorbed onto the surface of pyrite.

At low surfactin concentration (2 and 4 mg/L), surfactin showed little to no effect on the zeta potential of pyrite in the acidic pH range (pH 2 - 6). In the neutral and alkaline pH range (pH 6 – 10), high surfactin concentration (15 mg/L) had a significant impact on the zeta potential of pyrite, indicating that ionisation of the surfactin molecule and the formation of micelles played a significant part in adsorption.

Summary

The zeta potential results indicated that surfactin interacts with both coal and pyrite, but that the probable adsorption mechanisms are different. Surfactin adsorbs onto coal through physisorption and onto pyrite through chemisorption. There was a higher effect of surfactin on the zeta potential of both

coal and pyrite in the neutral and alkaline pH range, indicating that the ionisation of surfactin played a significant role in adsorption. The surfactin seemed to have a limited number of adsorption sites on the surface of coal, whereas the pyrite surface did not indicate such a limitation.

Thus, the effect of the coal and pyrite surface charge on the adsorption of surfactin has been evaluated and the second objective achieved. This answered our key question: does surfactin attach to the surface of coal and pyrite? Yes, surfactin adsorbs onto both coal and pyrite, although through different mechanisms and depending on the coal and pyrite surface charge, which is dependent on pH.

3. Evaluate the attachment mechanism of surfactin to the surface of coal and pyrite.

Zeta potential analysis provided an initial indication of the adsorption/attachment mechanism of surfactin on the surface of coal and pyrite. FTIR analysis was used to verify and clarify the adsorption mechanism of surfactin onto the surface of coal and pyrite proposed in the zeta potential analysis. This was done by using FTIR analysis to evaluate the coal and pyrite surface functional groups that surfactin molecules interact with.

Coal

Zeta potential analysis indicated that the adsorption of surfactin on the surface of coal is through hydrophobic physisorption between the aliphatic functional groups of surfactin and the hydrophobic carbonaceous surface functional groups of coal.

The FTIR analysis revealed a clear indication that surfactin interacts with the coal surface at all pH values, as evidenced by the changes in the spectra peak areas. The interaction mechanism however seemed to be concentration dependent. Surfactin at low surfactin concentration (5 mg/L) had a cleaning effect on the surface of coal, especially in the alkaline pH range, rather than a clear attachment to the coal surface. High surfactin concentration (15 mg/L) showed surfactin interaction and attachment through hydrophobic interactions with the coal surface.

Pyrite

The change in zeta potential of pyrite with the addition of surfactin suggested that surfactin chemisorbed onto the surface of pyrite.

FTIR analysis confirmed that there is interaction between surfactin molecules and the pyrite surface at all pH values. The FTIR analysis revealed that there is a strong indication that surfactin does adsorb onto the surface of pyrite and that this adsorption is onto Fe-hydroxide sites. Furthermore, there was evidence that suggested that the amide groups of surfactin played a role in chelation and adsorption. Lastly surfactin also exhibited the cleaning effect, also seen with the interaction between coal and surfactin, and that the cleaning effect leads to the oxidation of sulfur to sulfite and sulfate.

Summary

Surfactin presented a cleaning effect on both the surface of coal and pyrite, which may contribute to the increase in hydrophobicity cause by surfactin in the microflotation analysis. The attachment mechanism

of surfactin to the surface of coal was confirmed to be due to hydrophobic physisorption, and the attachment mechanism of surfactin onto the surface of pyrite was through chemisorption to either Fe-hydroxide sites or though interaction of the surfactin amide groups with sulfur on the pyrite surface. This serves to satisfy objective 3, which is to evaluate the attachment mechanism of surfactin to the surface of coal and pyrite and answering the key question of which coal and pyrite surface sites surfactin molecules attached to.

4. Evaluate the effect of surfactin on the hydrophobicity of coal and pyrite.

The effect of surfactin on hydrophobicity of coal and pyrite was investigated by evaluating changes in the total cumulative flotation recovery and the respective flotation kinetics in a microflotation setup. The microflotation cell minimized the hydrodynamic effects of flotation and allowed the interaction between surfactin and coal or pyrite to be the main driver of flotation response and thus hydrophobicity.

Coal

Surfactin performed as a collector of coal and increased the hydrophobicity of coal at all tested pH values except pH 8. An increase in coal recovery was also seen with an increase in surfactin concentration. The smallest effect of surfactin on the hydrophobicity of coal was observed at pH 10 at 5 mg/L surfactin concentration, with an increase in coal recovery of less than 2% (45.9% to 47.8%), and the largest effect was seen at pH 3 and 15 mg/L, with an increase of more than 30% (74% - 42.9%). However, results suggested that a maximum coal recovery has been reached, which has also previously been noted in the zeta potential analysis of coal. Although surfactin showed some depressant effect at pH 8, it was not very effective. Surfactin proved to be an excellent collector of coal at other pH values, increasing the hydrophobicity of coal significantly, especially in the acidic pH range at high surfactin concentration.

Pyrite

A clear trend was observed with the addition of surfactin. The hydrophobicity and consequently the recovery of pyrite increased as surfactin concentration increased. The largest increase in pyrite recovery was seen at pH 10 and 15 mg/L, with an increase of almost 60% (22.4% to 81.6%), and the lowest increase in pyrite recovery was at pH 6 and 5 mg/L surfactin concentration, with an insignificant increase of little over 1% (15.9% to 17.1%). Overall, the greater increase in pyrite recovery with the addition of surfactin was observed in the alkaline pH range than for the acidic pH range.

Summary

Surfactin was observed to have a significant effect on the hydrophobicity of both coal and pyrite. Surfactin acted as a collector of both coal and pyrite at most operating conditions, however at 5 mg/L surfactin concentration, surfactin had little to no effect on the hydrophobicity of coal at pH 10, and the hydrophobicity of pyrite at pH 6. In the case of coal, surfactin also acted as a depressant at pH 8. There is no overlap between the operating conditions of the instances where surfactin has little or no significant effect on the hydrophobicity of coal and pyrite, and thus presents an opportunity for favourable pyrite or coal selectivity for the desulphurisation of coal. Consequently, to separate coal and pyrite, flotation at

low surfactin concentration (5 mg/L) at a pH of 6 would favour the flotation of coal, whereas preferential flotation of pyrite would be at a pH of 10.

5. Determine the potential desulphurisation operating conditions.

The objective was to determine the potential coal desulphurisation operating conditions using the preliminary data collected in this study. In order to desulphurise coal, pyrite needs to be collected while coal is depressed, or coal collected while pyrite is depressed. The microflotation analysis indicated that pyrite could only be collected using surfactin and thus the separation is dictated by that condition. The operating conditions were then selected at a pH and surfactin concentration which would provide the highest pyrite recovery, with minimal or reduced coal recovery. The operating conditions were determined to be at pH 10 and 5 mg/L surfactin, providing a 56.2% pyrite recovery and 47.8 % coal recovery. This was however based on the microflotation of coal and pyrite separately and it is unknown how surfactin will perform in a combined coal and pyrite flotation.

Based on this preliminary research, it is evident that coal desulphurisation using surfactin is possible, as at the suggested operating conditions, surfactin was shown to be an effective collector of pyrite and have no significant effect on coal recovery. Thus, it is possible to separate coal and pyrite using surfactin.

7 RECOMMENDATIONS

The novelty of using pure surfactin as a coal desulphurisation agent makes this preliminary study only the beginning of the required analysis to understand the complete system. However, the work done in this dissertation has shown that it would be possible to use surfactin as a desulphurisation agent, but further study is needed to gain more insight. A few further key objectives have been identified and are discussed below:

1. **Determine the effect of surfactin on the combined flotation of coal and pyrite.**

The preliminary study evaluated the effect of surfactin on the flotation of coal and pyrite separately. The next logical step is to combine the flotation of coal and pyrite, as would be the case in a desulphurisation system. It is unknown whether surfactin will prefer coal or pyrite in a combined system and this need to be investigated as it will have a significant impact on the flotation configuration.

2. **Determine the effect of hydrodynamic effects on the flotation of coal and pyrite using surfactin.**

This preliminary study investigated the effect of surfactin on the flotation of coal and pyrite in a microflotation cell setup that eliminates the hydrodynamic effects of flotation. Although this is useful for isolating the effect of surfactin on flotation, it is not entirely relatable to practical flotation setups. Thus, surfactin performance should be evaluated in a batch flotation setup, that includes the hydrodynamic effects associated with flotation, to gauge the effect hydrodynamics have on using surfactin as a desulphurisation agent.

3. **Evaluate the performance of surfactin in comparison with typical industrial surfactants in the desulphurisation of coal.**

Surfactin has been shown to be a possible green chemistry candidate to replace synthetic surfactants in the desulphurisation of coal. However, to be a viable candidate, surfactin needs to demonstrate superior or comparable performance in comparison to synthetic surfactants. Thus, an apples to apples comparison needs to be made using surfactin compared to the typical surfactants used in coal desulphurisation.

4. **Evaluate the effect of surfactin on the flotation pulp electrochemistry.**

Surfactin was shown to have a cleaning effect on both the surface of coal and pyrite. Thus, it is recommended that redox potential or pulp potential be evaluated to fully understand this cleaning effect and the consequences on the flotation operating conditions.

8 REFERENCES

Abdel-Khalek, M.A., El-Midany, A.A., 2013. Application of Bacillus subtilis for reducing ash and sulfur in coal. Environ. Earth Sci. 70, 753–760. https://doi.org/10.1007/s12665-012-2163-4

Abdel-Mawgoud, A.M., Aboulwafa, M.M., Hassouna, N.A., 2008. Characterization of Surfactin Produced by Bacillus subtilis Isolate BS5. Appl. Biochem. Biotechnol. 150, 289–303. https://doi.org/10.1007/s12010-008-8153-z

Abotsi, G.K., Bota, K.B., Saha, G., 1992. Interfacial Phenomena in Coal Impregnation with Catalysts. Energy and Fuels 6, 779–782. https://doi.org/10.1021/ef00036a013

Agency for Toxic Substances and Disease Registry, 2012. Public Health Statement: Carbon Disulfide.

Agrawal, A., Sahu, K.K., 2009. An overview of the recovery of acid from spent acidic solutions from steel and electroplating industries. J. Hazard. Mater. 171, 61–75. https://doi.org/10.1016/j.jhazmat.2009.06.099

Ahmadi, M., Gharabaghi, M., Abdollahi, H., 2018. Effects of type and dosages of organic depressants on pyrite floatability in microflotation system. Adv. Powder Technol. 29, 3155–3162. https://doi.org/10.1016/j.apt.2018.08.015

Akcil, A., Koldas, S., 2006. Acid Mine Drainage (AMD): causes, treatment and case studies. J. Clean. Prod. 14, 1139–1145. https://doi.org/10.1016/j.jclepro.2004.09.006

Anawar, H.M., 2015. Sustainable rehabilitation of mining waste and acid mine drainage using geochemistry, mine type, mineralogy, texture, ore extraction and climate knowledge. J. Environ. Manage. 158, 111–121. https://doi.org/10.1016/j.jenvman.2015.04.045

Arima, K., Kakinuma, A., Tamura, G., 1968. Surfactin, a crystalline peptidelipid surfactant produced by Bacillus subtilis: Isolation, characterization and its inhibition of fibrin clot formation. Biochem. Biophys. Res. Commun. 31, 488–494. https://doi.org/10.1016/0006-291X(68)90503-2

Arutchelvi, J., Sangeetha, J., Philip, J., Doble, M., 2014. Self-assembly of surfactin in aqueous solution: Role of divalent counterions. Colloids Surfaces B Biointerfaces 116, 396–402. https://doi.org/10.1016/j.colsurfb.2013.12.034

Bach, L., Norregaard, R.D., Hansen, V., Gustavson, K., 2016. Review on environmental risk assessment of mining chemicals used for mineral separartion in the mineral resources industry and recommendations for Greenland.

Bastrzyk, A., Fiedot-Toboła, M., Polowczyk, I., Legawiec, K., Płaza, G., 2019. Effect of a lipopeptide biosurfactant on the precipitation of calcium carbonate. Colloids Surfaces B Biointerfaces 174, 145–152. https://doi.org/10.1016/j.colsurfb.2018.11.009

Benzaazoua, M., Bussière, B., Kongolo, M., McLaughlin, J., Marion, P., 2000. Environmental desulphurization of four Canadian mine tailings using froth flotation. Int. J. Miner. Process. 60, 57–74. https://doi.org/10.1016/S0301-7516(00)00006-5

Block, M., Pärt, P., 1986. Increased availability of cadmium to perfused rainbow trout (Salmo gairdneri, Rich.) gills in the presence of the complexing agents diethyl dithiocarbamate, ethyl xanthate and isopropyl xanthate. Aquat. Toxicol. 8, 295–302. https://doi.org/10.1016/0166-445X(86)90081-0

Bodour, A.A., Miller-Maier, R.M., 1998. Application of a modified drop-collapse technique for surfactant quantitation and screening of biosurfactant-producing microorganisms. J. Microbiol. Methods 32, 273–280.

Bognolo, G., 1999. Biosurfactants as emulsifying agents for hydrocarbons. Colloids Surfaces A Physicochem. Eng. Asp. 152, 41–52. https://doi.org/10.1016/S0927-7757(98)00684-0

Bois, D., Benzaazoua, M., Bussière, B., Kongolo, M., Poirier, P., 2005. A feasibility study on the use of

desulphurized tailings to control acid mine drainage. CIM Bull. 98, 74.

Bonmatin, J. -M, Genest, M., Labbé, H., Ptak, M., 1994. Solution three-dimensional structure of surfactin: A cyclic lipopeptide studied by 1H-nmr, distance geometry, and molecular dynamics. Biopolymers 34, 975–986. https://doi.org/10.1002/bip.360340716

Broadhurst, J.L., Kunene, M.C., Von Blottnitz, H., Franzidis, J.P., 2015. Life cycle assessment of the desulfurisation flotation process to prevent acid rock drainage: A base metal case study. Miner. Eng. 76, 126–134. https://doi.org/10.1016/j.mineng.2014.10.013

Buckley, A.N., Riley, K.W., 1991. Self-induced floatability of sulphide minerals: Examination of recent evidence for elemental sulphur as the hydrophobic entity. Surf. Interface Anal. 17, 655–659. https://doi.org/10.1002/sia.740170908

Cai, Y., Pan, Y., Xue, J., Su, G., 2009a. Surficial phase-identification and structural profiles from weathered natural pyrites: A grazing-incidence X-ray diffraction study. Appl. Surf. Sci. 255, 4066–4073. https://doi.org/10.1016/j.apsusc.2008.10.080

Cai, Y., Pan, Y., Xue, J., Sun, Q., Su, G., Li, X., 2009b. Comparative XPS study between experimentally and naturally weathered pyrites. Appl. Surf. Sci. 255, 8750–8760. https://doi.org/10.1016/j.apsusc.2009.06.028

Campbell, J., Sun, S., 1969. Special Research Report SR-74, Pennsylvania State University.

Carrillo, C., Teruel, J.A., Aranda, F.J., Ortiz, A., 2003. Molecular mechanism of membrane permeabilization by the peptide antibiotic surfactin. Biochim. Biophys. Acta - Biomembr. 1611, 91–97. https://doi.org/10.1016/S0005-2736(03)00029-4

Chamber of Mines of South Africa, 2018. National Coal Strategy for South Africa, National Coal Strategy.

Chander, S., Briceno, A., 1987. Kinetics of pyrite oxidation. Mining, Metall. Explor. 4, 171–176. https://doi.org/10.1007/BF03402687

Chernyshova, I. V, 2003. An in situ FTIR study of galena and pyrite oxidation in aqueous solution. J. Electroanal. Chem. 558, 83–98. https://doi.org/10.1016/S0022-0728(03)00382-6

Crawford, R.J., Mainwaring, D.E., 2001. The influence of surfactant adsorption on the surface characterisation of Australian coals. Fuel 80, 313–320.

de Faria, A.F., Teodoro-Martinez, D.S., de Oliveira Barbosa, G.N., Gontijo Vaz, B., Serrano Silva, Í., Garcia, J.S., Tótola, M.R., Eberlin, M.N., Grossman, M., Alves, O.L., Regina Durrant, L., 2011. Production and structural characterization of surfactin (C14/Leu7) produced by Bacillus subtilis isolate LSFM-05 grown on raw glycerol from the biodiesel industry. Process Biochem. 46, 1951–1957. https://doi.org/10.1016/j.procbio.2011.07.001

Deleu, M., Razafindralambo, H., Popineau, Y., Jacques, P., Thonart, P., Paquot, M., 1999. Interfacial and emulsifying properties of lipopeptides from Bacillus subtilis. Colloids Surfaces A Physicochem. Eng. Asp. 152, 3–10. https://doi.org/10.1016/S0927-7757(98)00627-X

Department of Minerals and Energy, 2001. National Inventory Discard And Duff Coal – 2001 Summary Report, Energy.

Desai, J.D., Banat, I.M., 1997. Microbial production of surfactants and their commercial potential. Microbiol. Mol. Biol. Rev. 61, 47–64. https://doi.org/10.1128/.61.1.47-64.1997

Dey, S., 2012. Enhancement in hydrophobicity of low rank coal by surfactants - A critical overview. Fuel Process. Technol. 94, 151–158. https://doi.org/10.1016/j.fuproc.2011.10.021

Dey, S., Pani, S., Singh, R., 2014. Study of interactions of frother blends and its effect on coal flotation. Powder Technol. 260, 78–83. https://doi.org/10.1016/j.powtec.2014.03.068

Didyk-Mucha, A., Pawlowska, A., Sadowski, Z., 2019. Modification of mineral surfaces by adsorption of biosurfactants produced by Streptomyces sp. Colloids Surfaces A Physicochem. Eng. Asp. 579, 123677. https://doi.org/10.1016/j.colsurfa.2019.123677

Dunn, J.G., Gong, W., Shi, D., 1993. A Fourier transform infrared study of the oxidation of pyrite. The influences of experimental variables. Thermochim. Acta 215, 247–254. https://doi.org/10.1016/0040-6031(93)80099-V

Ekmekçi, Z., Demirel, H., 1997. Effects of galvanic interaction on collectorless flotation behaviour of chalcopyrite and pyrite. Int. J. Miner. Process. 52, 31–48. https://doi.org/10.1016/S0301-7516(97)00050-1

Farrokhpay, S., 2011. The significance of froth stability in mineral flotation - A review. Adv. Colloid Interface Sci. 166, 1–7. https://doi.org/10.1016/j.cis.2011.03.001

Ferré, G., Besson, F., Buchet, R., 1997. Conformational studies of the cyclic L,D-lipopeptide surfactin by Fourier transform infrared spectroscopy. Spectrochim. Acta - Part A Mol. Biomol. Spectrosc. 53, 623–635. https://doi.org/10.1016/s1386-1425(96)01787-8

Fornasiero, D., Eijt, V., Ralston, J., 1992. An electrokinetic study of pyrite oxidation. Colloids and Surfaces 62, 63–73. https://doi.org/10.1016/0166-6622(92)80037-3

Fornasiero, D., Li, F., Ralston, J., Smart, R.S.C., 1994. Oxidation of galena surfaces I. x-ray photoelectron spectroscopic and dissolution kinetics studies. J. Colloid Interface Sci. https://doi.org/10.1006/jcis.1994.1175

Fuerstenau, D.W., Diao, J., 1992. Characterization of Coal Oxidation and Coal Wetting Behavior by Film Flotation. Coal Prep. 10, 1–17. https://doi.org/10.1080/07349349208905189

Fuerstenau, D.W., Herrera-Urbina, R., McGlashan, D.W., 2000. Studies on the applicability of chelating agents as universal collectors for copper minerals. Int. J. Miner. Process. 58, 15–33. https://doi.org/10.1016/S0301-7516(99)00058-7

Fuerstenau, D.W., Pradip, 2019. A Century of Research Leading to Understanding the Scientific Basis of Selective Mineral Flotation and Design of Flotation Collectors. Mining, Metall. Explor. 36, 3–20. https://doi.org/10.1007/s42461-018-0042-6

Fuerstenau, D.W., Pradip, 2005. Zeta potentials in the flotation of oxide and silicate minerals. Adv. Colloid Interface Sci. 114–115, 9–26. https://doi.org/10.1016/j.cis.2004.08.006

Fuerstenau, D.W., Rosenbaum, J.M., Laskowski, J., 1983. Effect of surface functional groups on the flotation of coal. Colloids and Surfaces 8, 153–173. https://doi.org/10.1016/0166-6622(83)80082-1

Gang, H., Liu, J., Mu, B., 2015. Binding structure and kinetics of surfactin monolayer formed at the air/water interface to counterions: A molecular dynamics simulation study. Biochim. Biophys. Acta - Biomembr. 1848, 1955–1962. https://doi.org/10.1016/j.bbamem.2015.05.016

Garten, V., Weiss, D., Willis, J., 1957. A new interpretation of the Acidic and Basic structures in Carbons. II. The Chromene-carbonium ion couple in Carbon. Aust. J. Chem. 10, 309. https://doi.org/10.1071/CH9570309

Geldenhuis, S., Bell, F.G., 1998. Acid mine drainage at a coal mine in the eastern Transvaal, South Africa. Environ. Geol. 34, 234–242. https://doi.org/10.1007/s002540050275

Geng, W., Nakajima, T., Takanashi, H., Ohki, A., 2009. Analysis of carboxyl group in coal and coal aromaticity by Fourier transform infrared (FT-IR) spectrometry. Fuel 88, 139–144. https://doi.org/10.1016/j.fuel.2008.07.027

Georgiou, G., Lin, S.C., Sharma, M.M., 1992. Surface-active compounds from microorganisms. Bio/Technology 10, 60–65. https://doi.org/10.1038/nbt0192-60

Georgopoulou, Z.J., Fytas, K., Soto, H., Evangelou, B., 1996. Feasibility and cost of creating an iron-phosphate coating on pyrrhotite to prevent oxidation. Environ. Geol. 28, 61–69. https://doi.org/10.1007/s002540050078

Gray, N.F., 1997. Environmental impact and remediation of acid mine drainage: A management problem. Environ. Geol. 30, 62–71. https://doi.org/10.1007/s002540050133

Güler, T., Şahbudak, K., Çetinkaya, S., Akdemir, Ü., 2013. Electrochemical study of pyrite-ovalbumin interaction in relation to flotation. Trans. Nonferrous Met. Soc. China (English Ed. 23, 2766–2775. https://doi.org/10.1016/S1003-6326(13)62795-8

Habe, H., Taira, T., Sato, Y., Imura, T., Ano, T., 2019. Evaluation of yield and surface tension-lowering activity of iturin a produced by bacillus subtilis RB14. J. Oleo Sci. 68, 1157–1162. https://doi.org/10.5650/jos.ess19182

Han, Y.S., Youm, S.J., Oh, C., Cho, Y.C., Ahn, J.S., 2017. Geochemical and eco-toxicological characteristics of stream water and its sediments affected by acid mine drainage. Catena 148, 52–59. https://doi.org/10.1016/j.catena.2015.11.015

Harrison, S., Broadhurst, J.L., van Hille, R., Oyekola, O., Bryan, C., Hesketh, A., Opitz, A., 2010. A systematic approach to sulphidic waste rock and tailings management to minimise acid rock drainage formation. South African Water Research Commission Report, No. 1831/1/10. Pretoria, South Africa.

Heerklotz, H., Seelig, J., 2001. Detergent-like action of the antibiotic peptide surfactin on lipid membranes. Biophys. J. 81, 1547–1554. https://doi.org/10.1016/S0006-3495(01)75808-0

Hesketh, A.H., Broadhurst, J.L., Harrison, S.T.L., 2010. Mitigating the generation of acid mine drainage from copper sulfide tailings impoundments in perpetuity: A case study for an integrated management strategy. Miner. Eng. 23, 225–229. https://doi.org/10.1016/j.mineng.2009.09.020

Holuszko, M.E., Mastalerz, M.D., 2015. Coal macerals chemistry and its implications for selectivity in coal floatability. Int. J. Coal Prep. Util. 35, 99–110. https://doi.org/10.1080/19392699.2014.967850

ICCP, 2001. New inertinite classification (ICCP System 1994). Fuel 80, 459–471. https://doi.org/10.1016/S0016-2361(00)00102-2

ICCP, 1998. The new vitrinite classification (ICCP System 1994). Fuel 77, 349–358.

Ishigami, Y., Osman, M., Nakahara, H., Sano, Y., Ishiguro, R., Matsumoto, M., 1995. Significance of β-sheet formation for micellization and surface adsorption of surfactin. Colloids Surfaces B Biointerfaces 4, 341–348. https://doi.org/10.1016/0927-7765(94)01183-6

Janek, T., Rodrigues, L.R., Gudiña, E.J., Czyznikowska, Z., 2019. Metal-Biosurfactant Complexes Characterization : Binding , Self-Assembly and Interaction with Bovine Serum Albumin. Int. J. Mol. Sci. 20, 2864.

Jauregi, P., Coutte, F., Catiau, L., Lecouturier, D., Jacques, P., 2013. Micelle size characterization of lipopeptides produced by B. subtilis and their recovery by the two-step ultrafiltration process. Sep. Purif. Technol. 104, 175–182. https://doi.org/10.1016/j.seppur.2012.11.017

Joshi, S., Bharucha, C., Desai, A.J., 2008. Production of biosurfactant and antifungal compound by fermented food isolate Bacillus subtilis 20B. Bioresour. Technol. 99, 4603–4608. https://doi.org/10.1016/j.biortech.2007.07.030

Kazadi Mbamba, C., Franzidis, J.P., Harrison, S.T.L., Broadhurst, J.L., 2013. Flotation of coal and sulphur from South African ultrafine colliery wastes. J. South. African Inst. Min. Metall. 113, 399–405.

Kazadi Mbamba, C., Harrison, S.T.L., Franzidis, J.P., Broadhurst, J.L., 2012. Mitigating acid rock drainage risks while recovering low-sulfur coal from ultrafine colliery wastes using froth flotation. Miner. Eng.

29, 13–21. https://doi.org/10.1016/j.mineng.2012.02.001

Kefeni, K.K., Msagati, T.A.M., Mamba, B.B., 2017. Acid mine drainage: Prevention, treatment options, and resource recovery: A review. J. Clean. Prod. 151, 475–493. https://doi.org/10.1016/j.jclepro.2017.03.082

Kelebek, S., Salman, T., Smith, G.W., 1982. An electrokinetic study of three coals. Can. Metall. Q. 21, 205–209. https://doi.org/10.1179/cmq.1982.21.2.205

Kershaw, J.R., Taylor, G.H., 1992. Properties of Gondwana coals with emphasis on the Permian coals of Australia and South Africa. Fuel Process. Technol. 31, 127–168. https://doi.org/10.1016/0378-3820(92)90016-J

Khan, S.U.M., Baltrus, J.P., Lai, R.W., Richardson, A.G., 1991. X-ray photoelectron spectroscopic study of the interaction of xanthate with coal pyrite and mineral pyrite surfaces. Appl. Surf. Sci. 47, 355–363. https://doi.org/10.1016/0169-4332(91)90088-2

Khoshdast, H., Sam, A., Vali, H., Noghabi, K.A., 2011. Effect of rhamnolipid biosurfactants on performance of coal and mineral flotation. Int. Biodeterior. Biodegrad. 65, 1238–1243. https://doi.org/10.1016/j.ibiod.2011.10.003

Klimpel, R.R., Hansen, R.D., 1988. The interaction of flotation chemistry and size reduction in the recovery of a porphyry copper ore. Int. J. Miner. Process. 22, 169–181. https://doi.org/10.1016/0301-7516(88)90062-2

Klimpel, R.R., Isherwood, S., 1991. Some industrial implications of changing frother chemical structure. Int. J. Miner. Process. 33, 369–381. https://doi.org/10.1016/0301-7516(91)90064-P

Knoblich, A., Matsumoto, M., Ishiguro, R., Murata, K., Fujiyoshi, Y., Ishigami, Y., Osman, M., 1995. Electron cryo-microscopic studies on micellar shape and size of surfactin, an anionic lipopeptide. Colloids Surfaces B Biointerfaces 5, 43–48. https://doi.org/10.1016/0927-7765(95)01207-Y

Korobetskii, I.A., Balabanova, N.V., Zaostrovskii, A.N., 1990. A new approach to the investigation of coal. Fuel Process. Technol. 24, 453–458.

Kowall, M., Vater, J., Kluge, B., Stein, T., Franke, P., Ziessow, D., 1998. Separation and characterization of surfactin isoforms produced by Bacillus subtilis OKB 105. J. Colloid Interface Sci. 204, 1–8. https://doi.org/10.1006/jcis.1998.5558

Kretschmer, A., Bock, H., Wagner, F., 1982. Chemical and Physical Characterization of Interfacial-Active Lipids from Rhodococcus erythropolis Grown on n-Alkanes. Appl. Environ. Microbiol. 44, 864–870. https://doi.org/10.1128/AEM.44.4.864-870.1982

Lang, S., 2002. Biological amphiphiles (microbial biosurfactants). Curr. Opin. Colloid Interface Sci. 7, 12–20. https://doi.org/10.1016/S1359-0294(02)00007-9

Li, Y., Zou, A.H., Ye, R.Q., Mu, B.Z., 2009. Counterion-induced changes to the micellization of surfactin-C16 aqueous solution. J. Phys. Chem. B 113, 15272–15277. https://doi.org/10.1021/jp9062862

Liu, J.F., Mbadinga, S.M., Yang, S.Z., Gu, J.D., Mu, B.Z., 2015. Chemical structure, property and potential applications of biosurfactants produced by Bacillus subtilis in petroleum recovery and spill mitigation. Int. J. Mol. Sci. 16, 4814–4837. https://doi.org/10.3390/ijms16034814

Lloyd, P.J., 2000. The potential of coal wastes in South Africa. J. South African Inst. Min. Metall. 69–72.

Long, X., He, N., He, Y., Jiang, J., Wu, T., 2017. Biosurfactant surfactin with pH-regulated emulsification activity for efficient oil separation when used as emulsifier. Bioresour. Technol. 241, 200–206. https://doi.org/10.1016/j.biortech.2017.05.120

Lotter, N.O., Bradshaw, D.J., Barnes, A.R., 2016. Classification of the Major Copper Sulphides into semiconductor types, and associated flotation characteristics. Miner. Eng. 96–97, 177–184.

https://doi.org/10.1016/j.mineng.2016.05.016

Macingova, E., Luptakova, A., 2012. Recovery of Metals from Acid Mine Drainage. Chem. Eng. Trans. 28, 109–114.

Maget-Dana, R., Ptak, M., 1992. Interfacial properties of surfactin. J. Colloid Interface Sci. 153, 285–291.

Mnif, I., Ghribi, D., 2015. Lipopeptides biosurfactants: Mean classes and new insights for industrial, biomedical, and environmental applications. Biopolymers 104, 129–147. https://doi.org/10.1002/bip.22630

Moslemi, H., Gharabaghi, M., 2017. A review on electrochemical behavior of pyrite in the froth flotation process. J. Ind. Eng. Chem. 47, 1–18. https://doi.org/10.1016/j.jiec.2016.12.012

Moslemi, H., Shamsi, P., Habashi, F., 2011. Pyrite and pyrrhotite open circuit potentials study: Effects on flotation. Miner. Eng. 24, 1038–1045. https://doi.org/10.1016/j.mineng.2011.05.001

Mulligan, C.N., 2009. Recent advances in the environmental applications of biosurfactants. Curr. Opin. Colloid Interface Sci. 14, 372–378. https://doi.org/10.1016/j.cocis.2009.06.005

Mulligan, C.N., Yong, R.N., Gibbs, B.F., 1999a. On the use of biosurfactants for the removal of heavy metals from oil-contaminated soil. Environ. Prog. 18, 50–54. https://doi.org/10.1002/ep.670180120

Mulligan, C.N., Yong, R.N., Gibbs, B.F., James, S., Bennett, H.P.J., 1999b. Metal removal from contaminated soil and sediments by the biosurfactant surfactin. Environ. Sci. Technol. 33, 3812–3820. https://doi.org/10.1021/es9813055

Nagaraj, D.R., Farinato, R.S., 2016. Evolution of flotation chemistry and chemicals: A century of innovations and the lingering challenges. Miner. Eng. 96–97, 2–14. https://doi.org/10.1016/j.mineng.2016.06.019

Naicker, K., Cukrowska, E., McCarthy, T.S., 2003. Acid mine drainage arising from gold mining activity in Johannesburg, South Africa and environs. Environ. Pollut. 122, 29–40. https://doi.org/10.1016/S0269-7491(02)00281-6

Nitschke, M., Pastore, G.M., 2006. Production and properties of a surfactant obtained from Bacillus subtilis grown on cassava wastewater. Bioresour. Technol. 97, 336–341. https://doi.org/10.1016/j.biortech.2005.02.044

Okolo, G.N., Neomagus, H.W.J.P., Everson, R.C., Roberts, M.J., Bunt, J.R., Sakurovs, R., Mathews, J.P., 2015. Chemical–structural properties of South African bituminous coals: Insights from wide angle XRD–carbon fraction analysis, ATR–FTIR, solid state 13 C NMR, and HRTEM techniques. Fuel 158, 779–792. https://doi.org/10.1016/j.fuel.2015.06.027

Osman, M., Høiland, H., Holmsen, H., Ishigami, Y., 1998. Tuning micelles of a bioactive heptapeptide biosurfactant via extrinsically induced conformational transition of surfactin assembly. J. Pept. Sci. 4, 449–458. https://doi.org/10.1002/(sici)1099-1387(199811)4:7<449::aid-psc164>3.0.co;2-%23

Pecci, Y., Rivardo, F., Martinotti, M.G., Allegrone, G., 2010. LC/ESI-MS/MS characterisation of lipopeptide biosurfactants produced by the Bacillus licheniformis V9T14 strain. J. Mass Spectrom. 45, 772–778. https://doi.org/10.1002/jms.1767

Peng, Y., Grano, S., 2010. Effect of grinding media on the activation of pyrite flotation. Miner. Eng. 23, 600–605. https://doi.org/10.1016/j.mineng.2010.02.003

Peng, Y., Grano, S., Fornasiero, D., Ralston, J., 2003. Control of grinding conditions in the flotation of galena and its separation from pyrite. Int. J. Miner. Process. 70, 67–82. https://doi.org/10.1016/S0301-7516(02)00153-9

Peppas, A., K, K., Halikia, I., 2000. Use of organic covers for acid mine drainage control. Miner. Eng. 13,

563–574.

Peypoux, F., Bonmatin, J.M., Wallach, J., 1999. Recent trends in the biochemistry of surfactin. Appl. Microbiol. Biotechnol. 51, 553–563. https://doi.org/10.1007/s002530051432

Pickel, W., Kus, J., Flores, D., Kalaitzidis, S., Christanis, K., Cardott, B.J., Misz-Kennan, M., Rodrigues, S., Hentschel, A., Hamor-Vido, M., Crosdale, P., Wagner, N., 2017. Classification of liptinite – ICCP System 1994. Int. J. Coal Geol. 169, 40–61. https://doi.org/10.1016/j.coal.2016.11.004

Polat, M., Polat, H., Chander, S., 2003. Physical and chemical interactions in coal flotation. Int. J. Miner. Process. 72, 199–213. https://doi.org/10.1016/S0301-7516(03)00099-1

Poortinga, A.T., Bos, R., Norde, W., Busscher, H.J., 2002. Electric double layer interactions in bacterial adhesion to surfaces, Surface Science Reports. https://doi.org/10.1016/S0167-5729(02)00032-8

Raichur, A.M., Wang, X.H., Parekh, B.K., 2001. Estimation of surface free energy of pyrites by contact angle measurements. Miner. Eng. 14, 65–75. https://doi.org/10.1016/S0892-6875(00)00160-6

Reddick, J.F., Von Blottnitz, H., Kothuis, B., 2007. A cleaner production assessment of the ultra-fine coal waste generated in South Africa. J. South. African Inst. Min. Metall. 107, 811–816.

Rosenberg, E., Ron, E.Z., 1999. High- and low-molecular-mass microbial surfactants. Appl. Microbiol. Biotechnol. 52, 154–162. https://doi.org/10.1007/s002530051502

Saikia, B.K., Boruah, R.K., Gogoi, P.K., 2007a. FT-IR and XRD analysis of coal from Makum coalfield of Assam. J. Earth Syst. Sci. 116, 575–579. https://doi.org/10.1007/s12040-007-0052-0

Saikia, B.K., Boruah, R.K., Gogoi, P.K., 2007b. XRD and FT-IR investigations of sub-bituminous Assam coals. Bull. Mater. Sci. 30, 421–426. https://doi.org/10.1007/s12034-007-0068-8

Sarikaya, M., Özbayoğlu, G., 1995. Flotation characteristics of oxidized coal. Fuel 14, 291–294.

Sen, R., Swaminathan, T., 2005. Characterization of concentration and purification parameters and operating conditions for the small-scale recovery of surfactin. Process Biochem. 40, 2953–2958. https://doi.org/10.1016/j.procbio.2005.01.014

Shen, H.H., Lin, T.W., Thomas, R.K., Taylor, D.J.F., Penfold, J., 2011. Surfactin structures at interfaces and in solution: The effect of pH and cations. J. Phys. Chem. B 115, 4427–4435. https://doi.org/10.1021/jp109360h

Simate, G.S., Ndlovu, S., 2014. Acid mine drainage: Challenges and opportunities. J. Environ. Chem. Eng. 2, 1785–1803. https://doi.org/10.1016/j.jece.2014.07.021

Singh, R., 1998. Development of flotation reagents with chelating functional groups. Froth Flotat. Recent Trends 68–78. https://doi.org/http://eprints.nmlindia.org/4358

Song, C.S., Ye, R.Q., Mu, B.Z., 2007. Molecular behavior of a microbial lipopeptide monolayer at the air-water interface. Colloids Surfaces A Physicochem. Eng. Asp. 302, 82–87. https://doi.org/10.1016/j.colsurfa.2007.01.055

Stonestreet, P., Franzidis, J.-P., 1988. REVERSE FLOTATION OF COAL - A NOVEL WAY FOR THE BENEFICIATION OF COAL FINES. Miner. Eng. I, 343–349.

Suli, L.M., Ibrahim, W.H.W., Aziz, B.A., Deraman, M.R., Ismail, N.A., 2017. A Review of Rare Earth Mineral Processing Technology. Chem. Eng. Res. Bull. 19, 20. https://doi.org/10.3329/cerb.v19i0.33773

Suraj, G., Iyer, C.S.P., Rugmini, S., Lalithambika, M., 1997. The effect of micronization on kaolinites and their sorption behaviour. Appl. Clay Sci. 12, 111–130. https://doi.org/10.1016/S0169-1317(96)00044-0

Sýkorová, I., Pickel, W., Christanis, K., Wolf, M., Taylor, G.H., Flores, D., 2005. Classification of huminite - ICCP System 1994. Int. J. Coal Geol. 62, 85–106. https://doi.org/10.1016/j.coal.2004.06.006

Szymanska, A., Sadowski, Z., 2010. Effects of biosurfactants on surface properties of hematite. Adsorption 16, 233–239. https://doi.org/10.1007/s10450-010-9251-0

Taira, T., Yanagisawa, S., Nagano, T., Zhu, Y., Kuroiwa, T., Koumura, N., Kitamoto, D., Imura, T., 2015. Selective encapsulation of cesium ions using the cyclic peptide moiety of surfactin: Highly efficient removal based on an aqueous giant micellar system. Colloids Surfaces B Biointerfaces 134, 59–64. https://doi.org/10.1016/j.colsurfb.2015.06.034

Tao, D.P., Li, Y.Q., Richardson, P.E., Yoon, R.H., 1994. The incipient oxidation of pyrite. Colloids Surfaces A Physicochem. Eng. Asp. 93, 229–239. https://doi.org/10.1016/0927-7757(94)02892-3

Thimon, L., Peypoux, F., Michel, G., 1992. Interactions of surfactin, a biosurfactant from Bacillus subtilis, with inorganic cations. Biotechnol. Lett. 14, 713–718. https://doi.org/10.1007/BF01021648

Trahar, W.J., Senior, G.D., Shannon, L.K., 1994. Interactions between sulphide minerals - the collectorless flotation of pyrite. Int. J. Miner. Process. 40, 287–321. https://doi.org/10.1016/0301-7516(94)90049-3

Tsan, P., Volpon, L., Besson, F., Lancelin, J.M., 2007. Structure and dynamics of surfactin studied by NMR in micellar media. J. Am. Chem. Soc. 129, 1968–1977. https://doi.org/10.1021/ja066117q

Van Niekerk, D., Pugmire, R.J., Solum, M.S., Painter, P.C., Mathews, J.P., 2008. Structural characterization of vitrinite-rich and inertinite-rich Permian-aged South African bituminous coals. Int. J. Coal Geol. 76, 290–300. https://doi.org/10.1016/j.coal.2008.08.014

Vazquez, G., Alvarez, E., Navaza, J.M., 1995. Surface Tension of Alcohol Water + Water from 20 to 50 .degree.C. J. Chem. Eng. Data 40, 611–614. https://doi.org/10.1021/je00019a016

Wang, X., Forssberg, E., 1990. EDTA-induced flotation of sulfide minerals. J. Colloid Interface Sci. 140, 217–226. https://doi.org/10.1016/0021-9797(90)90337-N

Weerasooriya, R., Makehelwala, M., Bandara, A., 2010. Probing reactivity sites on pyrite-oxidative interactions with 4-chlorophenol. Colloids Surfaces A Physicochem. Eng. Asp. 367, 65–69. https://doi.org/10.1016/j.colsurfa.2010.06.023

Wei, Y.H., Chu, I.M., 1998. Enhancement of surfactin production in iron-enriched media by Bacillus subtilis ATCC 21332. Enzyme Microb. Technol. 22, 724–728. https://doi.org/10.1016/S0141-0229(98)00016-7

Wen, B., Xia, W., Sokolovic, J.M., 2017. Recent advances in effective collectors for enhancing the flotation of low rank/oxidized coals. Powder Technol. 319, 1–11. https://doi.org/10.1016/j.powtec.2017.06.030

Wills, B.A., Napier-Munn, T., 2005. Froth flotation, in: Wills' Mineral Processing Technology (Seventh Edition). pp. 267–352. https://doi.org/http://dx.doi.org/10.1016/B978-075064450-1/50014-X

Xu, Y., Lay, J.P., Korte, F., 1988. Fate and effects of xanthates in laboratory freshwater systems. Bull. Environ. Contam. Toxicol. 41, 683–689. https://doi.org/10.1007/BF02021019

Yoon, R.H., Tao, D.P., Lu, M.X., Richardson, P.E., Luttrell, G.H., 1997. Improving pyrite rejection by galvanic control. Coal Prep. 18, 53–68. https://doi.org/10.1080/07349349708905138

Zachwieja, J.B., McCarron, J.J., Walker, G.W., Buckley, A.N., 1989. Correlation between the surface composition and collectorless flotation of chalcopyrite. J. Colloid Interface Sci. 132, 462–468. https://doi.org/10.1016/0021-9797(89)90260-9

Zajic, J.E., Guignard, H., Gerson, D.F., 1977. Properties and biodegradation of a bioemulsifier from Corynebacterium hydrocarboclastus. Biotechnol. Bioeng. 19, 1303–1320. https://doi.org/10.1002/bit.260190905

Zanotto, A.W., Valério, A., de Andrade, C.J., Pastore, G.M., 2019. New sustainable alternatives to reduce

the production costs for surfactin 50 years after the discovery. Appl. Microbiol. Biotechnol. 103, 8647–8656. https://doi.org/10.1007/s00253-019-10123-7

Zdziennicka, A., Krawczyk, J., Szymczyk, K., Jańczuk, B., 2018. Macroscopic and Microscopic Properties of Some Surfactants and Biosurfactants. Int. J. Mol. Sci. 19, 1934. https://doi.org/10.3390/ijms19071934

Zhu, H., Li, H.L., Ou, Z.S., Wang, D.Z., 2002. Analysis of surface modification on coal pyrite. J. South African Inst. Min. Metall. 102, 315–318.

Zouboulis, A.I., Matis, K.A., Lazaridis, N.K., Golyshin, P.N., 2003. The use of biosurfactants in flotation: Application for the removal of metal ions. Miner. Eng. 16, 1231–1236. https://doi.org/10.1016/j.mineng.2003.06.013

APPENDIX A - XRD

XRD analysis – Coal diffractogram

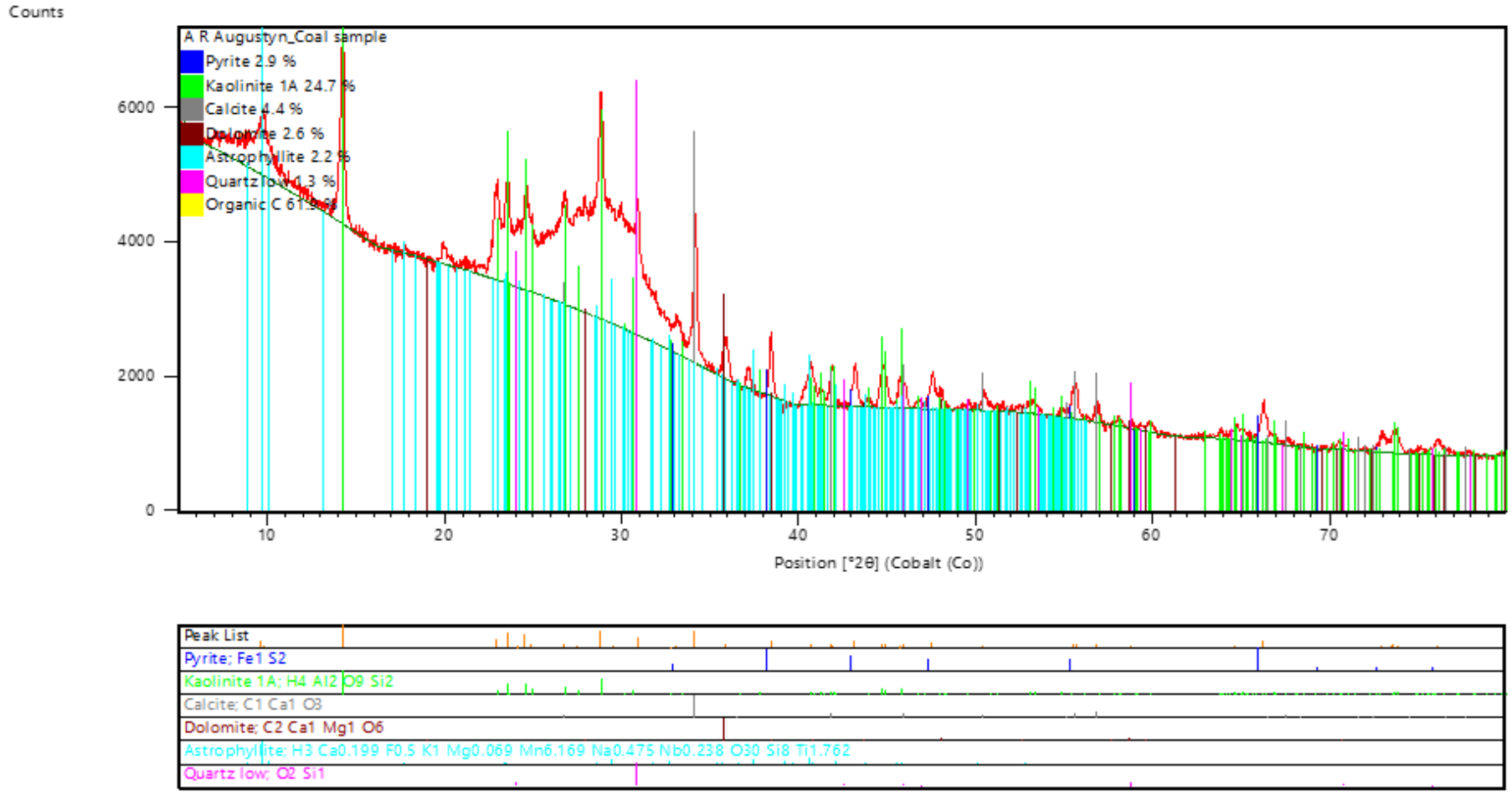

Figure 36: XRD analysis diffractograms for the coal sample.

XRD analysis – Pyrite diffractogram

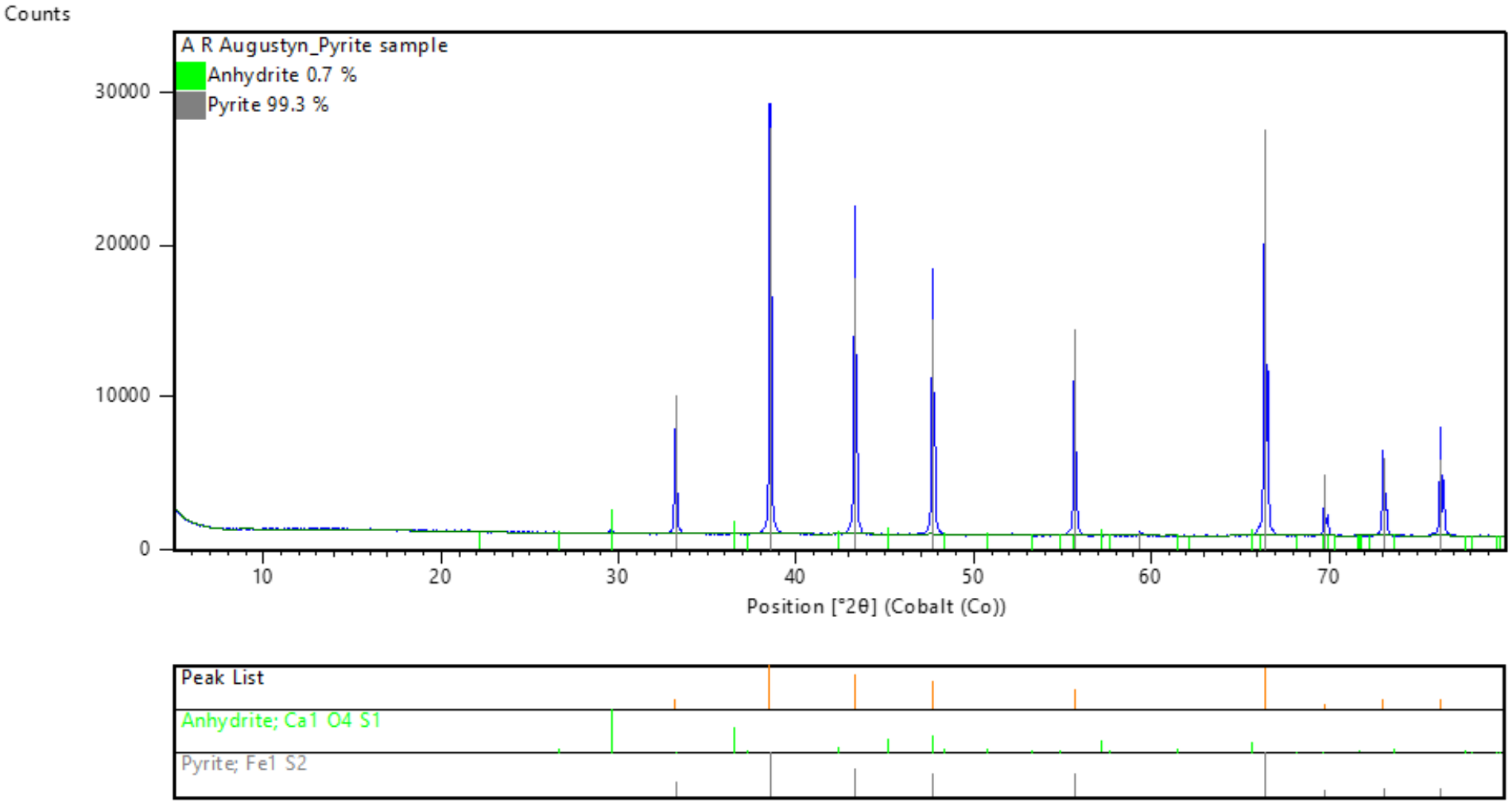

Figure 37: XRD analysis diffractograms for the pyrite sample.

APPENDIX B - LC-MS

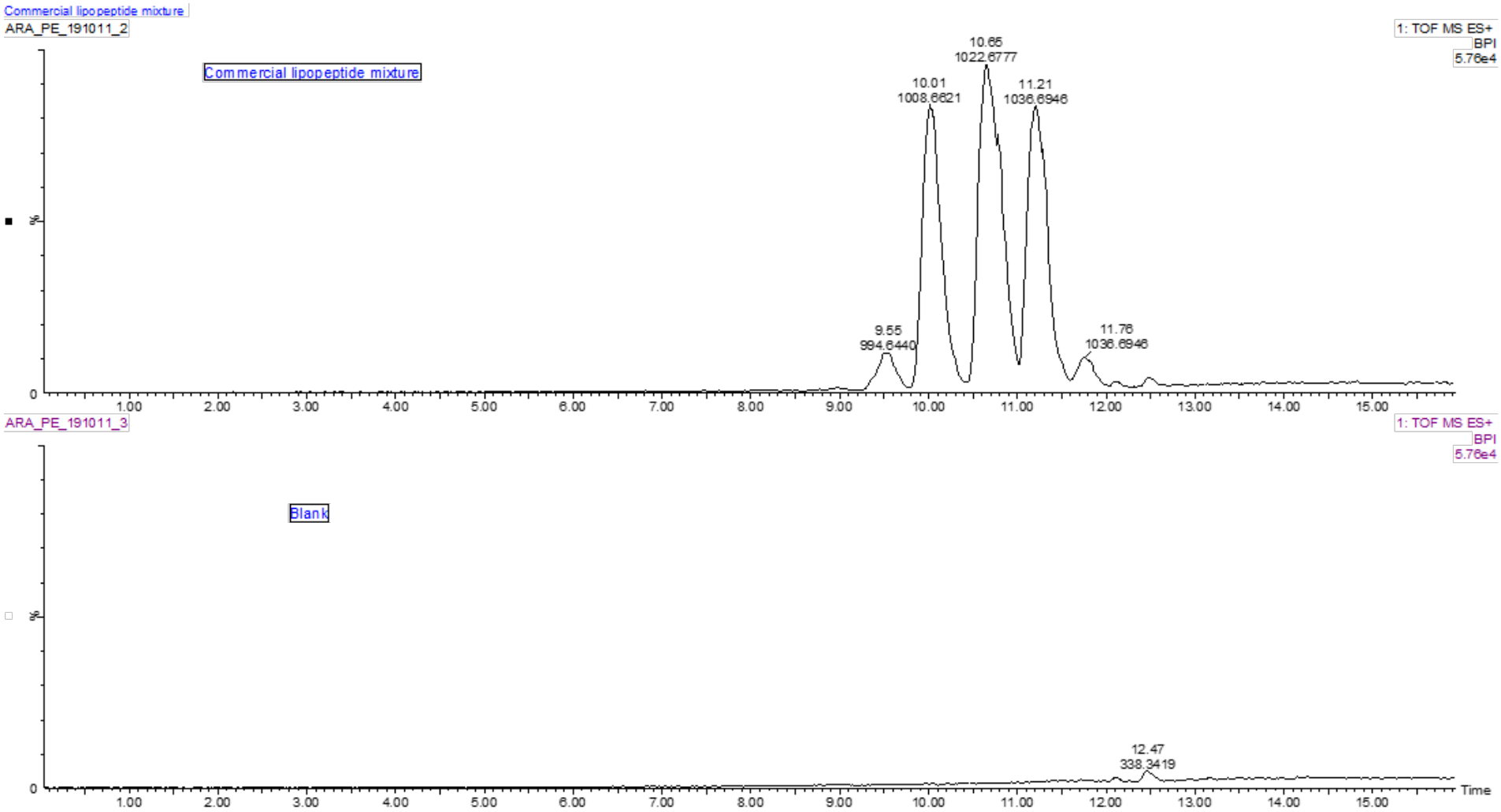

Figure 38: LC-MS chromatogram for the surfactin sample and the blank used.

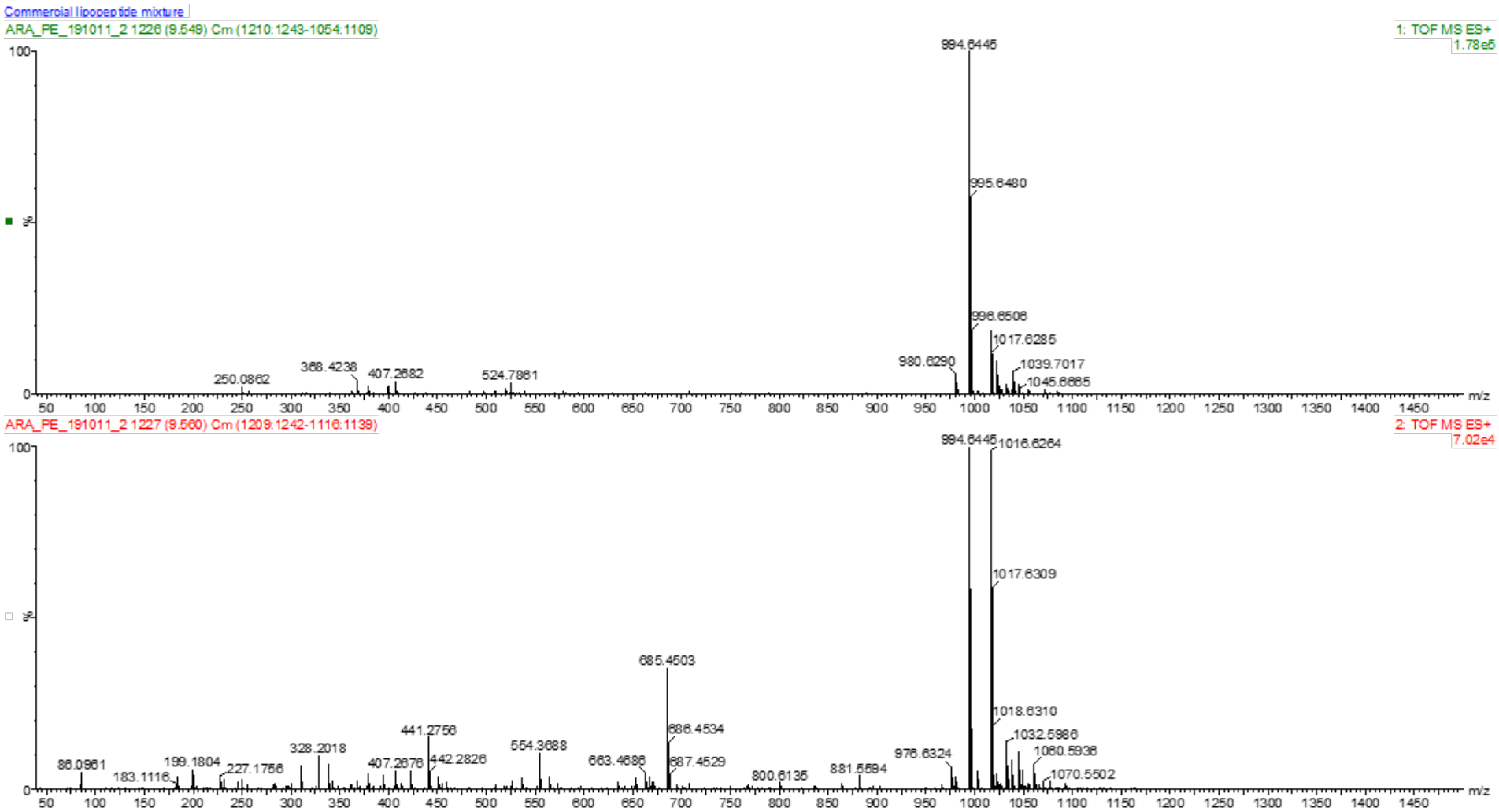

Figure 39: Mass spectra corresponding to the peaks around 9.5 min retention time.

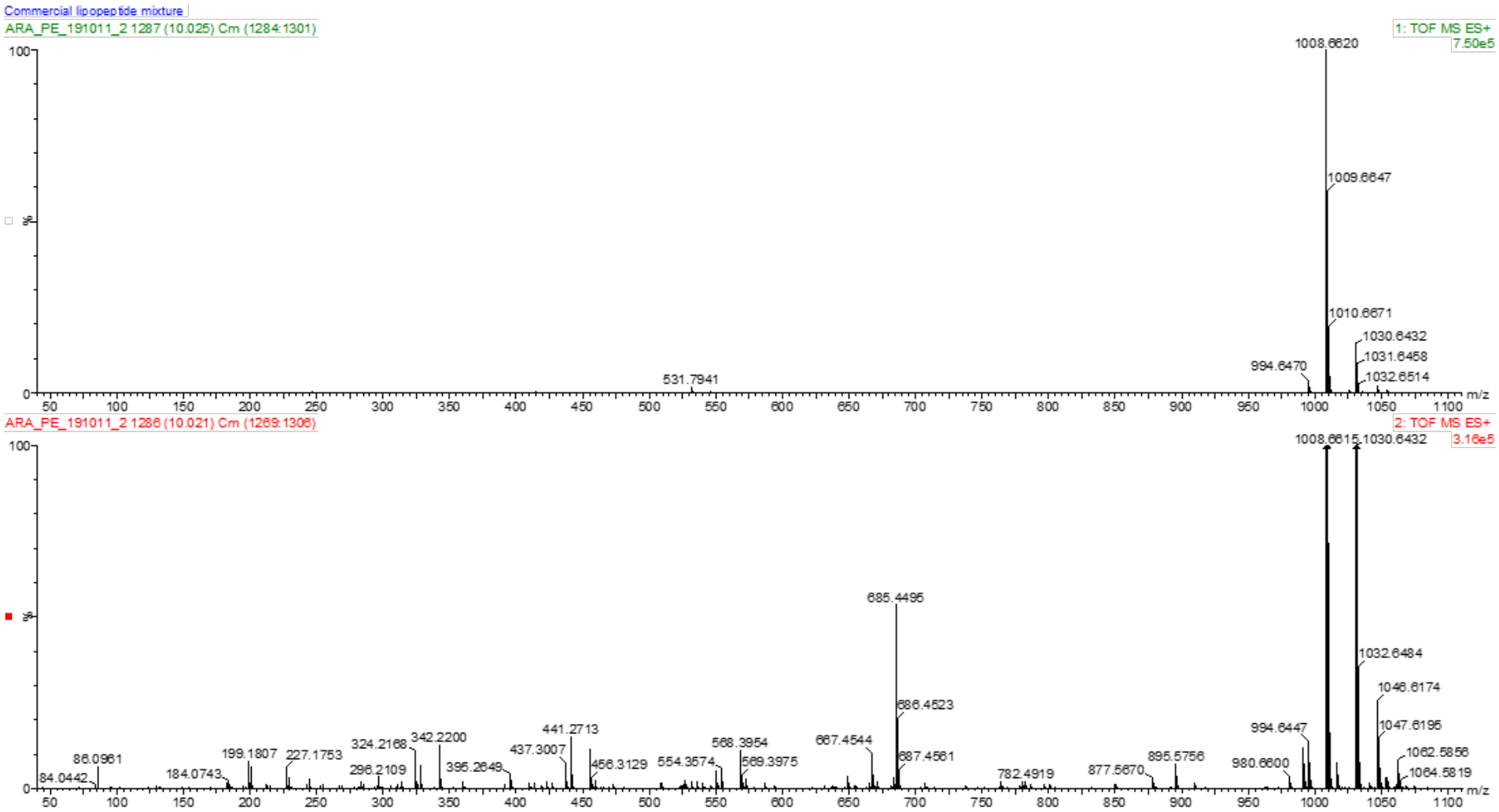

Figure 40 Mass spectra corresponding to the peaks around 10 min retention time.

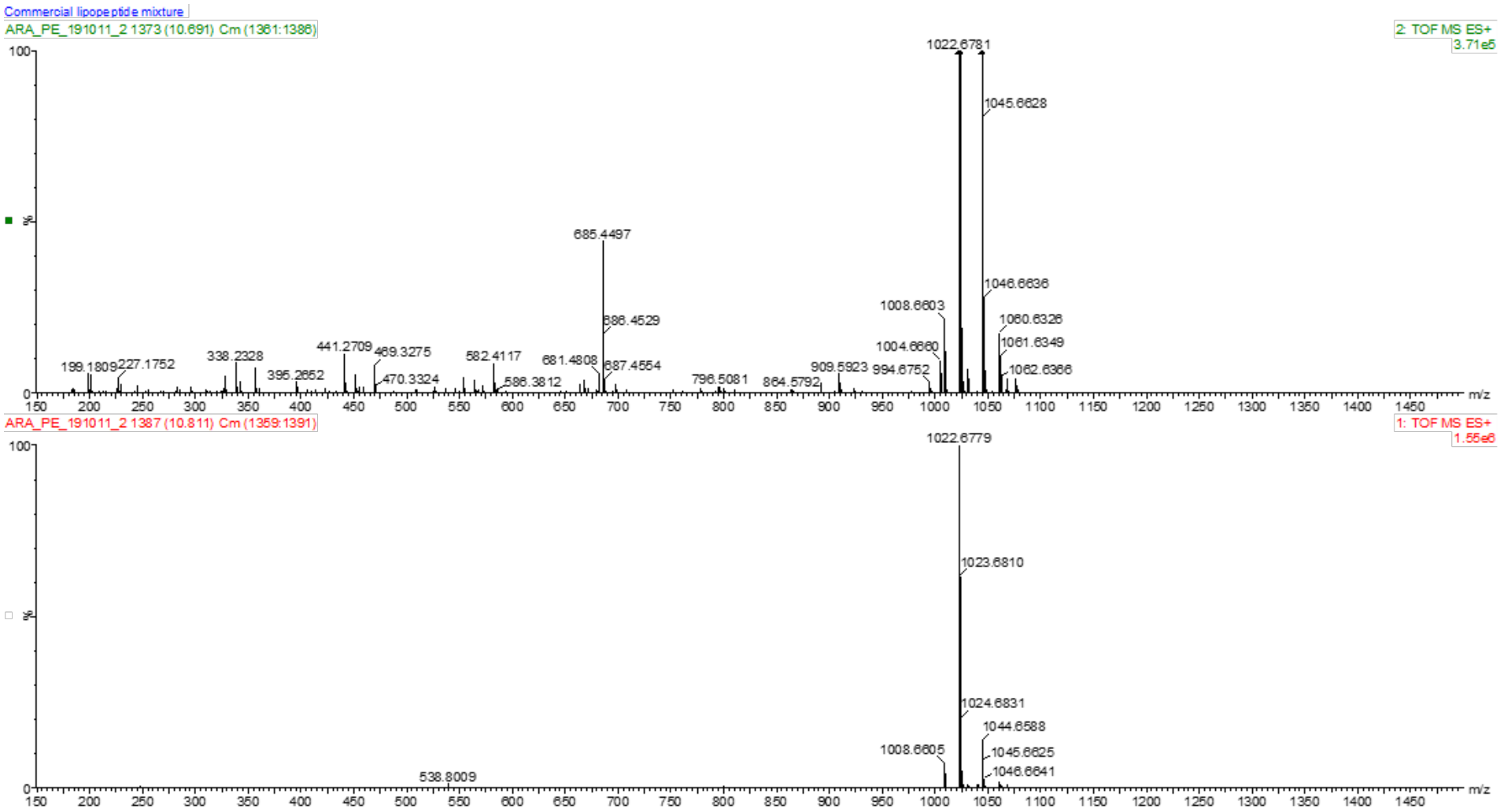

Figure 41: Mass spectra corresponding to the peaks around 10.7 min retention time.

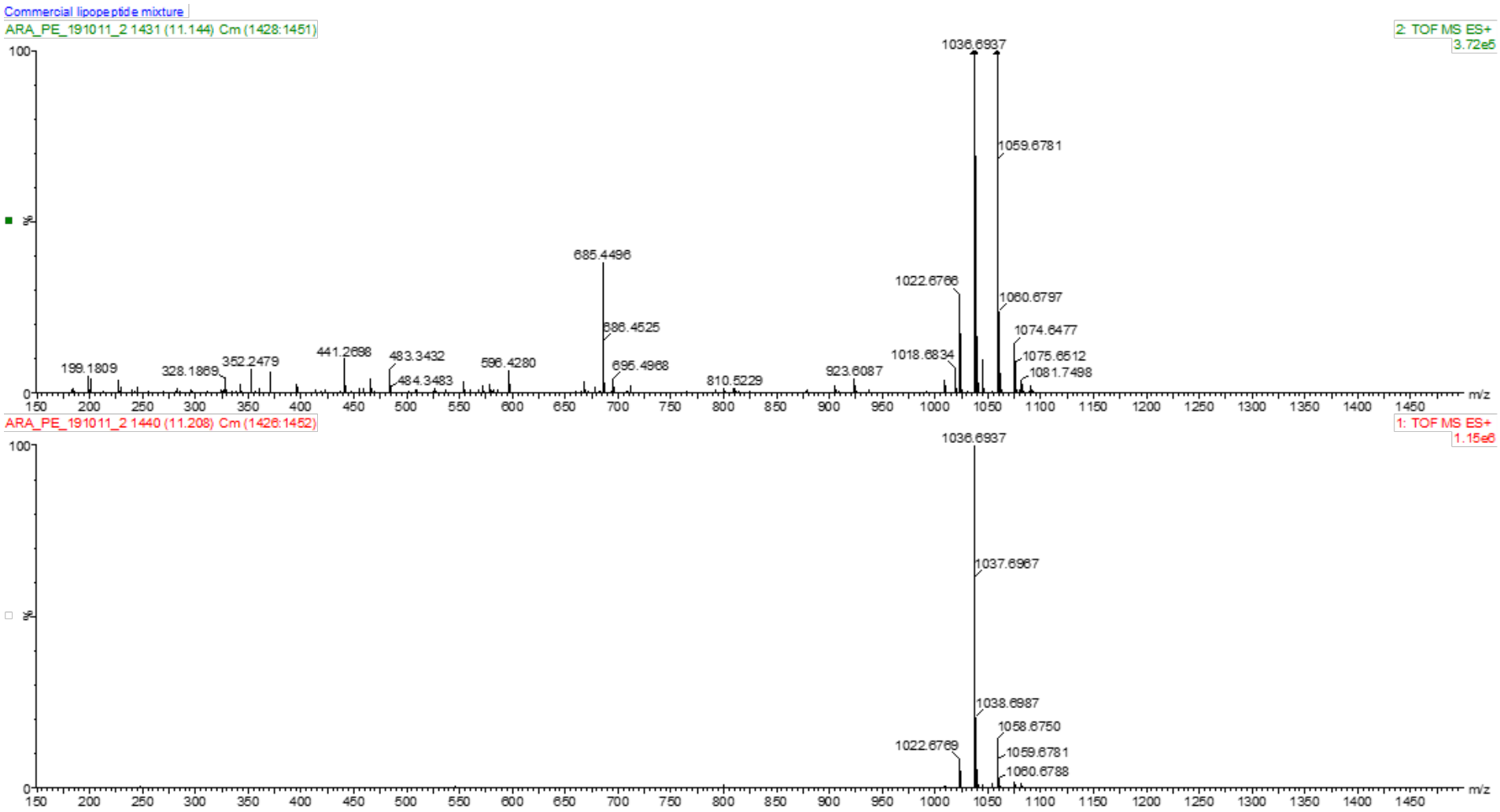

Figure 42: Mass spectra corresponding to the peaks around 11.2 min retention time.

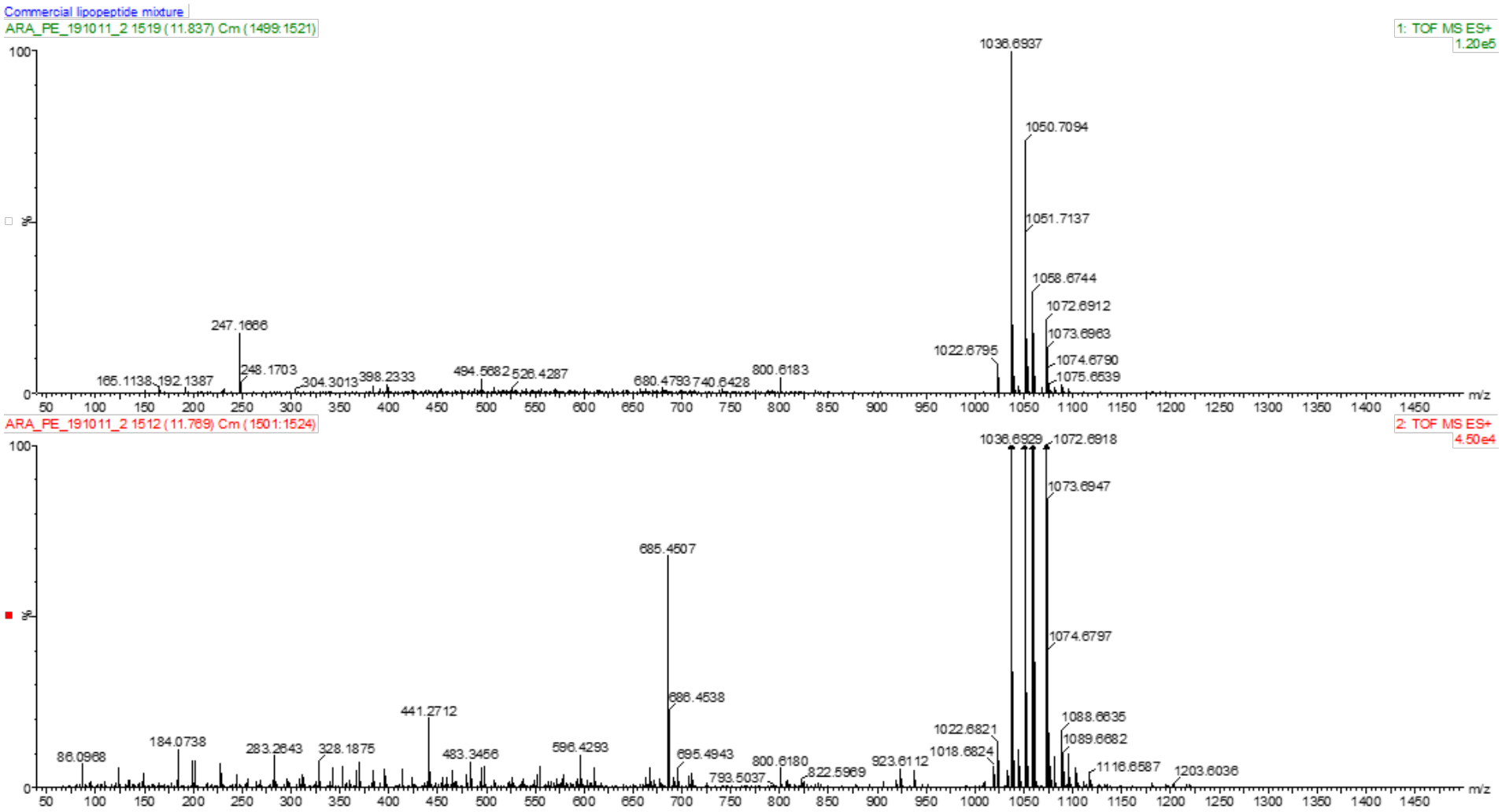

Figure 43: Mass spectra corresponding to the peaks around 11.8 min retention time.

APPENDIX C – PROCESSED DATA

Table 21: Surface tension data

Surfactin concentration (mg/L)	Surface tension (mN/m) (Huh-Mason correction)	Standard deviation
0	71.63	0.62
1	71.22	1.44
1.5	71.49	-
2	65.56	-
2.5	51.78	-
3	47.04	0.08
3.5	38.83	-
4	38.86	2.01
4.5	35.67	-
5	36.94	-
6	35.33	1.28
7	33.92	2.16
8	33.26	-
9	32.83	0.40
10	32.80	1.15
20	32.01	-
30	31.86	-
40	30.13	1.52
50	30.51	-
60	29.88	1.35
70	29.84	-
80	30.27	-
90	28.71	1.44
100	29.85	-

Table 22: Zeta potential data of coal at 0 mg/L surfactin concentration.

pH	Zeta potential (mV)	Standard deviation
2	16.34	0.66
3	15.02	1.28
4	3.65	0.61
5	-4.94	0.90
6	-9.69	3.84
7	-16.14	2.55
8	-21.87	1.30
9	-26.66	1.19
10	-27.34	1.81

Table 23: Zeta potential data of coal at 2 mg/L surfactin concentration.

pH	Zeta potential (mV)	Standard deviation
2	14.58	0.12
3	11.75	1.58
4	-3.52	2.62
5	-12.77	4.52
6	-14.92	5.02
7	-23.43	0.05
8	-24.85	0.87
9	-27.37	0.90
10	-28.40	0.71

Table 24: Zeta potential data of coal at 4 mg/L surfactin concentration.

pH	Zeta potential (mV)	Standard deviation
2	12.00	1.13
3	9.56	0.88
4	-5.82	3.49
5	-15.70	2.73
6	-16.88	2.85
7	-24.72	1.11
8	-25.13	0.85
9	-27.22	1.96
10	-28.25	1.53

Table 25: Zeta potential data of coal at 15 mg/L surfactin concentration.

pH	Zeta potential (mV)	Standard deviation
2	2.06	0.68
3	-0.88	1.14
4	-7.51	1.17
5	-17.98	1.25
6	-19.42	2.19
7	-25.43	2.78
8	-28.88	1.86
9	-32.28	2.66
10	-35.60	2.88

Table 26: Zeta potential data of pyrite at 0 mg/L surfactin concentration.

pH	Zeta potential (mV)	Standard deviation
2	2.06	1.93
3	-0.04	1.69
4	-2.14	0.59
5	-2.98	0.14
6	-2.59	0.32
7	-6.55	4.06
8	-8.22	2.31
9	-11.34	4.38
10	-13.22	1.58

Table 27: Zeta potential data of pyrite at 2 mg/L surfactin concentration.

pH	Zeta potential (mV)	Standard deviation
2	1.02	0.31
3	-0.83	0.27
4	-1.56	0.70
5	-3.31	1.05
6	-3.95	2.01
7	-8.57	4.85
8	-9.39	5.39
9	-13.39	5.72
10	-13.63	3.16

Table 28: Zeta potential data of pyrite at 4 mg/L surfactin concentration.

pH	Zeta potential (mV)	Standard deviation
2	1.30	1.59
3	-0.79	0.04
4	-4.46	2.05
5	-6.45	1.14
6	-7.46	0.79
7	-10.37	0.52
8	-13.55	1.86
9	-16.25	4.55
10	-16.88	2.99

Table 29: Zeta potential data of pyrite at 15 mg/L surfactin concentration.

pH	Zeta potential (mV)	Standard deviation
2	0.29	4.79
3	-3.10	3.51
4	-8.44	4.76
5	-9.22	3.09
6	-17.97	2.55
7	-21.97	1.04
8	-21.18	1.44
9	-20.13	2.83
10	-24.93	2.88

Table 30: Total coal recovery data for coal microflotation.

Surfactin concentration (mg/L)	pH	Total coal recovery (%)	Standard deviation
0	3	42.9%	15%
5	3	69.3%	12.0%
15	3	74.0%	4.4%
0	6	44.9%	15%
5	6	59.7%	6%
15	6	61.8%	6.9%
0	8	68.6%	9%
5	8	63.3%	11.1%
15	8	60.7%	10.5%
0	10	45.9%	2%
5	10	47.8%	11.4%
15	10	73.7%	3.8%

Table 31: Total pyrite recovery data for pyrite microflotation.

Surfactin concentration (mg/L)	pH	Total pyrite recovery (%)	Standard deviation
0	3	14.5%	4%
5	3	31.5%	7%
15	3	41.3%	0%
0	6	15.9%	1%
5	6	17.1%	3%
15	6	42.4%	6%
0	8	15.9%	7%
5	8	32.6%	16%
15	8	61.1%	23%
0	10	22.4%	4%
5	10	56.2%	19%
15	10	81.6%	2%